2020

3-D HOMOLOGY MODELING OF ORGANIC ANION TRANSPORTERS (OATs): DEFINING THE BIOCHEMICAL BASIS FOR OAT-SUBSTRATE INTERACTIONS

Christopher Jay
Virginia Commonwealth University

3-D HOMOLOGY MODELING OF ORGANIC ANION TRANSPORTERS (OATS): DEFINING THE BIOCHEMICAL BASIS FOR OAT-SUBSTRATE INTERACTIONS

A thesis/dissertation submitted in partial fulfillment of the requirements for the degree of Doctor of Philosophy at Virginia Commonwealth University.

By

Christopher Edward Jay
Bachelor of Science, University at Buffalo, Buffalo, New York, 2015

Director: Douglas H. Sweet, Ph.D.
Professor, Chair
Department of Pharmaceutics, School of Pharmacy

Virginia Commonwealth University (VCU)
Richmond, Virginia
June, 2020

ACKNOWLEDGEMENTS

The guidance provided by my advisor, Dr. Douglas Sweet, was unquestionably the driving force to complete my work as a PhD candidate. Through countless hours of discussion, interpretation, editing, and instruction, Dr. Sweet has been (and probably will be) the single greatest boss I have had the pleasure to work with. No matter how big or small the issue, Dr. Sweet made every attempt to push me outside my knowledge comfort zone and use critical thinking. Even with my busy day-to-day school schedule, Dr. Sweet allowed me to pursue other avenues to aid in a successful career outside academia, including allowing me to partake in courses outside the department to allowing me to participate in fellowship opportunities. As a mentor, a scholar, and as a friend, I cannot thank Dr. Sweet enough for giving me the chance to join his lab and show not only him, but the entire pharmaceutical world what I can accomplish as a scientist.

To my research committee members, including Dr. Phillip Gerk, Dr. Sandro da Rocha, Dr. Philip Mosier, and Dr. Adam VanWert, I sincerely thank you for your constant feedback in my research project. From the tough questions to the numerous instances of needed guidance, my committee members have been unequivocal assets to my future success as a scientist. As a teaching assistant for Dr. Gerk, I have learned from one of the most patient and knowledgeable professors in the Pharmaceutics Department, and I owe him everything for introducing a new passion of mine: Pharmacokinetics. I also thank Dr. Mosier for his countless hours of instruction on 3-D homology modeling, a new but exciting topic I was able to master, which became a substantial portion of my research.

I thank VCU School of Pharmacy, the Pharmaceutics Department, and the Graduate School in general for providing numerous instances of both educational and financial support to aid in my future career. The Pharmaceutics Department and the School of Pharmacy are lucky to have such kind and devoted staff, specifically Keyetta Tate, Laura Georgiadis and Sha-kim Craft, as through their efforts, the school runs smoothly and efficiently, not to mention these three are the nicest individuals on the planet.

To my lab-mates, Dr. Raymond Lai and Dr. Hebing Liu: I cannot thank you two enough for your help, as your support got me accustomed to “lab life” and how to be successful in it. I truly have made lasting friendships with these two individuals and I appreciate all the time and guidance they provided during my doctoral career.

Finally, to my family: while being born and raised in Buffalo, NY, certainly had its struggles, I owe all my success as a hardworking and dedicated individual to my parents, whom never quit when the going gets tough. While I have siblings, cousins, aunts, uncles, and grandparents that were supportive throughout my educational career, I unfortunately can’t list them all due to the endless amount of names. I love you all and could not have gotten through this journey without your support, especially the support from my loving and caring parents, Kathleen and Edward.

TABLE OF CONTENTS

LIST OF TABLES

LIST OF FIGURES

LIST OF ABBREVIATIONS

2-D	Two-dimensional
3-D	Three-dimensional
ADME	Absorption Distribution Metabolism Elimination
α-KG	Alpha-Ketoglutarate
ANOVA	Analysis of Variance
AP	Alkaline Phosphatase
APS	Ammonium Persulfate
BLAST	Basic Local Alignment Search Tool
BSA	Bovine Serum Albumin
CDER	Center for Drug Evaluation and Research
CHO	Chinese Hamster Ovary
DAPI	4’, 6-diamidino-2-phenylindol
DMEM/F12	Dulbecco's Modified Eagle's Medium/F12
DNA	Deoxyribonucleic Acid
DOPE	Discrete Optimized Protein Energy
DPX	Dibutylphthalate Polystyrene Xylene
EDTA	Ethylenediaminetetraacetic acid
ES	Estrone Sulfate
EtBr	Ethidium Bromide
FBS	Fetal Bovine Serum
FDA	Food and Drug Administration
FITC	Fluorescein Isothiocyanate

G418	Geneticin
GlpT	Glycerol-3-Phosphate Transporter
GOLD	Genetic Optimized Ligand Docking
GFP	Green Fluorescent Protein
HCl	Hydrochloride Acid
hCMV	Human Cytomegalovirus
HEK	Human Embryonic Kidney
HEPES	4-(2-hydroxyethyl)-1-piperazineethanesulfonic acid
HINT	Hydropathic Interactions
hOAT	Human Organic Anion Transporter
IDT	Integrated DNA Technologies
IgG	Immunoglobulin G
K_m	Michaelis-Menten Constant
L2K	Lipofectamine 2000
L3K	Lipofectamine 3000
LB	Luria Broth
MeOH	Methanol
MFS	Major Facilitator Superfamily
NaCl	Sodium Chloride
NaOH	Sodium Hydroxide
NBT/BCIP	Nitro Blue Tetrazolium Chloride / 5-Bromo-4-Chloro-3-Indolyl Phosphate
OAT	Organic Anion Transporter
PAH	*Para*-aminohippuric Acid

PBS	Phosphate Buffered Saline
PCR	Polymerase Chain Reaction
PDB	Protein Data Bank
PFA	Paraformaldehyde
PiPT	*Piriformospora Indica* High Affinity Phosphate Transporter
PVDF	Polyvinylidene Difluoride
RIPA	Radioimmunoprecipation Assay
RPM	Rotations Per Minute
SD	Standard Deviation
SDS	Sodium Dodecyl Sulfate
SE	Standard Error
SLC	Solute Carrier
TB	Transport Buffer
TBST	Tris Buffered Saline – Tween 20
TMD	Transmembrane Domain
UniProt	Universal Protein Resource
UV	Ultra-Violet
WT	Wild-Type

ABSTRACT

3-D HOMOLOGY MODELING OF ORGANIC ANION TRANSPORTERS (OATS): DEFINING THE BIOCHEMICAL BASIS FOR OAT-SUBSTRATE INTERACTIONS

By Christopher Edward Jay
Bachelor of Science, University at Buffalo, Buffalo, New York, USA

A dissertation submitted in partial fulfillment of the requirements for the degree of Doctor of Philosophy at Virginia Commonwealth University

Virginia Commonwealth University, 2020

Director: Douglas H. Sweet,
Professor, Chair
Department of Pharmaceutics, School of Pharmacy

A goal in the drug development process, as indicated by the FDA, is to evaluate a drug's ADME profile, as potential drug interactions could exist, leading to adverse drug reactions or loss of efficacy. Transport proteins, specifically organic anion transporters (OATs) are involved in the absorption, distribution, and elimination of small, negatively charged compounds. Although there is an exhaustive list of structurally diverse organic anions which interact with OATs, interactions at a molecular level are still shrouded in mystery particularly due to the lack of a solved crystal structure. Therefore, *in silico* homology models (hOAT1, 2, 3) were generated using a crystalized protein as template. Amino acid contacts predicted to be involved in compound recognition were then altered through mutagenesis, followed by accumulation and kinetic studies to evaluate their role in compound translocation (hOAT1 and hOAT3).

Three-dimensional (3-D) homology models were generated for hOAT1, hOAT2 and hOAT3 utilizing *Piriformospora indica* high affinity phosphate transporter (PiPT) as

template. The prototypical substrates *para*-aminohippuric acid (PAH) and estrone sulfate (ES) were docked into hOAT1 and hOAT3, respectively. Five amino acid contacts were identified after docking within hOAT1-PAH (Arg15, Ile19, Tyr230, Asn439 and Arg466) and hOAT3-ES (Tyr342, Phe426, Phe430, Leu431, and Arg454). Initial accumulation studies revealed hOAT1 substitutions at positions Arg15Ala, Ile19Ala, Tyr230Ala, Asn439Gln, Asn439Ala, and Arg466Ala abolished PAH transport mediated by hOAT1. Initial accumulation studies revealed hOAT3 substitutions at positions Tyr342Phe, Tyr342Ala, Phe426Ser, Leu431Ala, and Arg454Lys abolished ES transport mediated by hOAT3. Kinetic analysis revealed hOAT3 Phe430Ser substitution had a statistically significant increase in K_m as compared to hOAT3 WT. Additionally, numerous structurally divergent compounds were docked within the generated hOAT1, hOAT2, and hOAT3 models, revealing additional amino acid contacts potentially critical to compound recognition and translocation.

Initial *in silico* studies revealed amino acid contacts potentially critical in hOAT1, hOAT2, and hOAT3 compound recognition. hOAT1 and hOAT3 *in vitro* studies further validated the generated *in silico* models, as well as emphasized significance in residues involved in substrate recognition. Development of these homology models could serve as an invaluable tool to support targeted rational drug design in addition to predicting drug-drug interactions.

CHAPTER 1

Innovation and Specific Aims

1A. INNOVATION

The proposed studies were the first to use the recently crystallized MFS member, PiPT, as a template to generate 3-D homology models of SLC22 family members human organic anion transporters (hOAT) 1, 2 and 3. Prior studies on hOAT1 used the glycerol 3-phosphate transporter (GlpT, SLC37A2) as the protein template [1], however, PiPT offers the advantages of belonging to the same transporter superfamily, sharing higher sequence identity and similarity with hOATs than GlpT, being crystalized in its occluded state, and being even more closely related evolutionarily as it is eukaryotic whereas GlpT is prokaryotic. Using these generated *in silico* homology models for hOAT1 and hOAT3, potentially critical amino acid contacts were identified and tested through *in vitro* efforts. Our hypothesis is that substituting amino acid contacts identified will result in changes in compound transport mediated by hOAT1 and hOAT3.

1B. SPECIFIC AIMS

Specific Aim 1

To identify amino acid residues critical for compound-transporter interaction through:

a. *In-silico* 3-D homology modeling of OATs using the crystal structure of PiPT as the template.
b. *In-silico* ligand docking studies using prototypical substrates (PAH for hOAT1, ES for hOAT3) to determine the putative binding pocket for each OAT.
c. Identification of amino acids within each transporter's putative binding pocket that mediate interaction with the aforementioned substrates (PAH or ES, respectively).

Specific Aim 2

To mutate amino acids identified as critical in specific aim 1 and observe quantitative changes in affinity of OAT substrate recognition by:

a. Introducing conservative and non-conservative point mutations through use of site-directed mutagenesis, thus altering the amino acid residues at previous predicted positions.
b. Establish stably transfected cell lines expressing each OAT mutant.
c. Perform activity assays to identify mutants as either active or inactive.
d. Conduct saturation analysis studies on active mutants to determine affinity for the associated prototypical substrate (PAH or ES).
e. Verification of proper membrane targeting of inactive OAT mutants.

Specific Aim 3

To dock additional structurally divergent compounds to further characterize hOAT1-hOAT3 binding interactions by:

a. *In-silico* docking of structurally divergent OAT compounds: PAH, ES, penicillin G, α-ketoglutarate (α-KG), acyclovir, salicylate, probenecid, and fluorescein, and then identify additional amino acids critical to compound-transporter interaction.
b. Comparing amino acids critical to compound-transporter interactions across hOAT1, hOAT2, and hOAT3.

CHAPTER 2 –HUMAN ORGANIC ANION TRANSPORTER 1 (hOAT1)

Elucidating hOAT1-PAH binding interactions through homology modeling and mutational analysis

2A. INTRODUCTION

Organic anion transporters are integral membrane proteins directly involved in barrier tissue translocation of small, negatively charged compounds, including drugs, xenobiotics, and endogenous molecules. OATs are transport proteins which indirectly utilize cellular energy through the stored energy of concentration gradients as the main driving force for compound translocation [2]. OATs belong within the solute carrier (SLC) 22 transporter family, which encompasses organic cation/anion/zwitterion transporters, and mediate the cellular entry and exit of anionic and zwitterionic organic molecules. Since the initial discovery of human OAT1 (hOAT1) in 1998 [3], extensive functional analysis has established primary hOAT1 localization within the basolateral membrane of renal proximal tubule cells [3,4].

There is an exhaustive list of structurally diverse organic anions which interact with OATs, including drugs classified as diuretics, antihypertensives, antibiotics, antivirals, and anticancer agents. Further, various anionic substances intermingle with OATs, including endogenous substances such as metabolic intermediates and hormones, in addition to environmental toxins and toxicants, such as mycotoxins and pesticides [2]. However, interactions at a molecular level are still shrouded in mystery based on the lack of structural information available for OATs, particularly lack of a solved crystal structure. Thus, alternative methodology has been utilized to predict the 3-D structure of a protein sequence based on alignment of a structurally determined crystallized template protein,

also known as comparative modeling [5]. This strategy serves as a viable option for hOAT1 until hOAT1's crystal structure is determined. Thus, it is imperative to identify the most suitable template for subsequent analysis. Given the structural elements fundamental to OATs, including 12 transmembrane domain (TMD) spanning α-helices, intracellular orientation of both N-&-C termini, a large extracellular loop between TMD 1 & 2, and a large intracellular loop between TMD 6 & 7, crystallized proteins within the major facilitator superfamily (MFS) were considered. Previous attempts utilizing MFS proteins as a template based on structural characteristics and sequence similarities, including the prokaryotic glycerol-3-phosphate transporter (GlpT, SLC37A2), have been conducted [1]. While most appropriate at the time, subsequent to these studies additional MFS proteins have been successfully crystalized, including the eukaryotic transporter, *Piriformospora indica* phosphate transporter, or PiPT [6]. Using PiPT as a template for hOAT1 homology modeling offers the advantages of: 1) belonging to the same transporter superfamily, 2) sharing higher sequence identity and similarity with hOAT1 than GlpT, 3) being crystalized in its occluded state, and 4) being more closely related evolutionarily as it is eukaryotic whereas GlpT is prokaryotic. Given this information, comparative homology models based on PiPT's structure were constructed for hOAT1, followed by continued deductions regarding which residues contribute to hOAT1-compound recognition, using the prototypical substrate *para*-aminohippuric acid (PAH).

Amino acid residues predicted to be involved in substrate recognition were subsequently altered via site-directed mutagenesis in order to evaluate their potential role in PAH translocation. Wild-type (WT) and mutated hOAT1 constructs were then expressed in Chinese hamster ovary (CHO) cells to allow for their functional analysis.

Initial investigation suggested three conservative mutants (Arg15Lys, Ile19Leu, Tyr230Phe) exhibited significant changes in PAH accumulation as compared to parental CHO cells, albeit with no changes in affinity, as compared to WT hOAT1. All non-conservative substitutions led to loss of transport activity, indicating some rigidity in these positions in regards to PAH recognition. This information provides correlative support of the generated *in silico* hOAT1 homology model.

2B. MATERIALS AND METHODS

Chemicals and Reagents - [^{3}H] PAH was purchased from PerkinElmer Life and Analytical Science (Waltham, MA). Unlabeled PAH, probenecid, and DAPI (4',6-diamidino-2-phenylindol) ready-made solution were purchased from Sigma-Aldrich (St. Louis, MO). Specific primers for mutation reactions were purchased from Integrated DNA Technologies (IDT, Coralville, IA). QuikChange Lightning Site-Directed Mutagenesis Kit was purchased from Agilent Technologies (Santa Clara, CA). Lipofectamine transfection reagents and Dulbecco's modified eagle's/Ham's F12 medium were purchased from Thermo Fisher Scientific (Waltham, MA). QIAprep spin mini and midiprep kits were purchased from QIAGEN (Germantown, MD). GoTaq green master mix was purchased from Promega (Madison, WI). Abcam plasma membrane protein extraction kit and rabbit anti-c-Myc polyclonal antibody were purchased from Abcam (Cambridge, United Kingdom). Immuno-Blot assay kit was purchased from Bio-Rad (Hercules, CA). Primary actin antibody, alkaline phosphatase (AP) and FITC conjugated secondary antibodies were purchased from Santa Cruz Biotechnology (Dallas, TX).

Molecular Model Building – There were essentially four stages to the comparative modeling (Figure 2.1). In summary, the recently solved crystal structure for *Pirformospora indica* high-affinity phosphate transporter (PiPT) was identified as the most suitable currently available template molecule and its sequence was downloaded from Protein Data Bank (PDB ID: 4J05). The hOAT1 FASTA protein sequence was downloaded from the Universal Protein Resource (UniProt, UniProtKB ID: Q4U2R8). Looped regions between TMD 1 & 2 and 6 & 7 in the final crystalized form of PiPT were excluded based on their inability to resolve these regions [6]. In order to properly align the

target (hOAT1) peptide sequence with the known template (PiPT) peptide sequence, hOAT1 secondary structures, including potential TMD helices, were predicted using PredictProtein v1 [7]. Looped regions between TMD 1 & 2 and 6 & 7 were excluded from hOAT1 due to lack of resolved sequence within the PiPT crystal structure. The curated sequences were aligned using the multiple sequence alignment software ClustalX v2 [8], followed by manual modifications to avoid repetitive regions of non-alignment within predicted transmembrane helices, which would negatively impact the model building. The final alignment for PiPT-hOAT1 was visualized using ALINE v1.0.025 [9]. Based on this alignment, one hundred comparative protein models were generated, using the software MODELLER v9.17 [10]. The stereochemical integrity of the generated models was evaluated through Discrete Optimized Protein Energy (DOPE) scoring v9.17, [11] and Ramachandran plots (PROCHECK v9.17, [12]), both of which ensure bond lengths, angles, and torsions within the *in silico* model were within acceptable and feasible limits.

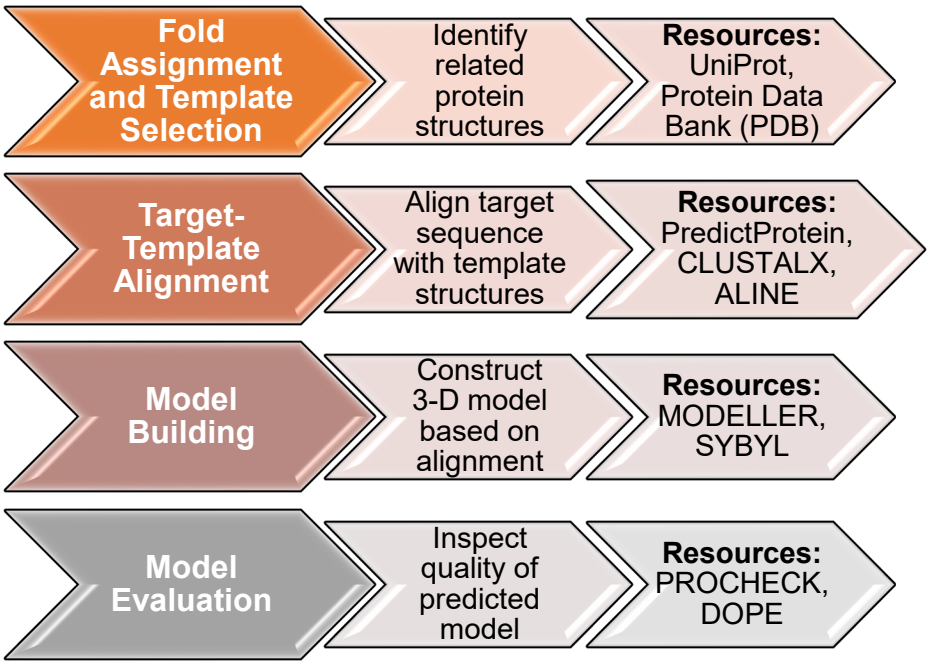

Figure 2.1 Summarized Steps to Comparative Modeling

Generalized scheme to initiate the model building procedure utilizing comparative modeling techniques. Information summarized using additional references [5].

Substrate Docking – An ionized, energy minimized structure for the prototypical hOAT1 substrate, PAH, was generated using the computer-aided molecular modeling design tool SYBYL-X v2.1 [13]. Proper confirmation and atom type for the sketched *in silico* molecule was evaluated and followed by energy minimization based on Gasteiger-Huckel charges. Ligand docking studies were initiated using the docking algorithm Genetic Optimization for Ligand Docking (GOLD) v5.4 provided from the Cambridge Crystallographic Data Centre [14]. Briefly, a GOLD configuration file was generated that referenced the previously generated one hundred hOAT1 models as the corresponding "receptor" and the *in silico* PAH molecule as the "ligand". A spherical region 30Å in diameter was designated, which virtually encapsulated the entire transporter. One thousand possible combinations were evaluated, and the top combination was selected based on GOLD score, DOPE score, and number of clusters. The specific hOAT1-PAH combination was then visually inspected using SYBYL-X v2.1, which allows 3-D manipulation, thus permitting identification of amino acids deemed potentially critical for the formation of the compound-transporter complex. Further validation of these predicted critical amino acids was obtained using the empirical molecular modeling system Hydropathic Interactions (HINT) [15], which evaluates and scores the binding interactions between hOAT1 and PAH.

Mutagenesis – hOAT1 constructs containing single conservative or non-conservative substitutions at each position hypothesized to be part of the hOAT1-PAH binding complex were generated, based upon the physiochemical properties of amino acids, amongst other supportive information [16]. Substitutions were introduced into pcDNA 3.1 (+) hOAT1 plasmid (Figure 2.2) using the QuikChange Lightning Site-Directed Mutagenesis Kit (Agilent Technologies, Santa Clara, CA). Oligonucleotide primers used to introduce the mutations were designed online using QuikChange Primer Design software (Agilent Technologies, Santa Clara, CA, [17]) and reported in Table 2.1. Cycling parameters for QuikChange Mutagenesis Method were as follows: denature at 95°C for 2 min, 18 cycles of 95°C denature for 20 sec, 60°C annealing for 10 sec, 68˚C elongation for 30 sec per kb of plasmid length (8kb plasmid, 4 min); with a final elongation at 68°C for 5 min. Samples were subsequently incubated with Dpn1 restriction enzyme at 37°C to degrade the WT hOAT1 parental template strands.

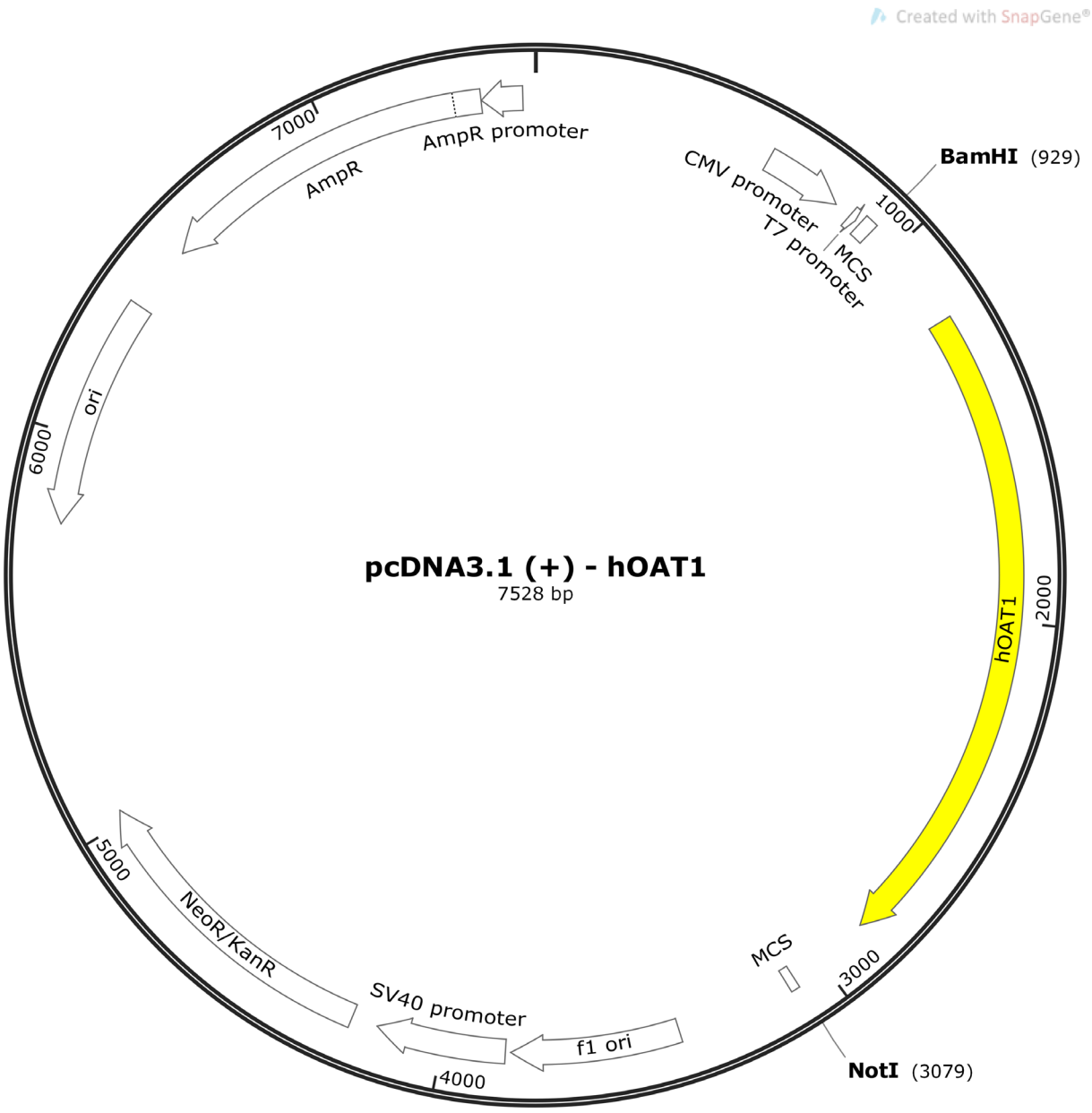

Figure 2.2 Plasmid Map of hOAT1 Template

Full length hOAT1 cDNA sequence was subcloned into pcDNA3.1 (+) plasmid vector (Invitrogen, Carlsbad, CA) using BamHI/NotI restriction enzyme sites. Location of hOAT1 insert is highlighted in yellow. Image generated using SnapGene.

Table 2.1 Oligonucleotide primer sequences used for site-directed mutagenesis

Position	Substitution	Primer	Primer Sequence (5' to 3')
Arginine 15	Lysine	Forward	GTGGGGGGTGTCGGC**AAG**TTCCAGCAGATCCAG
		Reverse	CTGGATCTGCTGGAA**CTT**GCCGACACCCCCCAC
	Alanine	Forward	GGGGGGTGTCGGC**GCC**TTCCAGCAGATC
		Reverse	GATCTGCTGGAA**GGC**GCCGACACCCCCC
Isoleucine 19	Leucine	Forward	CCGCTTCCAGCAG**TTG**CAGGTCACCCTGG
		Reverse	CCAGGGTGACCTG**CAA**CTGCTGGAAGCGG
	Alanine	Forward	GCCGCTTCCAGCAG**GCC**CAGGTCACCCTGG
		Reverse	CCAGGGTGACCTG**GGC**CTGCTGGAAGCGGC
Tyrosine 230	Phenylalanine	Forward	GGGCACCTTGATTGGCTATGTC**TTT**AGCCTGGGCCAG
		Reverse	CTGGCCCAGGCT**AAA**GACATAGCCAATCAAGGTGCCC
	Alanine	Forward	CCTTGATTGGCTATGTC**GCC**AGCCTGGGCCAGTTCC
		Reverse	GGAACTGGCCCAGGCT**GGC**GACATAGCCAATCAAGG
Asparagine 439	Glutamine	Forward	GTCTGGCTGCCTCCTTC**CAG**TGCATCTTCCTGTATAC
		Reverse	GTATACAGGAAGATGCA**CTG**GAAGGAGGCAGCCAGAC
	Alanine	Forward	TGTCTGGCTGCCTCCTTC**GCC**TGCATCTTCCTGTATAC
		Reverse	GTATACAGGAAGATGCA**GGC**GAAGGAGGCAGCCAGACA
Arginine 466	Lysine	Forward	GGCAGCACCATGGCC**AAG**GTGGGCAGCATCGTG
		Reverse	CACGATGCTGCCCAC**CTT**GGCCATGGTGCTGCC
	Alanine	Forward	CAGCACCATGGCC**GCA**GTGGGCAGCATC
		Reverse	GATGCTGCCCAC**TGC**GGCCATGGTGCTG

Position indicates native amino acid; Substitution indicates change (conservative or non-conservative) based on properties of amino acid position. Codon string for altered amino acid residue is indicated in bold within primer sequence.

Transformation – Dpn1 treated plasmids were incubated with XL10-Gold Ultracompetent Cells (Agilent Technologies, Santa Clara, CA). Preheated NZY+ Broth was added after heat-pulsing ultracompetent cells at 42˚C for 30 sec, followed by incubation at 37°C for one hr with constant shaking (225RPM). After incubation, 50, 100, and 200µL aliquots of cells were spread onto three separate LB agar plates containing 100 µg/mL ampicillin, adding a 200µL pool of NZY+ Broth for volumes less than 100µL to optimize spreading. Plates were incubated at 37°C for 16 hrs to allow adequate time for colony growth. Individual colonies were selected and grown in separate tubes containing 8mL NZY+ Broth and 100 µg/mL ampicillin, followed by overnight incubation at 37°C with constant shaking.

Plasmid preparation – Mini or midi-plasmid preparations were performed following manufacturer's protocol [18] (QIAGEN, Germantown, MD). Briefly, pelleted bacterial cultures were resuspended, lysed, neutralized, centrifuged at 13,000RPM for 10 min and supernatants transferred to supplied spin columns. After binding of plasmid DNA, columns were thoroughly washed prior to final DNA elution. Plasmid DNA concentration was determined using UV-Vis Spectroscopy.

Sequencing – Generated hOAT1 mutants were confirmed by DNA sequencing. Samples were sent with respective oligonucleotide sequencing primers (Table 2.2) for Sanger sequencing (Genewiz, South Plainfield, NJ). Sequencing files provided through Genewiz were compared to full length hOAT1 WT plasmid to ensure proper mutations were achieved.

Table 2.2 Oligonucleotide primers used for hOAT1 DNA sequencing

Primer	Primer Sequence (5' to 3')
hOAT1 Forward 1	CCCATCTACCATCGTGACTG
hOAT1 Forward 2	AGTCTGCAGAAGGAGCTGAC
hOAT1 Reverse 1	CATTGAGCAGGATGCAGATG
hOAT1 Reverse 2	AAGTTGGGTGCGAAGGCTGC

Cell Culture – CHO control, CHO-hOAT1 WT, and CHO-hOAT1 mutant cell lines were maintained at 37°C with 5% CO_2 in Dulbecco's Modified Eagle/Ham's F-12 Medium (DMEM/F12) containing 10% FBS, 1% Penicillin-Streptomycin (Pen-Strep) (Gibco-Invitrogen, Grand Island, NY) and 0.250 mg/mL G418. Once cells reached 80-90% confluency, passaging was performed. Briefly, the media was removed, cells were washed with 1x phosphate buffered saline (PBS), followed by cell dissociation using 0.25% Trypsin-EDTA (Gibco-Invitrogen, Grand Island, NY). Dislodged cells were resuspended in medium and passaged to a separate flask containing DMEM/F12, 10% FBS, 1% Pen-Strep, and 0.250 mg/mL G418. Cells were sub-cultured every three to four days and passages numbered 4 through 20 were used for experiments.

Transfection – CHO cells were grown in antibiotic-free DMEM/F12 (Gibco-Invitrogen, Grand Island, NY) with 10% Fetal Bovine Serum (FBS) at 37°C in 5% CO_2 until reaching 60 to 80% confluency. Stable transfections were performed according to the Lipofectamine® 2000 Reagent protocol [19]. One day before transfection, 7.0×10^4 CHO cells were seeded into 12-well tissue culture plates. On the day of transfection, Lipofectamine® 2000 (4µL) and OptiMEM medium (96µL) per transfection were incubated together for 5 min at room temperature. Plasmid DNA (1µg) was added to 100µL OptiMEM medium, combined with previous Lipofectamine® 2000/OptiMEM mixture, then incubated for 20 min at room temperature. After adding a fresh 1mL of medium to each well, the Lipofectamine® 2000/plasmid DNA/OptiMEM mixture (200µL) was added to each well and mixed gently. Cells were then incubated at 37°C for 24 to 48 hrs, followed by multiple weeks of antibiotic selection using 1 mg/mL Geneticin (G418) (Gibco-Invitrogen, Grand Island, NY).

Accumulation Assay – The procedure for cell accumulation assay has been described previously [20,21]. In summary, 2.5 x 10^5 cells were seeded with antibiotic-free culture medium in 24-well tissue culture plates 48 hrs before the experiment. The culture medium was removed and the cells were washed with 500µL transport buffer (TB) for 10 min. Cells were treated with 400µL TB containing 5µM PAH spiked with radiolabeled PAH (0.25 µCi/mL [^{3}H]PAH) in the absence or presence of the inhibitor probenecid (500µM) for 10 min. The treatment was removed, and the cells were rinsed three times with ice-cold TB. Cells were lysed in 200µL 1M NaOH and shaken for two hrs at room temperature. Afterward, cells were neutralized with 250µL 1M HCl and 200µL 10mM 4-(2-hydroxyethyl)-1-piperazineethanesulfonic acid (HEPES). Liquid scintillation was conducted using 400µL of samples with 5mL Ecoscint H cocktail (National Diagnostics, Atlanta, GA). Samples were normalized by protein content through Bradford protein assay using 10µL sample aliquots with 200µL protein assay dye (Bio-Rad Laboratories, CA). Screening data were reported as mean ± SD from triplicate samples.

Kinetic Analysis Assay – Michaelis-Menten constants (K_m) were determined for PAH uptake for active hOAT1 mutants through saturation analysis according to our previously published protocol [21]. In summary, 2.5 x 10^5 cells were seeded with antibiotic-free culture medium in 24-well tissue culture plates 48 hrs before the experiment. Culture medium was removed and the cells were washed with 500µL TB for 10 min. Cells were treated with 300µL TB containing increasing concentrations of PAH (1µM – 200µM; 0.25 µCi/mL [^{3}H]PAH) for one min. The treatment was removed and samples processed as described above for the accumulation assay. Data were plotted and analyzed by non-linear regression to generate K_m estimates (GraphPad v8.3.0).

Kinetic data was reported as mean ± SD from triplicate samples. Final K_m estimates were reported as mean ± SE from a minimum of three separate experiments

Verification of Genomic Integration – Cells were suspended in 500µL of lysis buffer (1 M Tris (pH 8.0), 5 M NaCl, 0.5 M EDTA, 10% SDS, and 0.4 mg/mL proteinase K) and incubated at 55°C overnight while shaking at 200RPM. The following day, genomic DNA was extracted using an equal volume of phenol/chloroform/isoamyl alcohol (25:24:1) and shaking for 10 min. Samples were centrifuged for 10 min at 15,000RPM in a table-top microcentrifuge. The upper aqueous phase was collected, mixed with an equal amount of isopropyl alcohol, and spun for an additional 15 min to obtain a DNA pellet. The pellet was rinsed with 70% ethanol, air-dried, and re-suspended in 200µL TE buffer (pH 8.0) containing 10mM Tris and 1mM EDTA. DNA concentration was determined using UV-Vis Spectroscopy. Genomic DNA ranging from 150 to 1,000ng, 2x GoTaq Green Master Mix (25µL), and 2.5µL primer pair mix (100µM T7: 5' – TAATACGACTCACTATAGGG – 3'; 100µM hOAT1Rev1: 5' – CATTGAGCAGGATGCAGATG – 3') were added to a final volume of 50µL and run in a thermocycler under the following conditions: denature at 95°C for two min, 30 cycles of denaturation at 95°C for 30 sec, annealing at 48°C for 30 sec, elongation at 72°C for one min. Final elongation proceeded at 72°C for five min, then samples were held at 4°C. PCR products were loaded onto a 1% agarose gel for separation using electrophoresis at 120V for one hr. Gel was stained in ethidium bromide (EtBr) for 10 min and visualized using a ChemiDoc Touch Imaging System (Bio-Rad Laboratories, Hercules, CA).

Western Blotting – COS7 cells expressing hOAT1 c-Myc were generously provided by Dr. Guofeng You (Rutgers University, Piscataway, NJ). Total COS7 hOAT1 cytosolic and plasma membrane fractions were isolated from COS7 hOAT1 c-Myc and CHO parent cell lines using a plasma membrane protein extraction kit (Abcam, Cambridge, United Kingdom). Briefly, approximately 5 x 10^7 cells were resuspended in homogenization buffer containing proteinase inhibitors and placed in a Dounce homogenizer. Cells were homogenized on ice for 10 min. Afterward, cell homogenates were spun at 700RPM for 10 min, then the supernatant was collected and transferred. The supernatant was spun at 10,000RPM for 30 min. Afterward, the supernatant was collected (cytosolic fraction) and the pellet, which contained total membrane protein, was resuspended in equal parts upper and lower phase. The resuspended pellet was spun at 3500RPM, and the upper phase was collected. Five volumes of diH_2O was added to the upper phase, then spun at 10,000RPM for 10 min. Afterward the pellet, which contained plasma membrane protein, was resuspended in radioimmunoprecipitation assay (RIPA) buffer containing proteinase inhibitors, then protein concentration was determined through a Bradford protein assay. Sodium dodecyl sulfate (SDS) loading buffer (5x) containing 2-mercaptoethanol was added to 60 µg protein samples. A Western blot gel was prepared consisting of both a 5% stacking gel portion (30% acrylamide, 1M Tris pH 6.8, 10% SDS, 10% APS, TEMED) and a 10% running gel portion (30% acrylamide, 1.5M Tris pH 8.7, 10% SDS, 10% APS, and TEMED). Samples were heated for one hr at 50°C then loaded onto the prepared gel submerged in 1x glycine running buffer. Electrophoresis was performed in two steps: 90V for 20 min, followed by 150V for one hr. Afterward, the gel was washed with diH_2O, then rinsed in 1x transfer buffer (glycine, Tris,

methanol) and transferred to polyvinylidene difluoride (PVDF) membrane. The transfer stage was run at 100mA for one hr with constant stirring. Afterward, the process was continued using the Immun-Blot goat anti-rabbit IgG (H + L) AP Assay Kit. The PVDF membrane was blocked with 3% gelatin in 1x TBS for one hr with constant shaking. The block was removed and the membrane was incubated with rabbit anti c-Myc antibody (1:500) overnight at 4°C. The next day, the primary antibody was removed and the membrane was incubated with goat anti-rabbit IgG-AP secondary antibody conjugate for one hr, followed by three separate, five minute washes with 1xTBST, then a final wash in 1x TBS. Next, 50uL of both AP Color Reagent A and B containing nitro blue tetrazolium chloride/5-bromo-4-chloro-3-indolyl phosphate (NBT/BCIP) was added to AP color development buffer, then the solution was added to the PVDF membrane until bands were visualized. The NBT/BCIP wash was removed and the membrane was submerged in diH_2O for 10 min. In addition, the membrane was probed for β-actin (goat anti-actin IgG (1:1000), donkey anti-goat IgG-AP (1:5000)) as a loading control.

hOAT1 Green Fluorescent Protein (GFP) Plasmid: Transfection & Microscopy – A hOAT1-GFP fusion protein expression construct was synthesized by GenScript (Piscataway, NJ) and confirmed by DNA sequencing. In summary, the coding region for hOAT1 was ligated into the pEGFP-C3 plasmid (Invitrogen, Carlsbad, CA) in-frame with the carboxyl terminal end of GFP using restriction enzymes KpnI/BamHI (Figure 2.3). The pEGFP-C3-hOAT1 plasmid was transformed into DH5-α cells, and plasmid DNA was extracted through use of a QIAprep miniprep kit. The hOAT1-GFP plasmid was transiently transfected into CHO cells (1.0 μg hOAT1-GFP plasmid DNA, incubated at 37°C for 24 hr) seeded onto glass coverslips. After 24 hrs, the medium was

removed, and the cells were fixed using 4% paraformaldehyde in 1x PBS for 10 min. Coverslips were then washed thrice in 1x PBS, followed by 1 µg/mL DAPI solution for two min. The DAPI was removed, the coverslips were washed twice in 1x PBS, once in diH_2O, and mounted onto a microscope slide using DPX Mountant. Fluorescence images were taken using an OLYMPUS IX51 microscope containing an X-Cite series 120 fluorescence lamp illuminator. Images were collected through use of an OLYMPUS XC30 digital color camera. Images were processed using both OLYMPUS cellSens Entry and ImageJ [22].

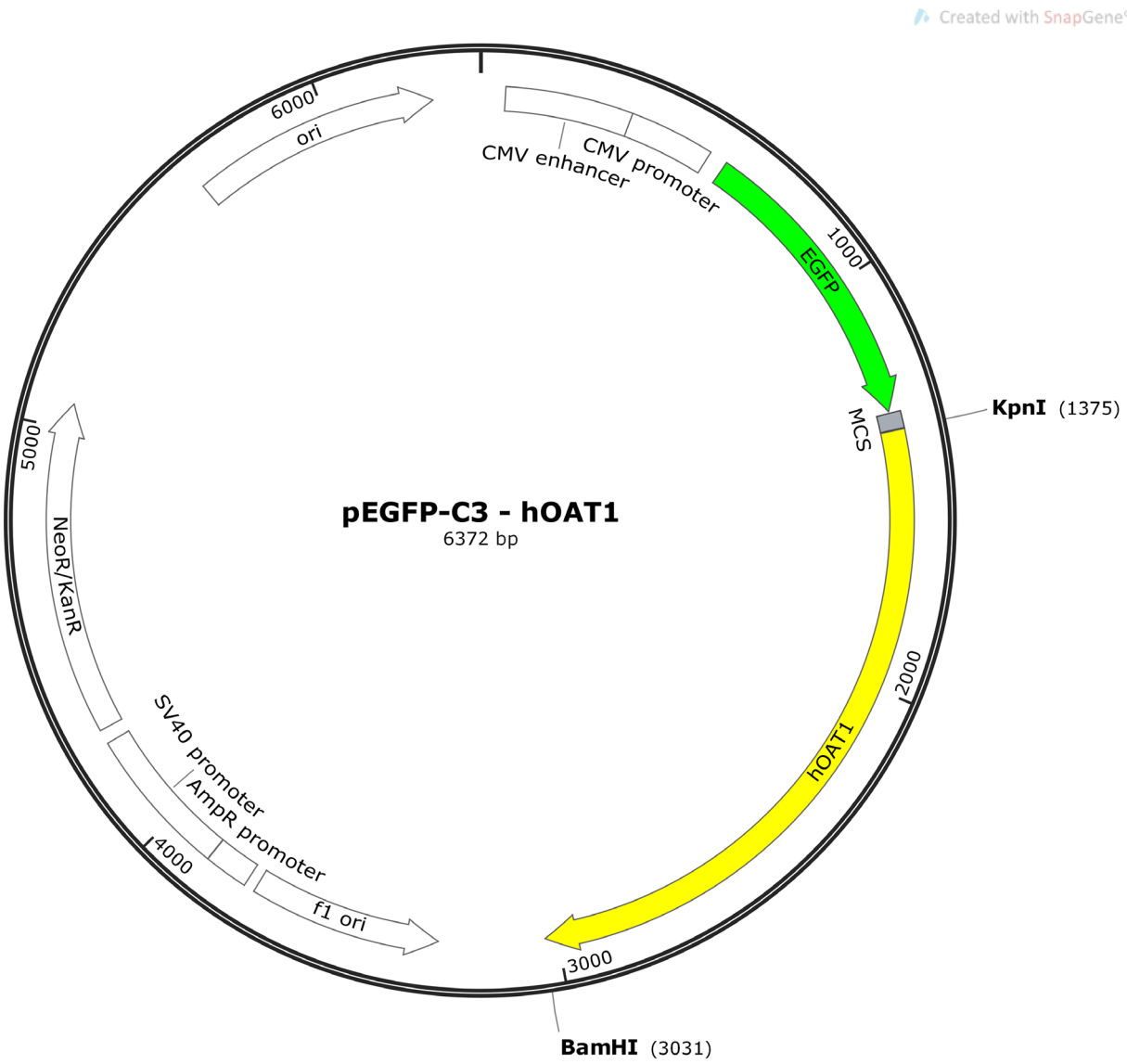

Figure 2.3 Plasmid Map of pEGFP-hOAT1

Full length hOAT1 sequence was ligated into a pEGFP-C3 plasmid using KpnI/BamHI restriction enzyme sites. Location of hOAT1 insert is highlighted in yellow and EGFP feature is highlighted in green. Image generated using SnapGene.

hOAT1 c-Myc Plasmid: Transfection & Microscopy – CHO cells were transfected with 1.0 µg hOAT1 c-Myc plasmid DNA and were incubated at 37°C for 24 hrs. After 24 hrs, the media was removed, and the cells fixed using 4% paraformaldehyde in 1x PBS for 10 min followed by permeabilization in 0.2% Tween 20 for 20 min. Coverslips were then washed thrice with 1x PBS, followed by antigen retrieval. Coverslips were added to a beaker containing 100°C sodium citrate buffer (pH 6.0) for 20 min, followed by cold diH2O for 10 min. Coverslips were then blocked with 1% BSA in 1x PBS for 2 hrs at room temperature. Anti c-Myc primary antibody was diluted with 1% BSA in TBST (1:100) and the coverslips were incubated overnight at 4°C. Primary antibody was removed, the coverslips were washed thrice in 1x PBS, followed by incubation with FITC labeled secondary antibody diluted in 1% BSA in TBST (1:100) for one hr at room temperature. Secondary antibody was removed and coverslips were processed as described above for hOAT1-GFP transfection and microscopy.

Cell Sorting – Due to the presence of antibiotic-resistant CHO cells with limited hOAT1-mediated transport, cells were sorted using a fluorescent substrate for hOAT1, fluorescein, using a BD FACSCanto II system. CHO parent cells (control) were incubated with 5µM fluorescein for 15 min then washed thrice in ice-cold TB containing 500µM probenecid. The cells were added after their final wash to the instrument to set the calibration curve. For the experimental conditions, multiple flasks of CHO hOAT1 WT or active mutants (Arg15Lys, Ile19Leu, Tyr230Phe) were separately incubated with 5µM fluorescein for 15 min, washed thrice in ice-cold TB containing 500µM probenecid, and maintained in the final wash before sorting. Experimental conditions were sterilely sorted based on FITC intensity, with the cells exhibiting the strongest fluorescence activity (top

5%) collected and transferred to a fresh flask containing DMEM/F12 with 10% FBS, 1% Pen Strep, and 0.250 mg/mL G418.

Mycoplasma Testing – All cell lines were tested for the presence of mycoplasma using a Universal Mycoplasma Detection Kit (ATCC, Manassas, VA). Briefly, adherent cells were harvested and resuspended in lysis buffer, heated at 95°C, then spun at 13,000RPM for five min. Supernatants were collected, followed by the addition of Universal PCR mix plus Universal Primers supplied through the kit, with the appropriate positive and negative controls. Following the PCR amplification procedure, a 3% agarose gel was prepared, and 10µL of PCR products were loaded. The gel was stained using EtBr, washed thrice in diH_2O, then observed under UV illumination. No instances of mycoplasma were detected in any generated CHO hOAT1 expressing cell lines (Figure 2.4).

Statistics – Data are plotted as mean ± SD for initial screening assay and individual saturation assays. Final K_m estimates are reported as mean ± SE. Statistical analysis was performed using GraphPad Prism v8.3.0 and R 3.6.0. Equal variance, one-way ANOVA with post-hoc Dunnett's multiple comparisons was used to evaluate differences compared to a single control where indicated. All differences were considered statistically significant if $p < 0.05$.

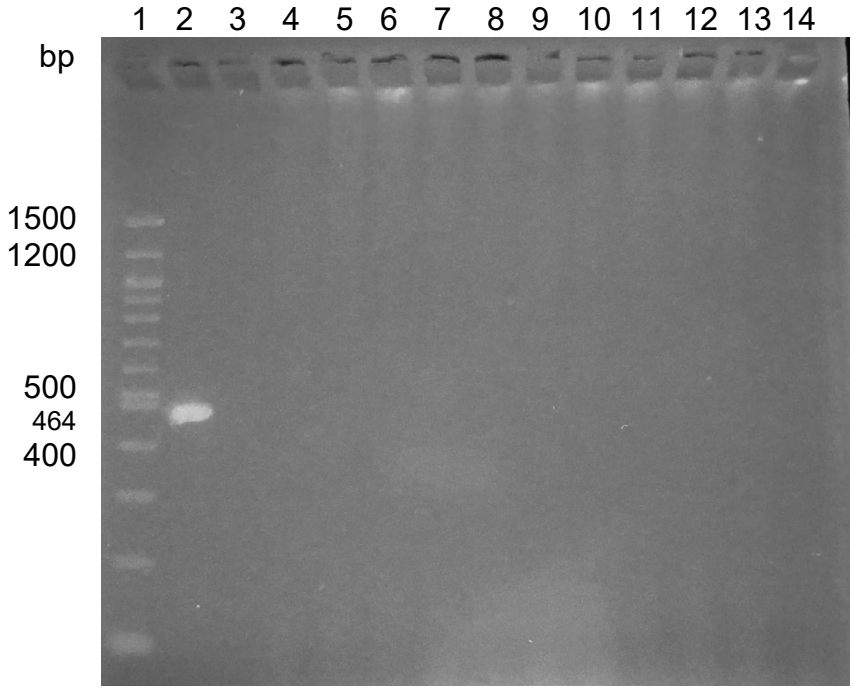

Figure 2.4 Mycoplasma Testing of Generated CHO cell lines

Mycoplasma testing of CHO hOAT1 cell lines along with parental CHO cells is shown. 10µL aliquots were loaded for 100bp DNA ladder, positive control, negative control, and CHO cell lines. Mycoplasma was detected for positive control only (Lane 2, 464bp). Lanes are as follows: (1) 100bp Ladder, (2) Positive Control, (3) Negative Control, (4) hOAT1 WT, (5) CHO Parent, (6) hOAT1 Arg15Lys, (7) hOAT1 Arg15Ala, (8) hOAT1 Ile19Leu, (9) hOAT1 Ile19Ala, (10) hOAT1 Tyr230Phe, (11) hOAT1 Tyr230Ala, (12) hOAT1 Asn439Gln, (13) hOAT1 Asn439Ala, (14) hOAT1 Arg466Ala.

2C. RESULTS

Comparative Modeling of hOAT1

An initial Basic Local Alignment Search Tool (BLAST) search of the non-redundant protein sequences database was performed using hOAT1 as the target to identify a suitable template for homology modeling. Search results indicated the peptide sequence of the recently crystallized protein, PiPT, shares 33% sequence similarity and 19% sequence identity with hOAT1, signifying PiPT as a more appropriate template than previously utilized GlpT (PDB ID: 1PW4), which shares 27% similarity and 16% identity with hOAT1. In addition to higher similarity and identity, PiPT offers further advantages as a template molecule such as also being a eukaryotic protein, inclusion in the major facilitator superfamily (MFS), a 12 TMD structure divided into two domains, and being crystallized in the occluded state therein maximizing the interaction within the compound-transporter complex. Thus, PiPT was selected to serve as the template.

Both PiPT and hOAT1 are predicted to have large sequence loops between TMDs 1 & 2 and 6 & 7. Due to their flexibility, these loops are not resolved in the PiPT crystal structure, thus there are no corresponding residues to model. Therefore, before alignment of hOAT1 and PiPT peptide sequences, the hOAT1 sequence (UniProtKB ID: Q4U2R8) was truncated from Ile44 – Ser129 (between TMDs 1 & 2) and Ser277 – Leu329 (between TMDs 6 & 7). The final sequence alignment is shown in Figure 2.5, showing the TMDs for PiPT (white) and hOAT1 (yellow) as well as exact positioned identities (white letters). This alignment file was fed into MODELLER, generating 100 separate *in silico* homology models for hOAT1.

Next, docking studies were conducted using GOLD v5.4 where the energy minimized PAH structure was docked into each model separately, ten times, generating a total of 1,000 different combinations between hOAT1 and PAH. To determine the top hOAT1-PAH combination, models were ranked through evaluation of their DOPE and GOLD scores as well as cluster analysis. As shown in Table 2.3, the top hOAT1 model was number 4 with PAH pose number 45. Overall, this combination had the highest GOLD score (65.30), the second-highest DOPE score (-45539.37), and the same number of clusters (1) as the top four GOLD ranked solutions reported. To further evaluate hOAT1 model 4, a Ramachandran plot was generated using the program PROCHECK v9.17 allowing visualization of all bond angles. Favorable bond angles appear in the red and yellow regions whereas disallowed angles are located in the white areas (Figure 2.6). Only three residues, Ser160, Ala331, and Tyr334, were identified as forming disallowed bond angles in this model. These residues are positioned on the outskirts of the *in silico* model, i.e. well outside the putative PAH binding domain, and thus likely exert no direct influence on the hOAT1-PAH binding complex in this model. It was also of interest to visualize all top PAH solutions docked, to better validate the top model chosen (Figure 2.7). The top PAH pose is displayed as a space-filling molecule to distinguish from all other PAH molecules docked. This molecule is positioned centrally within hOAT1, clustered amongst numerous additional PAH molecules that were separately docked. This provides further validation that the top PAH pose (45) is an appropriate representation of the GOLD docking results generated, in addition to providing further support to a clear single, centralized binding region. Thus, hOAT1 model 4 was selected as the best representation of hOAT1 in the occluded state with PAH (Figure 2.8). As

shown, the generated hOAT1 model has 12 predicted TMDs with intracellular amino and carboxyl termini, with multiple TMDs contributing to the binding pocket. PAH is represented with a space filling model while individual amino acids are represented with lines.

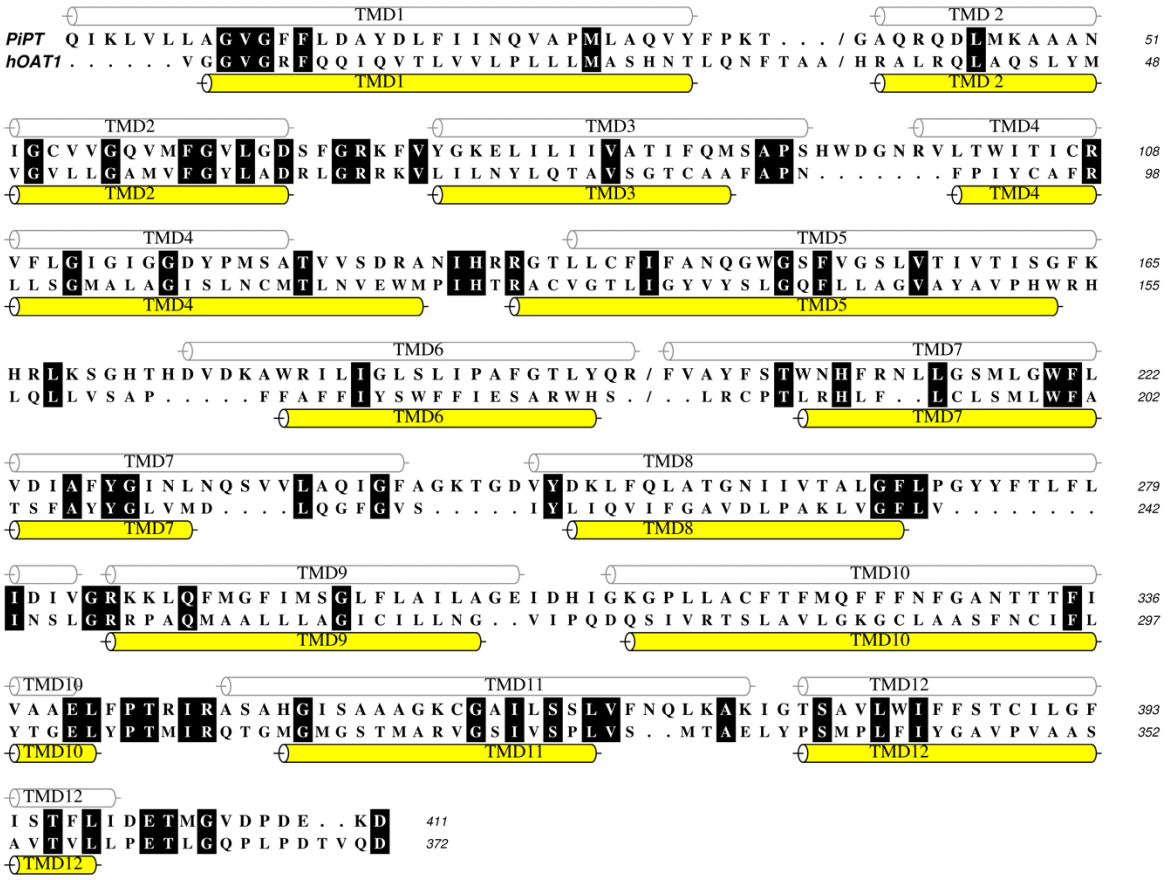

Figure 2.5 Peptide Sequence Alignment Between PiPT and hOAT1

Final peptide sequence alignment between PiPT (top) and hOAT1 (bottom). Transmembrane domain (TMD) regions for PiPT (white) documented and confirmed through crystallization of the protein. TMD regions for hOAT1 were initially predicted through PredictProtein v1 software, then regions were determined (yellow) upon final model generation. White letters indicate conserved amino acid residues between target and template. Image generated using the program ALINE v1.0.025.

Table 2.3 Summary of evaluative parameters and ranking for the top 15 hOAT1 models

GOLD Rank	GOLD Score	Model ID	Best hOAT1-PAH Pose	DOPE Score	# of Clusters
1	65.30	4	45	-45539.37	1
2	58.62	88	28	-45958.39	1
3	57.63	67	38	-45221.56	1
4	57.53	32	48	-45102.04	1
5	56.94	82	4	-44844.93	4
6	56.74	9	12	-45426.21	2
7	56.07	76	2	-45471.81	5
8	55.86	68	15	-45063.06	2
9	54.90	93	11	-44951.75	3
10	54.74	83	31	-45153.58	1
11	54.50	86	14	-45219.59	2
12	54.47	10	55	-45286.07	1
13	53.86	29	1	-45127.43	7
14	53.76	51	17	-45499.86	2
15	52.34	75	13	-45448.21	2

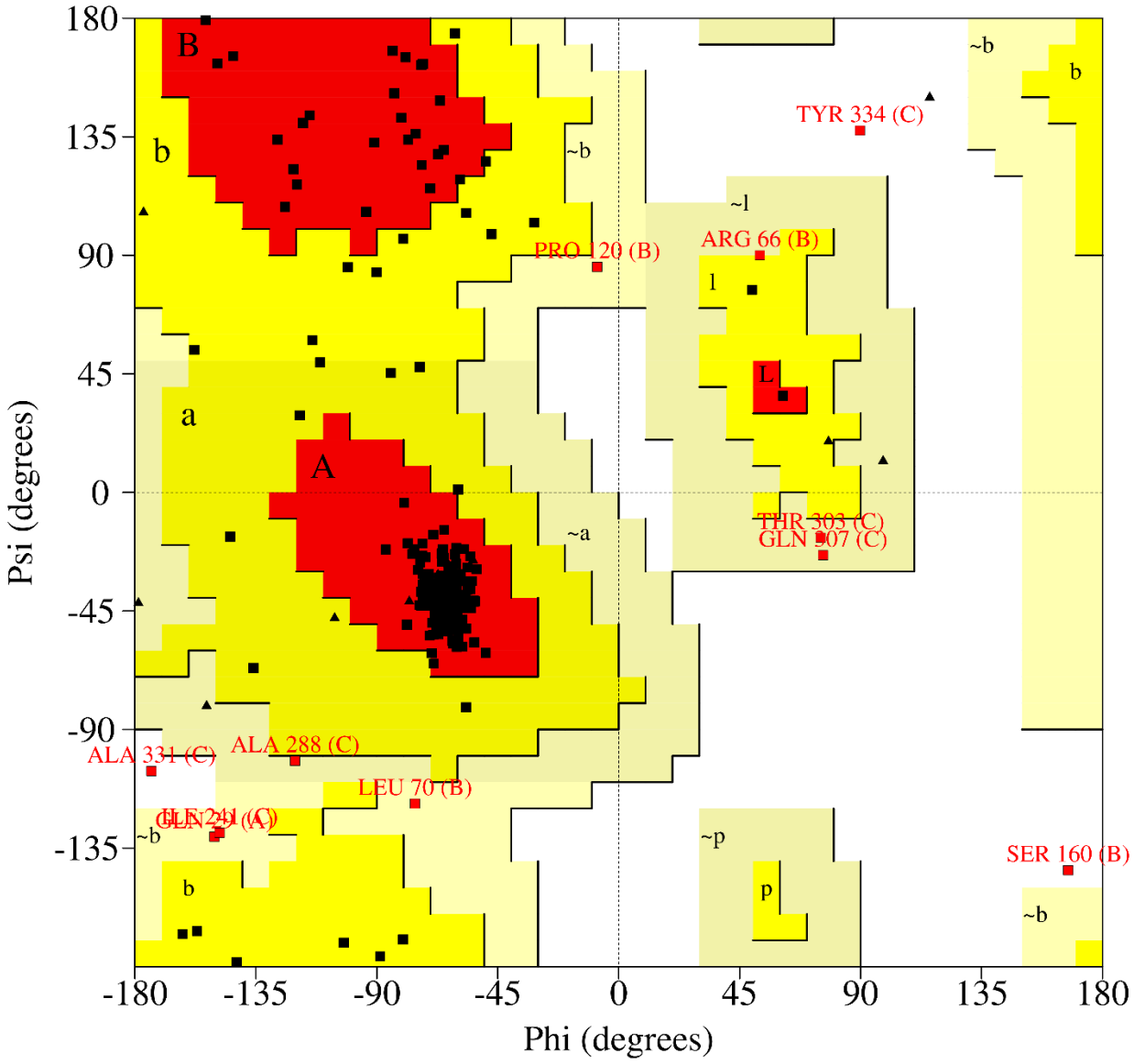

Figure 2.6 Ramachandran Plot of Top hOAT1 Homology Model

Axes indicate degree value of rotatable bonds present between neighboring amino acid residues with specific model generated. High percentage of amino acid residues were reported within favorable regions (99%), with remaining residues (SER160, TYR334, ALA331) in unfavorable regions. Plot generated using PROCHECK.

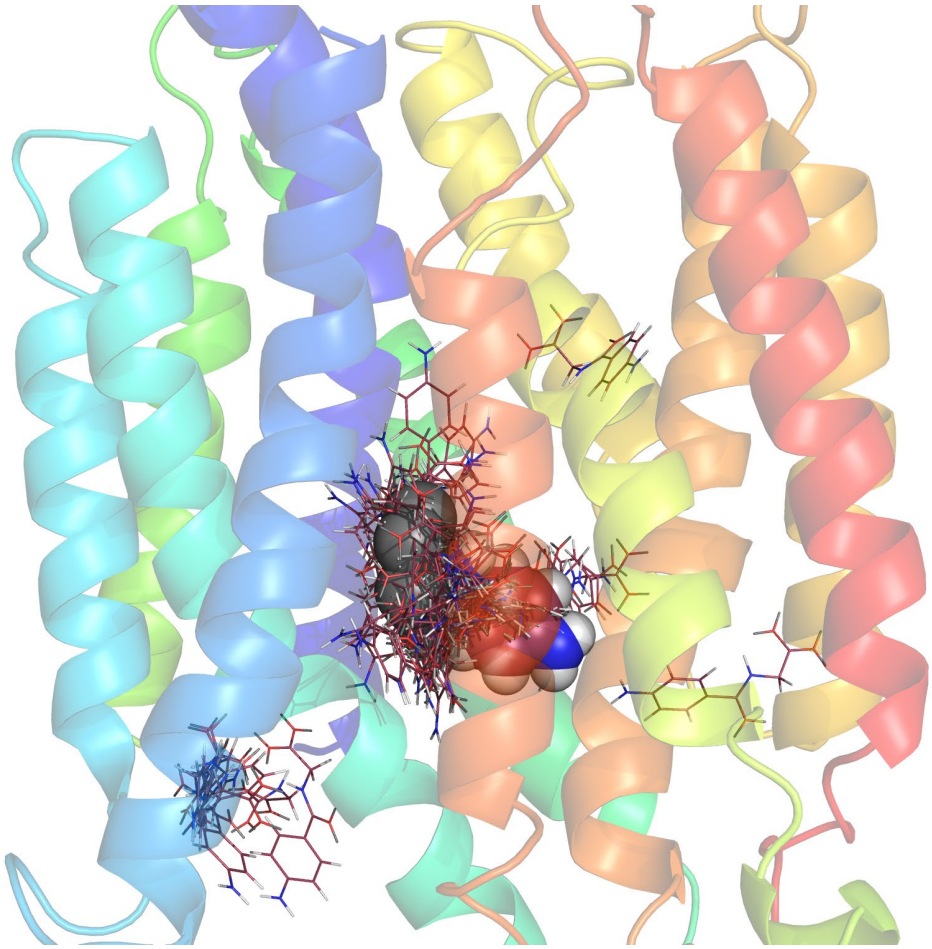

Figure 2.7 Summary of All PAH Docked Poses within hOAT1

The summary of all PAH locations upon successful GOLD docking studies. The PAH locations for all modeling studies are indicated as line molecules. The top PAH location (pose 45) is shown as a space-filling molecule. The multicolored helices represent the 12 TMD regions for hOAT1. Image file generated using PyMOL 1.8.

Using PyMOL v1.8, further analysis was focused within the suggested binding pocket to determine which amino acid contacts within the transporter are critical to PAH recognition (Figure 2.9 A & B). Five amino acids with potential PAH interactions were identified, specifically Arg15, Ile19, Tyr230, Asn439 and Arg466. The nature of the proposed interactions between each residue and PAH are summarized in Table 2.4. A hydrogen bond interaction was predicted for amino acids Arg15, Asn439 and Arg466. In addition, Ile19 was proposed to exhibit a hydrophobic interaction, and an edge-face aromatic interaction was identified for Tyr230. To directly examine these predicted amino acid – PAH interactions, conservative and non-conservative substitutions were introduced at each position and effects on transporter function examined *in vitro*.

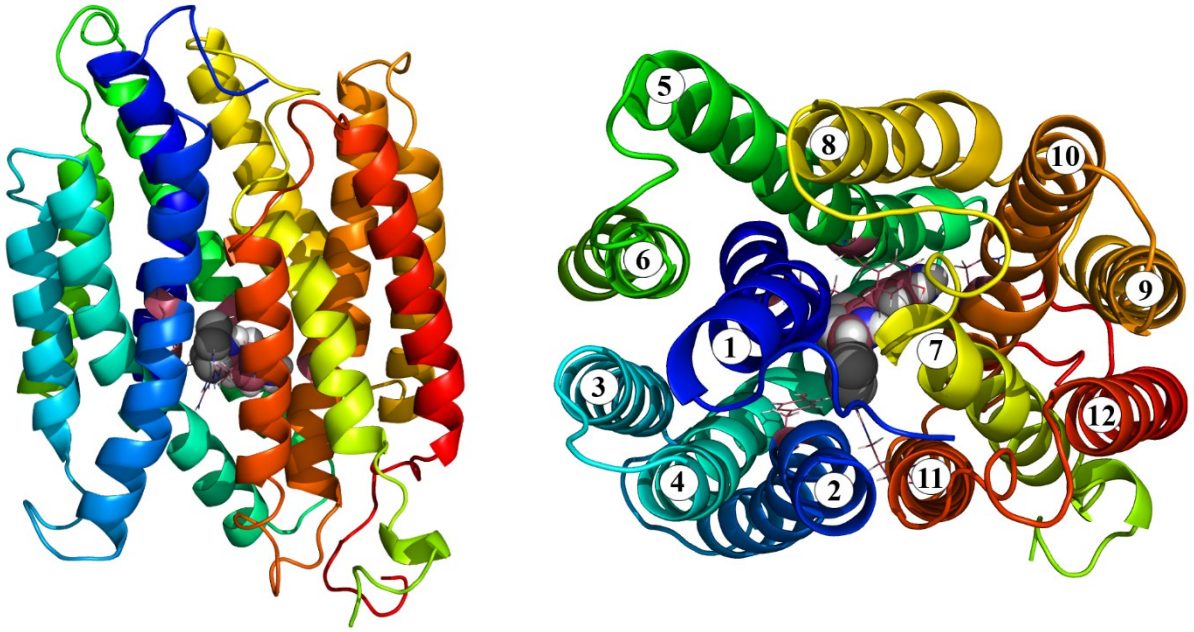

Figure 2.8 Three-Dimensional *in silico* hOAT1-PAH Model

Three-dimensional side view (left) and top view (right) of the generated hOAT1-PAH binding complex. The multicolored helices represent the 12 TMD regions for hOAT1 and are numbered in the top view. A space filling representation of PAH is shown with putative interacting amino acids indicated as line molecules. Image files generated using PyMOL 1.8.

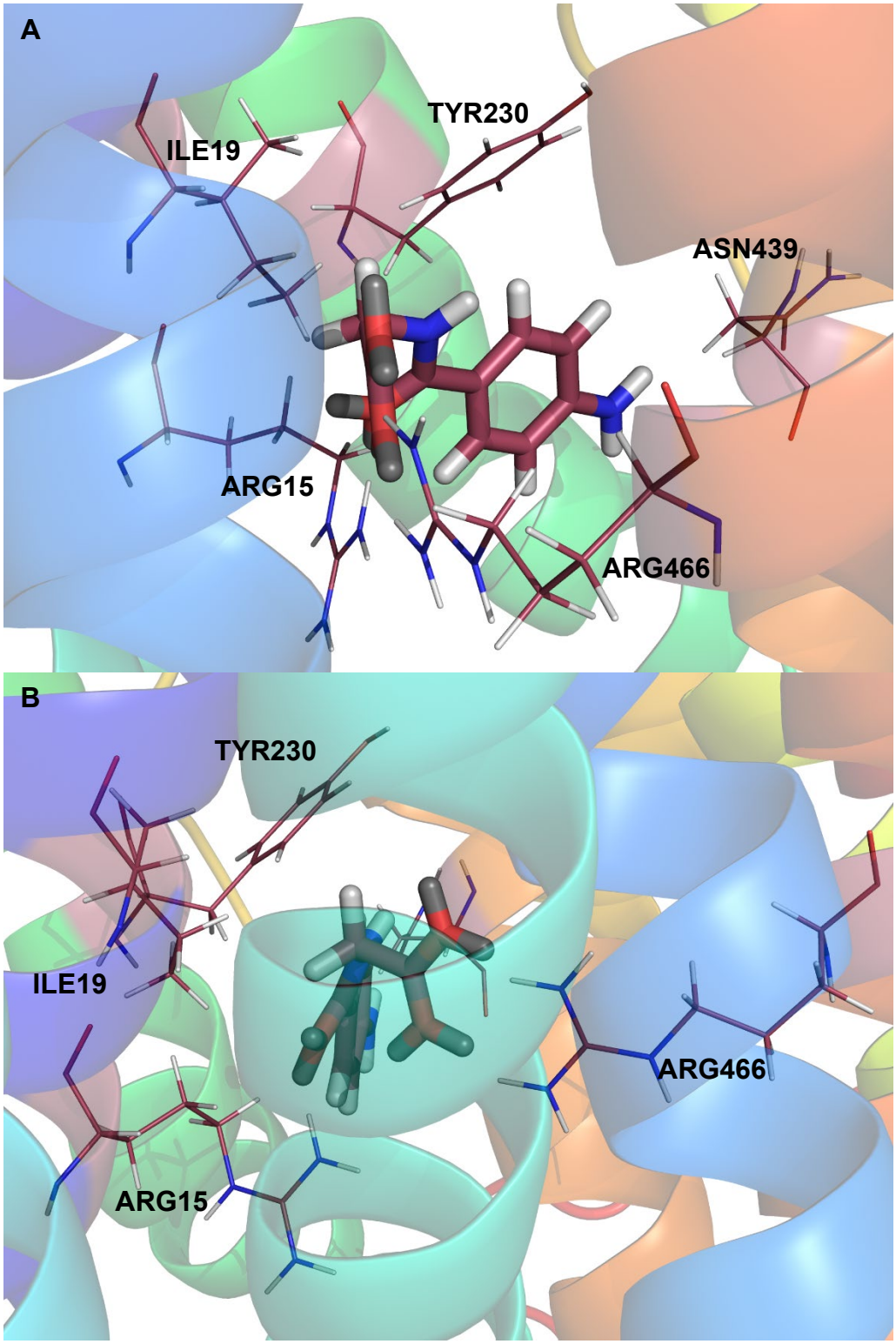

Figure 2.9 A & B Different Rotational Views of the hOAT1-PAH Binding Complex

The five amino acids predicted to be important for PAH binding and transport are indicated. Image files generated using PyMOL 1.8.

Table 2.4 Summary of putative PAH-hOAT1 complex forming amino acids, the predicted nature of each interaction and generated conservative and non-conservative hOAT1 mutations

TMD	Amino Acid	Interaction	Conservative	Non-conservative
1	Arg15	Hydrogen Bond	Lys	Ala
1	Ile19	Hydrophobic	Leu	Ala
5	Tyr230	Edge-Face Aromatic	Phe	Ala
10	Asn439	Hydrogen Bond	Gln	Ala
11	Arg466	Salt Bridge featuring Bidentate Hydrogen Bond	Lys	Ala

Interactions proposed are based on each amino acid's orientation with the docked substrate. Conservative and non-conservative substitutions were based on physiochemical properties of amino acids amongst additional supportive information [16].

In Vitro Testing

The identity of all hOAT1 mutant constructs was confirmed by DNA sequencing prior to functional examination. Representative chromatograms for both a hOAT1 conservative (Arg15Lys) and non-conservative (Arg15Ala) mutation are shown. In Figure 2.10 panel A the WT ‘CGC’ codon for arginine is clearly observed, while in panel B the codon has been mutated to ‘AAG’ which codes for lysine. Similarly, in Figure 2.11 it can be seen that the WT arginine codon has been altered to ‘GCC’ which codes for alanine. For undetermined reasons, the conservative substitution Arg466Lys could not be generated. Several attempts were made, however in each instance the mutagenesis primer sequence appeared in tandem thus significantly altering the hOAT1 coding sequence in the final construct. Further work involving this conservative substitution was discontinued. Confirmed mutant constructs were stably-transfected into CHO cells.

A

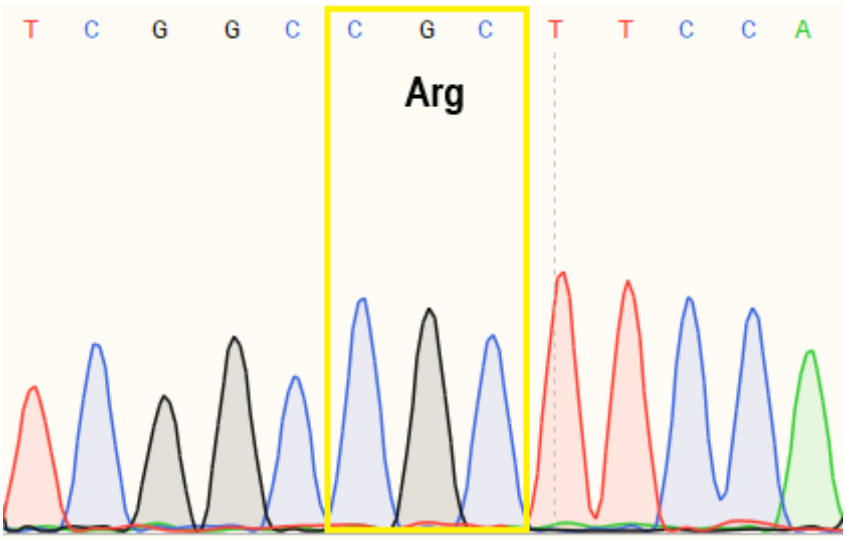

B

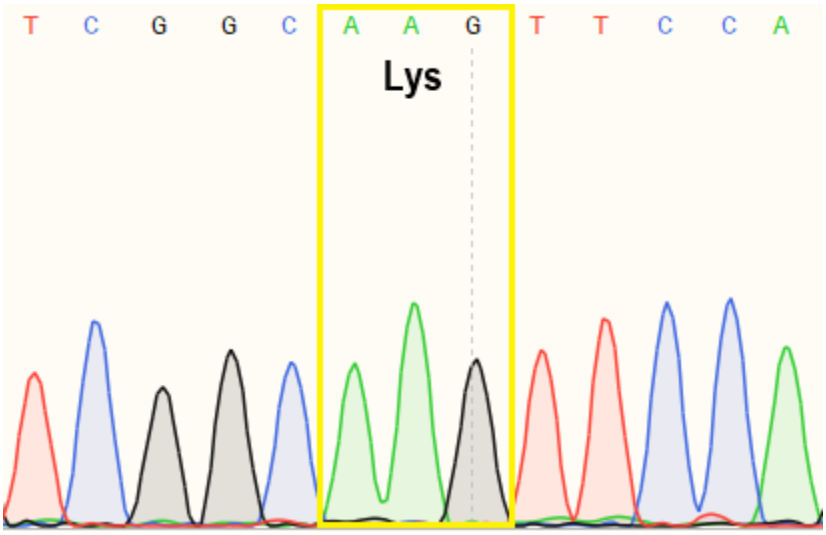

Figure 2.10 Representative Chromatogram for DNA Sequencing Confirmation of hOAT1 Conservative Mutants.

The chromatogram for hOAT1 WT (A) and hOAT1 Arg15Lys (B) sequence. The triplet codon region highlighted shows position of mutation. The three letter amino acid codon string is translated and displayed within the highlighted section. Image generated using SnapGene.

A

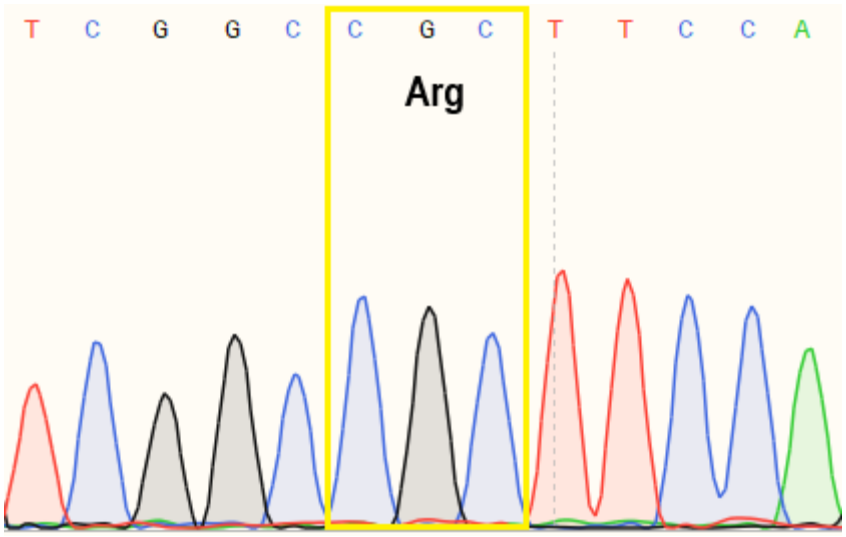

B

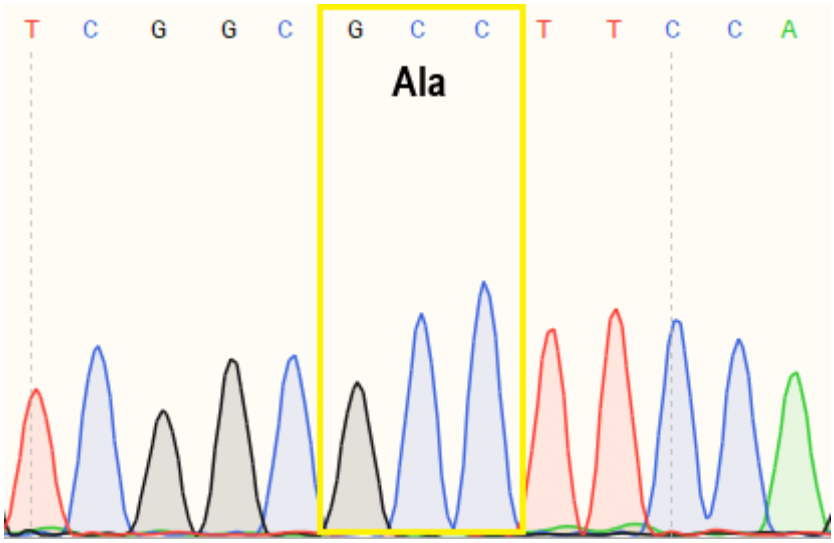

Figure 2.11 Representative Chromatogram for DNA Sequencing Confirmation of hOAT1 Non-conservative Mutants.

The chromatogram for hOAT1 WT (A) and hOAT1 Arg15Ala (B) sequence. The triplet codon region highlighted shows position of mutation. The three letter amino acid codon string is translated and displayed within the highlighted section. Image generated using SnapGene.

After establishing stably-expressing WT and mutated hOAT1 cell lines, initial accumulation assays were performed to quantify PAH transport activity. Cells were exposed to PAH (5μM) in the absence or presence of the inhibitor probenecid (Figure 2.12). As shown, hOAT1 WT cells showed marked accumulation of PAH (~55 fold) compared to CHO parental cells (275.6 ± 21.8 vs. 5.4 ± 1.0 pmol/mg protein/10 min, respectively). The known hOAT1 inhibitor probenecid (500μM) showed virtually complete inhibition of hOAT1-mediated PAH uptake, as accumulation was comparable between probenecid exposed hOAT1 WT cells and CHO parental cells (6.0 ± 0.5 vs. 5.0 ± 0.2 pmol/mg protein/10 min, respectively). Cell accumulation assay demonstrated that conservative substitutions Arg15Lys (230.4 ± 22.0 pmol/mg protein/10 min), Ile19Leu (407.5 ± 29.1 pmol/mg protein/10 min), and Tyr230Phe (252.9 ± 36.3 pmol/mg protein/10 min) all retained PAH transport activity as compared to CHO parental cells. One conservative (Asn439Gln) and all non-conservative (Arg15Ala, Ile19Ala, Tyr230Ala, Asn439Ala, Arg466Ala) substitutions abolished PAH transport mediated by hOAT1. To determine if hOAT1 mutant cell lines were considered transport active or inactive, equal variance ANOVA with Dunnett's multiple comparisons between hOAT1 mutant cell lines and CHO parental background cells was performed. Three cell lines (Arg15Lys, Ile19Leu, Tyr230Phe) were found to be statistically different from CHO parent ($p < 0.0001$), indicating these three cell lines are transport active mutants. The remaining cell lines (Arg15Ala, Ile19Ala, Tyr230Ala, Asn439Gln, Asn439Ala, Arg466Ala) were not statistically different from the parent ($p > 0.05$) and were thus treated as inactive mutants.

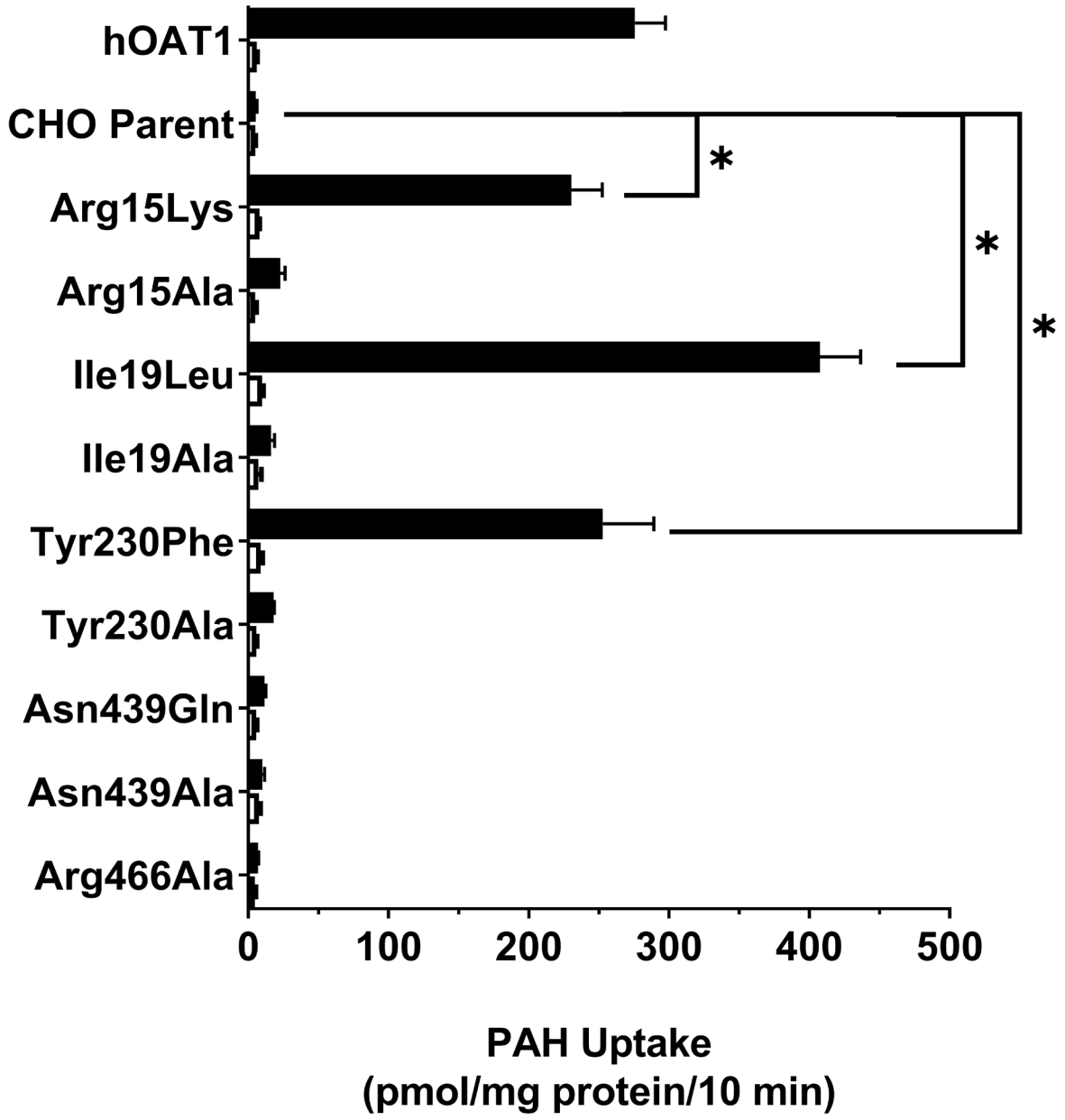

Figure 2.12 Initial PAH Transport Activity Assay Assessment of hOAT1 Mutants

Initial accumulation assay with 5μM PAH in the absence (black) and presence (white) of 500μM probenecid. Y-axis labels indicate the hOAT1 protein expressed in the stable cell line tested including hOAT1 WT (hOAT1), parental background (CHO Parent), and the generated conservative and non-conservative hOAT1 mutants. Accumulation was performed over a 10 min period and corrected by protein content. Values reported as mean ± SD of triplicate samples. Significance indicated by $*p < 0.0001$ as determined by one-way ANOVA followed by Dunnett's t-test in comparison to CHO Parent without probenecid.

For the active hOAT1 mutant cell lines, further kinetic analysis was conducted to determine if mutant cells exhibited changes in PAH affinity (K_m) as compared to hOAT1 WT. Cells were exposed to increasing concentrations of PAH (1μM – 200μM) for one minute and representative plots are shown in Figure 2.13. All constructs exhibited saturable transport activity and final K_m estimates are summarized in Table 2.5. As shown in Table 2.5, the hOAT1 mutants Arg15Lys and Tyr230Phe had reduced K_m estimates for PAH (16.1 ± 1.9 and 20.1 ± 3.5 μM, respectively), but the reductions were not significant at the $p < 0.05$ level. The Ile19Leu mutant (26.8 ± 3.6 μM) had virtually an unchanged K_m estimate as compared to hOAT1 WT (26.1 ± 2.1 μM).

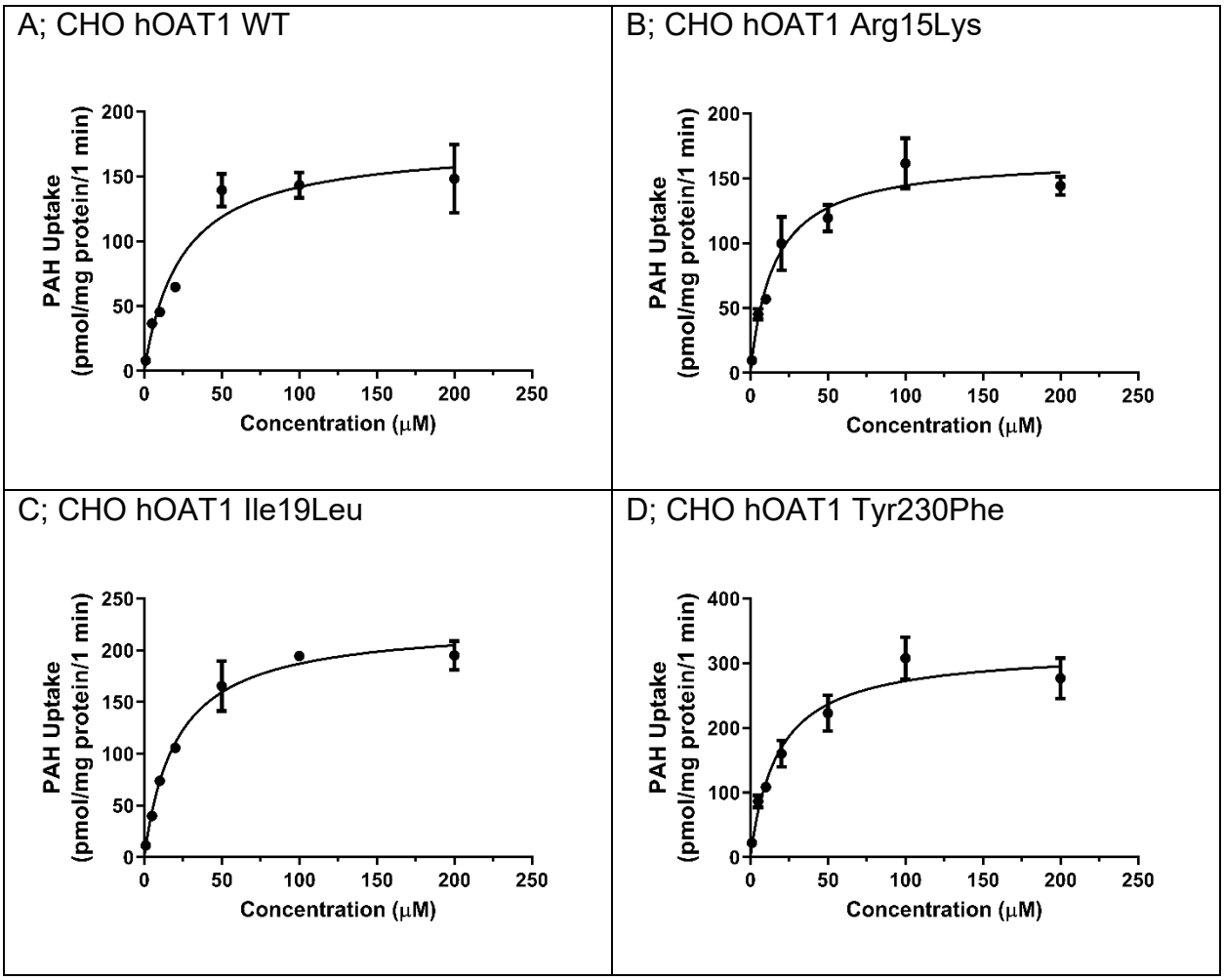

Figure 2.13 Saturation Analysis Conducted for hOAT1 WT and Active Mutants

One minute uptake of increasing concentrations of PAH (1μM – 200μM) spiked with [^{3}H]PAH (0.25 μCi/mL) in (A) CHO hOAT1 WT, (B) CHO hOAT1 Arg15Lys, (C) CHO hOAT1 Ile19Leu, and (D) CHO hOAT1 Tyr230Phe cell lines. Data were corrected for background measured in CHO Parent control cells. K_m values were determined using Michaelis-Menten nonlinear regression using GraphPad Prism. Experiments within each cell line were repeated a minimum of three times in triplicate with final K_m estimates reported as mean ± SE. Each panel consists of a representative curve, with values plotted as mean ± SD.

Table 2.5 Estimated K_m for hOAT1 WT and hOAT1 active mutants

Transporter	K_m (μM)	N
hOAT1 WT	26.1 ± 2.1	3
hOAT1 Arg15Lys	16.1 ± 1.9	4
hOAT1 Ile19Leu	26.8 ± 3.6	3
hOAT1 Tyr230Phe	20.1 ± 3.5	5

Values are reported as mean ± SE.

Genomic Integration of hOAT1 Mutant Constructs

To confirm successful transfections of transport inactive cell lines, genomic DNA from each transfected cell line was isolated and used as template for PCR. Primers consisted of the plasmid sequence specific T7 primer and the hOAT1 reverse 1 sequencing primer (Table 2.2) which should yield full length (~2,000bp) amplification of the hOAT1 insert. As shown in Figure 2.14, the expected product band was detected in every instance, except for non-transfected CHO Parent negative control (lane 2), confirming successful genome integration of all constructs during transfection.

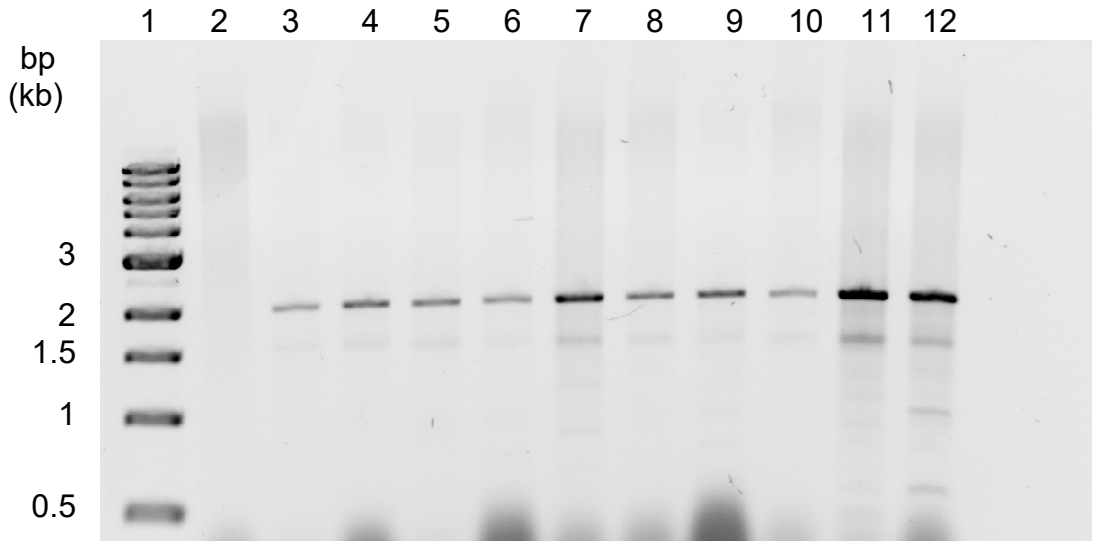

Figure 2.14 Confirmation of Construct Integration into Genomic DNA

Confirmation of successful genomic integration of mutant hOAT1 constructs. Lanes are as follows: (1) 1kb Ladder, (2) CHO Parent, (3) hOAT1 WT, (4) hOAT1 Arg15Lys, (5) hOAT1 Arg15Ala, (6) hOAT1 Ile19Leu, (7) hOAT1 Ile19Ala, (8) hOAT1 Tyr230Phe, (9) hOAT1 Tyr230Ala, (10) hOAT1 Asn439Gln, (11) hOAT1 Asn439Ala, (12) hOAT1 Arg466Ala.

Membrane Targeting of Inactive Mutants

Upon completion of the initial accumulation assay with PAH, six hOAT1 mutant cell lines (Arg15Ala, Ile19Ala, Tyr230Ala, Asn439Gln, Asn439Ala, Arg466Ala) failed to demonstrate PAH transport when compared to CHO parent. To initially investigate the translation and membrane targeting for hOAT1, full length hOAT1 cDNA was ligated into vector pEGFP-C3, forming the hOAT1-GFP plasmid which expresses a GFP-hOAT1 fusion protein. CHO cells transiently transfected with hOAT1-GFP plasmid were imaged and representative micrographs are shown in Figure 2.15. Cells expressing hOAT1-GFP showed strong fluorescence, with lack of signal detected in the nucleus (Panels C & D). However, given the high cytoplasmic fluorescence, membrane specific targeting of the WT hOAT1 fusion protein could not be conclusively demonstrated or ruled out, thus this technique was not explored further with inactive mutants. Cells were stained and imaged for DAPI signal (Panels A & B) to ensure cell monolayer was confluent with attached cells. Control transfections (Lipofectamine only) showed no fluorescent signal (data not shown).

A; DAPI, 20x

B; DAPI, 40x

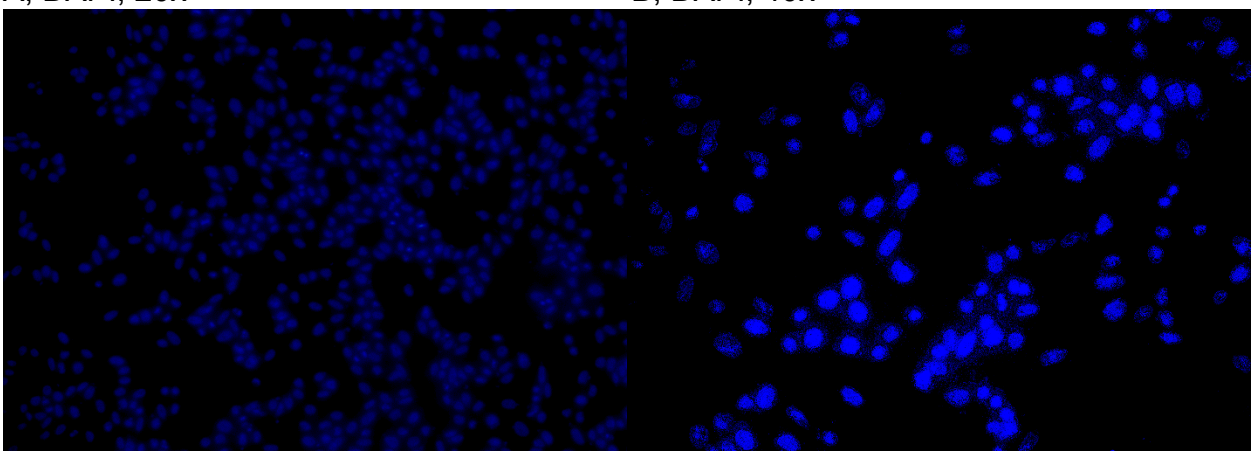

C; FITC, 40x

D; DAPI & FITC Merge, 40x

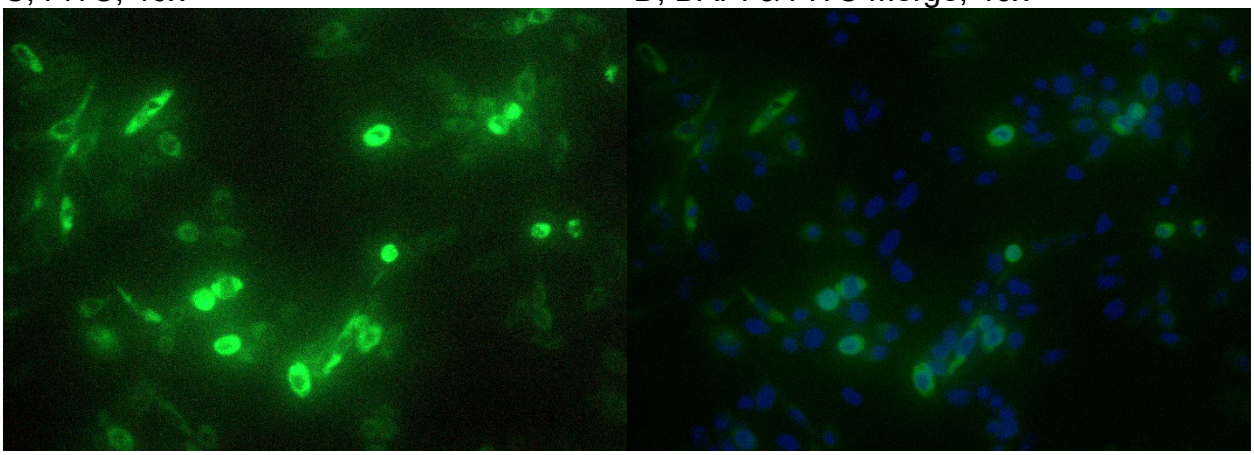

Figure 2.15 Expression Pattern of hOAT1-GFP

CHO cells transfected with pEGFP-C3/hOAT1 were fixed and mounted at 24 hrs post-transfection then viewed by fluorescence microscopy: (A) DAPI, 20x (B) DAPI, 40x (C) FITC, 40x and (D) DAPI & FITC Merge, 40x

As an alternative method for evaluating membrane targeting of non-functional hOAT1 mutants, use of an artificially c-Myc tagged hOAT1 construct was explored. CHO cells transiently transfected with hOAT1 c-Myc plasmid were imaged and representative micrographs are shown in Figure 2.16. The expression pattern of hOAT1 WT c-Myc showed strong nuclear fluorescence, with no detectable signal at the plasma membrane (Panel C). In addition, cells were stained for DAPI, which when merged with FITC signal, showed strong overlapping signal (Figure 2.16 Panel D), thus indicating endogenous c-Myc protein in the nucleus. Control transfections (lipofectamine only) showed a similar fluorescent pattern as compared to cells expressing hOAT1 WT c-Myc (data not shown). Since the COS7 hOAT1 c-Myc cells do exhibit transport activity [23], some of the tagged transporter clearly traffics to the cell surface, therefore, in the absence of observable signal at the cell surface in CHO hOAT1 c-Myc, this technique was not pursued further.

A; DAPI, 20x

B; DAPI, 40x

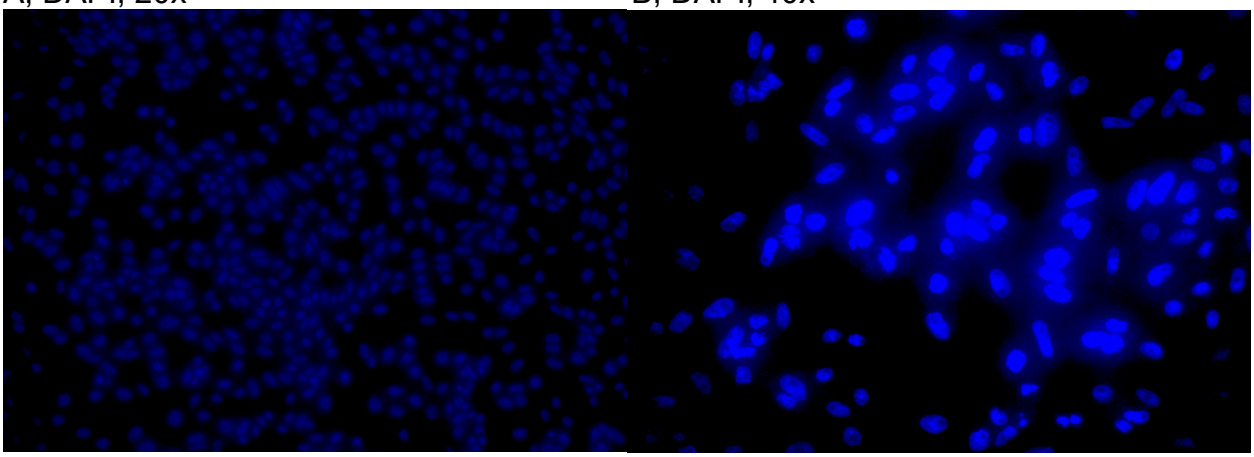

C; FITC, 40x

D; DAPI & FITC Merge, 40x

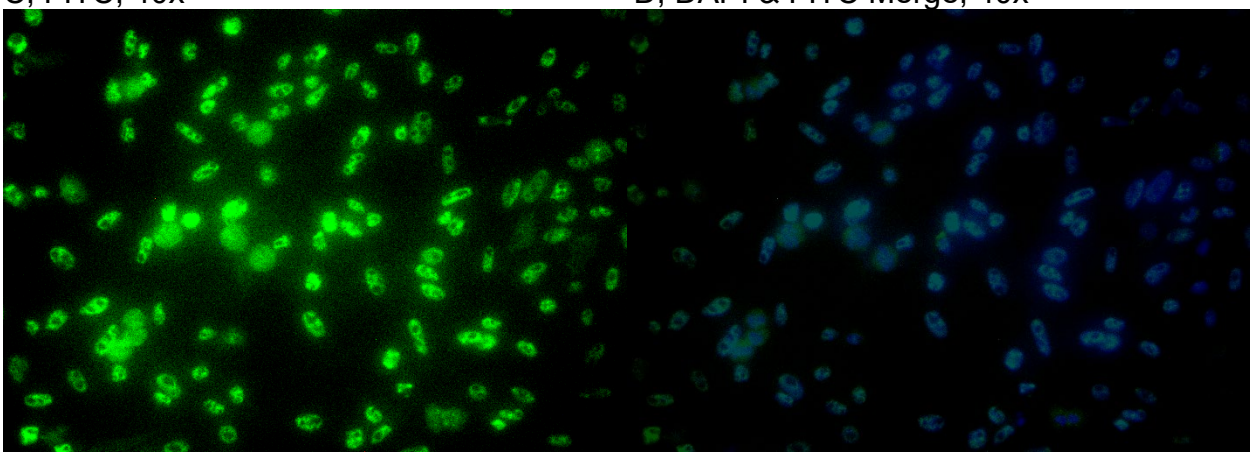

Figure 2.16 Immunohistochemistry of hOAT1 c-Myc Expressing Cells

CHO cells transfected with pcDNA3.1 hOAT1 c-Myc were fixed, permeabilized, subjected to heat antigen retrieval and mounted at 24 hrs post transfection, then viewed by fluorescence microscopy: (A) DAPI, 20x (B) DAPI, 40x (C) FITC, 40x and (D) DAPI & FITC Merge, 40x.

Finally, in addition to immunohistochemistry, Western blotting was performed on isolated cytoplasmic and plasma membrane fractions from COS7 cells expressing hOAT1 WT c-Myc using the c-Myc antibody. Protein bands were observed at the expected position of full length endogenous c-Myc protein (~48kD), however no detectable signal was observed in the hOAT1 WT c-Myc membrane fraction (~66kD, Figure 2.17 A). The membrane was additionally blocked then probed for β-actin as a loading control. Detection for β-actin was consistently observed (~43kD) in all lanes (Figure 2.17 B).

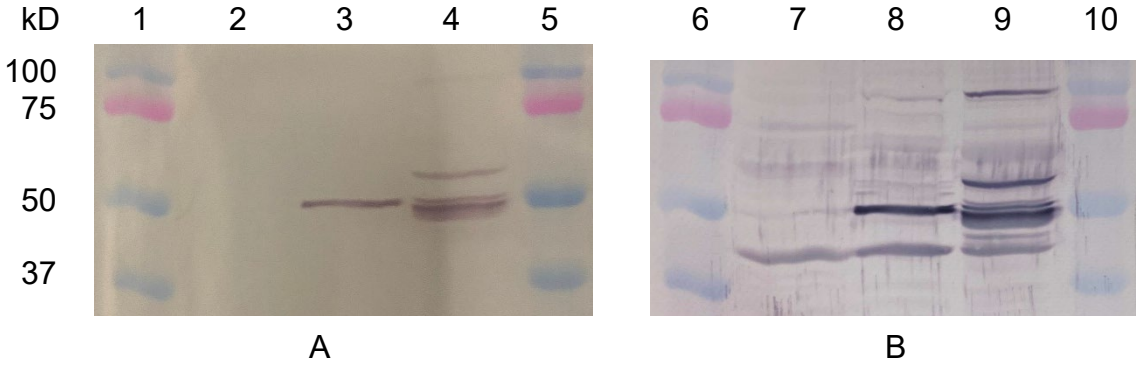

Figure 2.17 Immunoblotting of hOAT1 c-Myc Expressing Cells

Western blot images of cytosolic and membrane fractions from control and hOAT1 c-Myc expressing cells after probing for c-Myc (A) followed by β actin (B). Lanes are as follows: (1, 5, 6, 10) 5μL Ladder, (2, 7) COS7 hOAT1 c-Myc Membrane (60 μg), (3, 8) COS7 hOAT1 c-Myc Cytosolic (60 μg), and (4, 9) CHO Parent Cytosolic (60 μg).

2D. DISCUSSION

Although it has been over two decades since the first discovery of OATs, information is still lacking regarding the structural components that impact compound recognition at the molecular level. Thus far, attempts to crystallize SLC22 family members have been unsuccessful, thus, homology modeling has been employed. Previous work has been conducted using bacterial GlpT as template to develop a model for hOAT1 [1]. Recently, however, a protein within the MFS, PiPT, was crystallized and represents a more suitable template for hOAT1 modeling studies. PiPT belongs to the same transporter superfamily, shares higher protein sequence identity (19%) and similarity (33%) with hOAT1 than GlpT (16% and 27%, respectively), and is more closely related evolutionarily as it is a eukaryotic protein whereas GlpT is prokaryotic. In addition, the International Transporter Consortium has designated PiPT as the appropriate template for SLC22 transporters [24]. Finally, in a June 2019 article regarding current advances in studying clinically relevant transporters of the SLC family, PiPT was also identified as the preferred template for structure-based modeling [25]. Therefore, in this work molecular modeling studies were conducted using PiPT as template.

One hundred models were constructed to represent the proposed alignment between PiPT and hOAT1, which aids in distinguishing small bond angles and torsional rotations over the course of the model building procedure. Of the potential 1,000 combinations generated, the top 15 results are reported in Table 2.3. The best combinations between hOAT1 and PAH are listed in descending order of “GOLD Rank”. Choosing which model and pose combination to continue with was based on GOLD scores, DOPE scores, and number of clusters. DOPE scores aid through increasing the accuracy of the protein

structure assessment [11,26]. GOLD scoring takes into account hydrogen bond energy, protein-ligand van der Waals energy, ligand internal van der Waals energy, and ligand torsional strain energy to predict appropriate and feasible ligand binding positions [14]. Based upon these criteria, hOAT1 model 4 was selected (out of 100), and the best pose of PAH within this model was number 45. Further evaluation of model 4 was conducted via Ramachandran plot analysis. Such analysis provides an additional detailed check on the stereochemistry of the protein structure in the proposed model (Figure 2.6). This plot provides assessment of the overall quality of the structure and also highlights regions which may require further investigation [12]. As indicated, in model 4 99% of the residues exist in “allowable” or “favorable” conformations and only three residues, Ser160, Ala331, and Tyr334, were identified as having inappropriate bond angles between neighboring amino acids. Further visual inspection of the model confirmed these three residues reside towards the outer surface of the protein, a significant distance from the putative PAH binding domain identified herein. Therefore, these residues were viewed as likely being non-influential to the final hOAT1-PAH result. Finally, when all 1,000 PAH docking results were observed as a group it was clear a single, centralized binding region emerged and the top PAH pose (i.e pose 45, displayed as a space-filling molecule to distinguish from all other PAH molecules docked) is positioned within this centrally located region within hOAT1 (Figure 2.7). Thus, model 4 was selected (Figure 2.8).

Side (left) and top (right) views of the generated hOAT1 model illustrate the 12 TMD regions, along with the proposed binding pocket PAH occupies (indicated by the grey space-filling cluster). Initial investigation revealed amino acid residues predicted to interact with PAH, and they are labeled and visualized in Figure 2.9 A & B. Three residues,

Arg15, Asn439, and Arg466, have the potential for hydrogen bonding (Table 2.4). The guanidinium groups present within the arginine amino acids appear to align with the electronegative group of the carboxylic acid within PAH. For asparagine, the carboxylic acid group acts as an electronegative group to the positive amine group within PAH. Isoleucine 19 may exhibit what is known as a hydrophobic interaction: the nonpolar properties of the isoleucine group appear to associate with the benzene ring within PAH, and thus form in a hydrophobic pocket. Finally, the aromatic ring of Tyr230 appears to interact with the aromatic ring of PAH, leading to an edge-face aromatic interaction. Based on the structure of a benzene ring, electronegativity is subject to moving freely above and below the ring, leading to an overall positive charge on the benzene edge. Therefore, it is proposed that the electronegativity below the tyrosine ring interacts with the positivity on the edge of the ring within PAH (Figure 2.9 B).

Previous hOAT1 modeling based upon the GlpT template preliminarily identified positions Tyr230, Lys431 and Phe438 as important for PAH/hOAT1 interactions [1]. We also identified Tyr230 as possibly contributing to PAH binding (as discussed above). However, unlike the previous study, Lys431 and Phe438 were not identified as possible interacting residues. In the current PiPT based hOAT1 model, Lys431 is located well outside of the putative binding pocket and poorly positioned to contribute to PAH interactions in this conformation and thus was not considered. Phe438, on the other hand, was identified within the confines of the hOAT1-PAH binding pocket. Upon further HINT analysis, however, this residue was also deemed non-influential in PAH recognition. There were several differences in the modeling approaches that likely explain these discrepancies, (1) different template molecules were used (GlpT vs PiPT), (2) the GlpT

structure did not have substrate included whereas PiPT was crystallized in the occluded state and (3) the previous investigation did not actively dock PAH within the proposed hOAT1 model (thus limiting visual conformation that specific residues are located within the binding pocket), but rather identified favorable active site positions based on size, shape and burial extent of protein void volumes using Putative Active Sites with Spheres (PASS) software [1].

In order to test whether the residues identified in the current study truly impact hOAT1-PAH interactions, conservative and non-conservative amino acid substitutions were introduced (Table 2.4). Initial transport activity assays confirmed three hOAT1 mutants, Arg15Lys, Ile19Leu and Tyr230Phe, mediated inhibitor-sensitive PAH uptake that was significantly ($p < 0.0001$) greater than CHO parental background (Figure 2.12). All other mutants were determined to be transport inactive, as PAH accumulation was not significantly different from background. Every non-conservative substitution led to inactivity. This was likely due to the drastic change of the initial amino acid to alanine, a residue devoid of a physiochemical influencing functional group, thus limiting the potential interaction with the substrate, PAH. One conservative substitution, Asn439Gln, was also inactive, potentially indicating the importance of asparagine at this position; e.g. the hydrogen bond between it and PAH is crucial for PAH translocation and altering this residue disrupts substrate recognition.

While the three hOAT1 conservative mutants still recognized and transported PAH to some degree, it was unknown whether mutation led to altered affinity for PAH. Therefore, these mutants were subjected to saturation (kinetic) analysis in order to estimate the K_m for PAH and directly compare this to the hOAT1 WT K_m (Figure 2.13).

The hOAT1 WT K_m for PAH determined in these studies was 26.1 ± 2.1μM, which is in good agreement with the previous literature [27,28]. Estimated K_m values for both Arg15Lys and Tyr230Phe trended lower (16.1 ± 1.9 and 20.1 ± 3.5μM, respectively), while Ile19Leu had a similar K_m value of 26.8 ± 3.6μM (Figure 2.13 and Table 2.5). Regardless, no active mutant K_m estimates were found to be statistically different from hOAT1 WT ($p > 0.05$). Further studies are required to determine if multiple substitutions within the same molecule (i.e., double or triple mutants) will result in notable changes in transporter affinity.

Several explanations exist for the lack of PAH transport activity by Arg15Ala, Ile19Ala, Tyr230Ala, Asn439Gln, Asn439Ala and Arg466Ala; 1) failed integration of full length hOAT1 cDNA into the genomic DNA during transfection, 2) substitution of the native amino acid truly impacted substrate recognition based on a critical interaction with PAH, or 3) substitution disrupted proper folding and/or targeting of the protein to the plasma membrane following translation. Genomic integration of intact cDNA for all hOAT1 constructs was confirmed by PCR (Figure 2.14), demonstrating at the very least successful genomic integration. In order to examine proper targeting of the inactive hOAT1 mutants to the membrane, numerous techniques were attempted. The first method tried was based on previous successes utilizing transporter-GFP fusion proteins to directly visualize plasma membrane targeting of rat Oat1 and rat Oct2 [29,30]. A similar approach was designed and performed, as hOAT1 was fused to the C-terminus of GFP to evaluate membrane targeting of inactive hOAT1 mutants (Figure 2.15). While fluorescent signal was clearly excluded from the nucleus, indicating expression of the intact hOAT1 - GFP fusion construct, excessive cytoplasmic signal prevented conclusive

examination at the cell surface. A second technique involved introducing a c-Myc epitope tag at the carboxyl terminus of hOAT1 [31]. COS7 cells expressing the hOAT1-c-Myc tagged protein were subjected to immunohistochemistry utilizing a commercial c-Myc antibody (Figure 2.16). The observed expression pattern showed abundant endogenous c-Myc localized in the nucleus (merged images show complete overlap of DAPI and FITC signals within the nucleus (Figure 2.16 D)) however, no discernable signal was associated with the cell surface. Control transfections indicated a similar pattern: strong FITC and DAPI signal within the nucleus (data not shown). Thus, despite remaining transport active, there may be insufficient hOAT1 c-Myc protein at the cell surface to visualize with this technique. Finally, Western blotting was conducted on plasma membranes isolated from hOAT1 c-Myc expressing COS7 cells. Again, however, the anti c-Myc antibody failed to detect hOAT1-c-Myc (~66kD), but did successfully detect native c-Myc (~48kD) for both COS7 hOAT1 c-Myc and CHO background fractions (Figure 2.17 A). The blot was additionally probed for β-actin as a control to ensure sample integrity, leading to a detectable band (~43kD) in all lanes (Figure 2.17 B). Human OAT1 expression levels below assay limits of detection also could be the issue here. The detection kit utilized is able to detect “sub-nanogram” levels of protein. However, targeted proteomics studies in both rat and mouse kidney have reported 10.6 fmol/μg protein and 12.7 fmol/μg protein [32,33], in proximal tubule basolateral membrane or renal cortex fractions, respectively. Therefore, if hOAT1 c-Myc expression level in COS7 cells is equivalent to native expression levels, 60 μg of membrane might have ~636 fmol of hOAT1 c-Myc and a one hundred fold overexpression would result in ~63.6 pmol of hOAT1 c-Myc. Thus, potentially indicating these standard detection techniques lack sufficient sensitivity to

detect target and that a targeted proteomics approach is required for detection/quantification.

In summary, a novel *in silico* homology model for hOAT1 based on the solved structure of PiPT was successfully constructed and validated. Upon successful docking of the prototypical substrate, PAH, into the generated hOAT1 model, residues Arg15, Ile19, Tyr230, Asn439 and Arg466 (involving four separate TMDs) were identified as potentially critical to PAH recognition. Regardless of position, non-conservative substitution to alanine led to complete loss of transport activity. Conservative substitutions at positions 15, 19, and 230 did not significantly alter transport affinity for PAH, demonstrating a degree of tolerance at these positions in hOAT1 without loss of transporter function. The loss of transport activity for the conservative substitution at position 439 suggests that there is less flexibility at this position or that asparagine is required at this position for effective PAH transport. Future work will be focused on confirming non-functional hOAT1 mutants in regards to membrane targeting to further strengthen our conclusions. Ideally, such models will serve as invaluable tools supporting future targeted rational drug design strategies, the prediction of potential transporter-mediated drug interactions, and *in silico* modeling and prediction of drug pharmacokinetic profiles of new chemical entities and investigational drug products.

CHAPTER 3 – HUMAN ORGANIC ANION TRANSPORTER 3 (hOAT3)

Elucidating hOAT3-ES binding interactions through homology modeling and mutational analysis

3A. INTRODUCTION

Organic anion transporters are integral membrane proteins involved in the translocation of small, negatively charged compounds, including but not limited to drugs, xenobiotics, and endogenous molecules. Within the SLC transporter family lies another specific anion transporter: human organic anion transporter 3 (hOAT3), which was first characterized in human renal proximal tubules in 1999 [4,34].

Pre-clinical studies involving drug transport protein function are essential, as transporters have clinically relevant effects on the pharmacokinetics and pharmacodynamics of drugs through impacting their absorption, distribution, and elimination [35]. Further, there are increasing examples in the literature where these transporter proteins are the site of deleterious drug-drug interactions in the clinic [36–38]. In fact, such information is now recognized as being so vital to the drug development and approval process that the Center for Drug Evaluation and Research (CDER) within the United States Food and Drug Administration (FDA) has outlined a guidance for the pharmaceutical industry in regards to *in vitro* metabolism and transporter mediated drug-drug interaction studies. Within this FDA guidance, OAT1 and OAT3 are specifically identified as renal transporters possibly requiring *in vitro* studies to determine whether an investigational drug is a substrate for either transporter, and to evaluate the potential for significant impact on clinical efficacy or drug-drug interactions involving transporters.

Due to the significance of OAT1 and OAT3 within this guidance, it was apparent that a greater understanding of their structure, mechanism of action, and specifics of

substrate recognition, binding and translocation are needed. To begin to shed light on these aspects of substrate-transporter interactions for hOAT3, a comparative homology model was constructed. The prototypical hOAT3 substrate, estrone sulfate (ES), was docked within the model via *in silico* simulation to identify a potential binding pocket and residues critical to forming the compound-transporter binding complex.

Amino acids predicted to be involved in ES recognition were altered through site-directed mutagenesis in order to evaluate their potential role in ES translocation. Wild type (WT) and mutated hOAT3 constructs were then expressed in Human Embryonic Kidney (HEK) 293 cells to allow for their functional analysis. Initial investigation revealed five mutants, Phe426Tyr, Phe430Tyr, Phe430Ser, Leu431Ile and Arg454Ala, supported significant ES accumulation as compared to parental HEK 293 cells. In addition, the Phe430Ser mutant exhibited a significant change in ES affinity as compared to WT hOAT3. The five remaining substitutions, Tyr342Phe, Tyr342Ala, Phe426Ser, Leu431Ala and Arg454Lys, led to complete loss of transport activity, indicating some rigidity in these positions in regards to ES recognition. In general, this hOAT3 homology model provides an *in silico* option to screen new drug candidates which may interact with hOAT3 and serve as a tool to advance pre-clinical development of investigational drug products.

3B. MATERIALS AND METHODS

Chemicals and Reagents - [^{3}H] ES was purchased from PerkinElmer Life and Analytical Science (Waltham, MA). Unlabeled ES, probenecid, and DAPI readymade solution were purchased from Sigma-Aldrich (St. Louis, MO). Specific primers for mutation reactions were purchased from IDT (Coralville, IA). QuikChange Lightning Site-Directed Mutagenesis Kit was purchased from Agilent Technologies (Santa Clara, CA). Lipofectamine transfection reagents and HyClone DMEM/High glucose medium with L-glutamine and sodium pyruvate were purchased from Thermo Fisher Scientific (Waltham, MA). QIAprep spin mini- and midiprep kits were purchased from QIAGEN Inc. (Germantown, MD). GoTaq Green Master Mix was purchased from Promega (Madison, WI).

Molecular Model Building - The recently solved crystal structure for *Pirformospora indica* high-affinity phosphate transporter, PiPT, was identified as the most suitable currently available template molecule and its sequence was downloaded from the Protein Data Bank (PDB ID: 4J05). The hOAT3 FASTA protein sequence was downloaded from UniProt (UniProtKB ID: Q8TCC7). Looped regions between TMD 1 & 2 and 6 & 7 in the final crystalized form of PiPT were excluded based on their inability to resolve these regions [6]. In order to properly align the target (hOAT3) peptide sequence with the known template (PiPT) peptide sequence, hOAT3 secondary structures, including potential TMD helices, were predicted using PredictProtein v1 [7]. Looped regions between TMD 1 & 2 and 6 & 7 were excluded from hOAT3 due to lack of resolved sequence within the PiPT crystal structure. The curated sequences were aligned using the multiple sequence alignment software ClustalX v2 [8], followed by manual

modifications to avoid repetitive regions of non-alignment within predicted transmembrane helices, which would negatively impact the model building. The final alignment for PiPT-hOAT3 was visualized using ALINE v1.0.025 [9]. Based on this alignment, one hundred comparative protein models were generated, using the software MODELLER v9.17 [10]. The stereochemical integrity of the generated models was evaluated through DOPE scoring v9.17 [11,26] and Ramachandran plots (PROCHECK v9.17, [12]), both of which ensure bond lengths, angles, and torsions within the *in silico* model were within acceptable and feasible limits.

Substrate Docking – An ionized, energy minimized structure for the prototypical hOAT3 substrate, ES, was generated using the computer-aided molecular modeling design tool SYBYL-X 2.1 [13]. Proper confirmation and atom type for the sketched *in silico* molecule was evaluated and followed by energy minimization based on Gasteiger-Huckel charges. Ligand docking studies were initiated using the docking algorithm GOLD v5.4 provided from the Cambridge Crystallographic Data Centre [14]. Briefly, a GOLD configuration file was generated that referenced the previously generated one hundred hOAT3 models as the corresponding “receptor” and the *in silico* ES molecule as the “ligand”. A spherical region 30Å in diameter was designated , which virtually encapsulated the entire transporter. One thousand possible combinations were evaluated, and the top combination was selected based on GOLD score, DOPE score, and number of clusters. The specific hOAT3-ES combination was then visually inspected using SYBYL-X v2.1, which allows 3-D manipulation, thus permitting identification of amino acids deemed potentially critical for the formation of the compound-transporter complex. Further validation of these predicted critical amino acids was obtained using the empirical molecular modeling system HINT [15], which evaluates and scores the binding interactions between hOAT3 and ES.

Mutagenesis – hOAT3 constructs containing single conservative or non-conservative substitutions at each position hypothesized to be part of the hOAT3-ES binding complex were generated, based upon the physiochemical properties of amino acids, amongst other supportive information [16]. Substitutions were introduced into pcDNA 3.1 (+) / V5-His-TOPO – hOAT3 plasmid (Figure 3.1) using the QuikChange Lightning Site-Directed Mutagenesis Kit (Agilent Technologies, Santa Clara, CA). Oligonucleotide primers used to introduce the mutations were designed online using QuikChange Primer Design software (Agilent Technologies, Santa Clara, CA, [17]) and reported in Table 3.1. Cycling parameters for QuikChange Mutagenesis Method were as follows: denature at 95°C for two min, 18 cycles of 95°C denature for 20 sec, 64°C annealing for 10 sec, 68°C elongation for 30 sec per kb of plasmid length (8kb plasmid, 4 min); with a final elongation at 68°C for 5 min. Samples were subsequently incubated with Dpn1 restriction enzyme at 37°C to degrade the WT hOAT3 parental template strands.

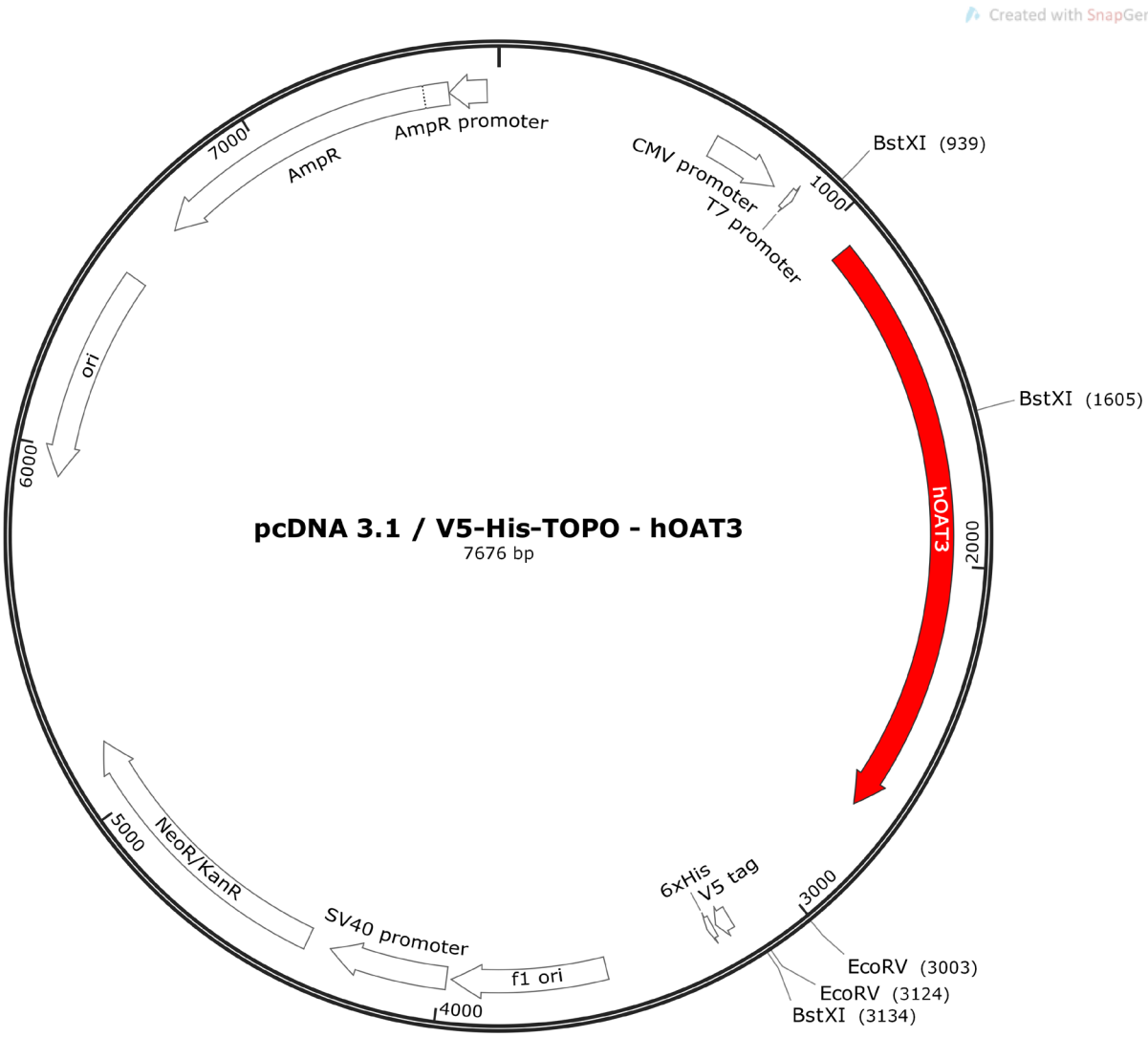

Figure 3.1 Plasmid Map of hOAT3 Template

Full length hOAT3 cDNA sequence was subcloned into pcDNA3.1/V5-His-TOPO expression vector (Invitrogen, Carlsbad, CA) using BstX1/EcoRV restriction enzyme sites [39]. Location of hOAT3 insert is highlighted in red. Image generated using SnapGene.

Table 3.1 Oligonucleotide primer sequences used for site-directed mutagenesis

Position	Substitution	Primer	Primer Sequence (5' to 3')
Tyrosine 342	Phenylalanine	Forward	TACCGGTTTTGCCTAC**TTT**AGTTTGGCTATGGGTG
		Reverse	CACCCATAGCCAAACT**AAA**GTAGGCAAAACCGGTA
	Alanine	Forward	TGCTACCGGTTTTGCCTAC**GCT**AGTTTGGCTATGGGTGTG
		Reverse	CACACCCATAGCCAAACT**AGC**GTAGGCAAAACCGGTAGCA
Phenylalanine 426	Tyrosine	Forward	CCTATCCAGCTCC**TAC**AGCTGCCTCTTCC
		Reverse	GGAAGAGGCAGCT**GTA**GGAGCTGGATAGG
	Serine	Forward	CCTATCCAGCTCC**TCC**AGCTGCCTCTTCC
		Reverse	GGAAGAGGCAGCT**GGA**GGAGCTGGATAGG
Phenylalanine 430	Tyrosine	Forward	GCTCCTTCAGCTGCCTC**TAC**CTCTACACAAGT
		Reverse	ACTTGTGTAGAG**GTA**GAGGCAGCTGAAGGAGC
	Serine	Forward	GCTCCTTCAGCTGCCTC**TCC**CTCTACACAAGT
		Reverse	ACTTGTGTAGAG**GGA**GAGGCAGCTGAAGGAGC
Leucine 431	Isoleucine	Forward	CTCCTTCAGCTGCCTCTTC**ATC**TACACAAGTGAATTATA
		Reverse	TATAATTCACTTGTGTA**GAT**GAAGAGGCAGCTGAAGGAG
	Alanine	Forward	CTCCTTCAGCTGCCTCTTC**GCC**TACACAAGTGAATTATAC
		Reverse	GTATAATTCACTTGTGTA**GGC**GAAGAGGCAGCTGAAGGAG
Arginine 454	Lysine	Forward	GTAAGTAACCTGTGGACC**AAG**GTGGGAAGCATGGTGTCC
		Reverse	GGACACCATGCTTCCCAC**CTT**GGTCCACAGGTTACTTAC
	Alanine	Forward	GTAACCTGTGGACC**GCC**GTGGGAAGCATGG
		Reverse	CCATGCTTCCCAC**GGC**GGTCCACAGGTTAC

Position indicates native amino acid; Substitution indicates change (conservative or non-conservative) based on properties of amino acid position. Codon string for altered amino acid residue is indicated in bold within primer sequence.

Transformation – Dpn1 treated plasmids were incubated with XL10-Gold Ultracompetent Cells (Agilent Technologies, Santa Clara, CA). Preheated NZY+ broth was added after heat-pulsing the ultracompetent cells at 42˚C for 30 sec, followed by incubation at 37˚C for 1 hr with constant shaking (225RPM). After incubation, 50, 100, and 200µL aliquots of cells were spread onto three separate LB agar plates containing 100 µg/mL ampicillin, adding a 200µL pool of NZY+ Broth for volumes less than 100µL to optimize spreading. Plates were incubated at 37˚C for 16 hrs to allow adequate time for colony growth. Individual colonies were selected and grown in separate tubes containing 8mL NZY+ Broth and 100 µg/mL ampicillin, followed by overnight incubation at 37°C with constant shaking.

Plasmid preparation – Mini or midi-plasmid preparation was performed following the manufacturer's protocol [18] (QIAGEN, Germantown, MD). Briefly, pelleted bacterial cultures were resuspended, lysed, neutralized, centrifuged at 13,000RPM for 10 min and supernatants transferred to supplied spin columns. After binding of plasmid DNA, columns were thoroughly washed prior to final DNA elution. Plasmid DNA concentration was determined using UV-Vis Spectroscopy.

Sequencing – Generated hOAT3 mutants were confirmed by DNA sequencing. Samples were sent with respective oligonucleotide sequencing primers (Table 3.2) for Sanger sequencing (Genewiz, South Plainfield, NJ). Sequencing files provided through Genewiz were compared to full length hOAT3 WT plasmid to ensure proper mutations were achieved.

Table 3.2 Oligonucleotide primers used for hOAT3 DNA sequencing

Primer	Primer Sequence (5' to 3')
hOAT3 Forward 1	TGGTCTTCCGCTTCCTGTG
hOAT3 Forward 2	CTTAAGCTACCTGGGCC
hOAT3 Reverse 1	CTAGGATCAGTCTCTGGAGG
hOAT3 Reverse 2	CCTCCGAGGACTTTCCAGAC

Cell Culture – HEK 293, HEK-hOAT3 WT and HEK-hOAT3 mutant cell lines were maintained at 37°C with 5% CO_2 in DMEM containing 10% FBS, 1% Pen-Strep (Gibco-Invitrogen, Grand Island, NY) and 0.250 mg/mL G418. Once cells reached 80-90% confluency, passaging was performed. Briefly, the media was removed, cells were washed with 1x PBS, and followed by cell dissociation using 0.25% Trypsin-EDTA (Gibco-Invitrogen, Grand Island, NY). Dislodged cells were resuspended in medium and passaged to a separate flask containing DMEM, 10% FBS, 1% Pen-Strep, and 0.250 mg/mL G418. Cells were sub-cultured every three to four days and passages numbered 4 through 20 were used for experiments.

Transfection – HEK 293 cells were grown in antibiotic-free DMEM containing 4.5g/L D-Glucose, L-glutamine and 110 mg/L sodium pyruvate (Gibco-Invitrogen, Grand Island, NY) with 10% FBS at 37°C in 5% CO_2 until reaching 60 to 80% confluency. Stable transfections were performed according to the Lipofectamine® 2000 Reagent protocol [19]. One day before transfection, 2.0 x 10^5 HEK 293 cells were seeded into 12-well tissue culture plates. On the day of transfection, Lipofectamine® 2000 (4µL) and OptiMEM medium (96µL) per transfection were incubated together for 5 min at room temperature. Plasmid DNA (1µg) was added to 100µL OptiMEM medium, combined with previous Lipofectamine® 2000/OptiMEM mixture, then incubated for 20 min at room temperature. After adding a fresh 1mL of medium to each well, the Lipofectamine® 2000/plasmid DNA/OptiMEM mixture (200µL) was added to each well and mixed gently. Cells were then incubated at 37°C for 24 to 48 hrs, followed by multiple weeks of antibiotic selection using 1 mg/mL Geneticin (G418) (Gibco-Invitrogen, Grand Island, NY).

Accumulation Assay – The procedure for cell accumulation assay has been described previously [20,21]. In summary, 3.5 x 10^5 cells were seeded with antibiotic-free culture medium in 24-well tissue culture plates coated with 0.1 mg/mL poly-D-lysine 48 hrs before the experiment. The culture medium was removed and the cells were washed with 500µL TB for 10 min. The cells were treated with 400µLTB containing 5µM ES spiked with radiolabeled ES (0.25 µCi/mL [^{3}H]ES) in the absence or presence of the inhibitor probenecid (500µM) for 10 min. The treatment was removed, and the cells were rinsed three times with ice-cold TB. Cells were lysed in 200µL 1M NaOH and shaken for 2 hrs at room temperature. Afterward, cells were neutralized with 250µL 1M HCl and 200µL 10mM HEPES. Liquid scintillation was conducted using 400µL of samples with 5mL Ecoscint H cocktail (National Diagnostics, Atlanta, GA). Samples were normalized by protein content through a Bradford protein assay using 10µL sample aliquots with 200µL protein assay dye (Bio-Rad Laboratories, CA). Screening data were reported as mean ± SD from triplicate samples.

Kinetic Analysis Assay - Michaelis-Menten constant (K_m) were determined for ES uptake for active hOAT3 mutants through saturation analysis according to our previously published protocol [21]. In summary, 3.5 x 10^5 cells were seeded with antibiotic-free culture medium in 24-well tissue culture plates coated with 0.1 mg/mL poly-D-lysine 48hrs before the experiment. Culture medium was removed and the cells were washed with 500µL TB for 10 min. Cells were treated with 300µL TB containing increasing concentrations of ES (1µM – 100µM; 0.25 µCi/mL [^{3}H]ES) for one min. The treatment was removed and samples processed as described above for the accumulation assay. Data were plotted and analyzed by non-linear regression to generate K_m estimates (GraphPad

v8.3.0). Kinetic data were reported as mean ± SD from triplicate samples. Final K_m estimates were reported as mean ± SE from a minimum of three separate experiments

Verification of Genomic Integration – Cells were suspended in 500µL of lysis buffer (1 M Tris (pH 8.0), 5 M NaCl, 0.5 M EDTA, 10% SDS, and 0.4 mg/mL proteinase K) and incubated at 55°C overnight while shaking at 200RPM. The following day, genomic DNA was extracted using an equal volume of phenol/chloroform/isoamyl alcohol (25:24:1) and shaking for 10 min. Samples were centrifuged for 10 min at 15,000RPM in a table-top microcentrifuge. The upper aqueous phase was collected, mixed with an equal amount of isopropyl alcohol, and spun for an additional 15 min to obtain a DNA pellet. The pellet was rinsed with 70% ethanol, air-dried, and re-suspended in 200µL TE buffer (pH 8.0) containing 10mM Tris and 1mM EDTA. DNA concentration was determined using UV-Vis Spectroscopy. Genomic DNA ranging from 150 to 1,000ng, 2x GoTaq Green Master Mix (25µL), and 2.5µL primer pair mix (100µM T7: 5' – TAATACGACTCACTATAGGG – 3'; 100µM hOAT3Rev1: 5' – CTAGGATCAGTCTCTGGAGG– 3') were added to a final volume of 50µL and run in a thermocycler under the following conditions: denature at 95°C for 2 min, 30 cycles of denaturation at 95°C for 30 sec, annealing at 52°C for 30 sec, elongation at 72°C for one min. Final elongation proceeded at 72°C for 5 min, then samples were held at 4°C. PCR products were loaded onto a 1% agarose gel for separation using electrophoresis at 120V for 1 hr. Gel was stained in EtBr for 10 min and visualized using ChemiDoc Touch Imaging System (Bio-Rad Laboratories, Hercules, CA).

Mycoplasma Testing – All cell lines were tested for the presence of mycoplasma using a Universal Mycoplasma Detection Kit (ATCC, Manassas, VA). Briefly, adherent cells were harvested and resuspended in lysis buffer, heated at 95°C, then spun at 13,000RPM for 5 min. Supernatants were collected, followed by the addition of Universal PCR mix plus Universal Primers supplied through the kit, with the appropriate positive and negative controls. Following the PCR amplification procedure, a 3% agarose gel was prepared, and 10µL of PCR products were loaded. The gel was stained using EtBr, washed thrice in diH_2O, then observed under UV illumination. No instances of mycoplasma were detected in any generated HEK hOAT3 expressing cell lines (Figure 3.2).

Statistics – Data are plotted as mean ± SD for initial screening assay and individual saturation assays. Final K_m estimates are reported as mean ± SE. Statistical analysis was performed using GraphPad Prism v8.3.0 and R 3.6.0. Equal variance, one-way ANOVA with post-hoc Dunnett's multiple comparisons was used to evaluate differences compared to a single control where indicated. All differences were considered statistically significant if $p < 0.05$.

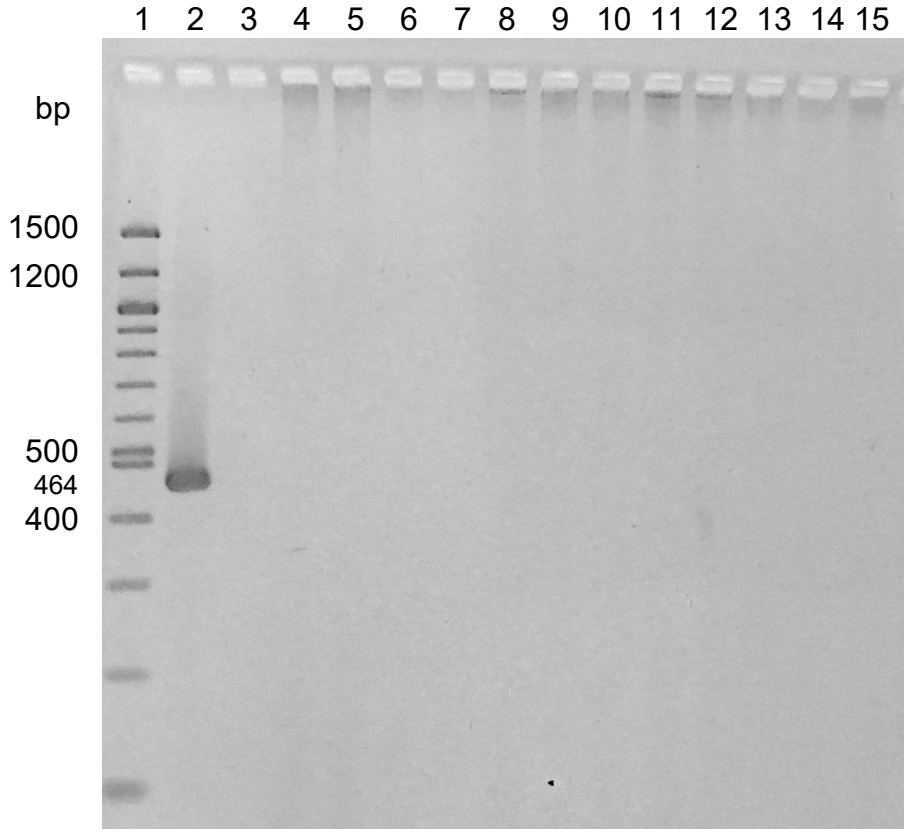

Figure 3.2 Mycoplasma Testing of Generated HEK cell lines

Mycoplasma testing of HEK hOAT3 cell lines along with parental HEK 293 cells is shown. 10µL aliquots were loaded for 100bp DNA ladder, positive control, negative control, and HEK cell lines. Mycoplasma was detected for positive control only (Lane 2, 464bp). Lanes are as follows: (1) 100bp DNA Ladder, (2) Positive Control, (3) Negative Control, (4) hOAT3 WT, (5) HEK 293, (6) hOAT3 Tyr342Phe, (7) hOAT3 Tyr342Ala, (8) hOAT3 Phe426Tyr, (9) hOAT3 Phe426Ser, (10) hOAT3 Phe430Tyr, (11) hOAT3 Phe430Ser, (12) hOAT3 Leu431Ile, (13) hOAT3 Leu431Ala, (14) hOAT3 Arg454Lys, (15) hOAT3 Arg454Ala.

3C. RESULTS

Comparative Modeling of hOAT3

An initial BLAST search of the non-redundant protein sequences database was performed using hOAT3 as the target to identify a suitable template for homology modeling. Search results indicated the peptide sequence of the recently crystalized protein, PiPT, shares 31% sequence similarity and 17% sequence identity with hOAT3, signifying PiPT as a more appropriate template than previously utilized GlpT (PDB ID: 1PW4), which shares 27% similarity and 16% identity with hOAT3. In addition to higher similarity and identity, PiPT offers further advantages as a template molecule such as being a eukaryotic protein, inclusion in the MFS, a 12 TMD structure divided into two domains, and being crystallized in the occluded state therein maximizing the interaction within the compound-transporter complex. Thus, PiPT was selected to serve as the template.

Both PiPT and hOAT3 are predicted to have large sequence loops between TMDs 1 & 2 and 6 & 7. Due to their flexibility, these loops are not resolved in the PiPT crystal structure, thus there are no corresponding residues to model. Therefore, before alignment of hOAT3 and PiPT peptide sequences, the hOAT3 sequence (UniProtKB ID: Q8TCC7) was truncated from Gln38 - Asn117 (between TMDs 1 & 2) and Val264 – Arg319 (between TMDs 6 & 7). The final sequence alignment is shown in Figure 3.3, showing the TMDs for PiPT (white) and hOAT3 (red) as well as exact positioned identities (white letters). This alignment file was fed into MODELLER, generating 100 separate *in silico* homology models for hOAT3.

Next, docking studies were conducted using GOLD v5.4 where the energy minimized ES structure was docked into each model separately, ten times, generating a total of 1,000 different combinations between hOAT3 and ES. To determine the top hOAT3-ES combination, models were ranked through evaluation of their DOPE and GOLD scores, as well as cluster analysis. As shown in Table 3.3, the top hOAT3 model was number 1 with ES pose number 2. Overall, this combination had the highest GOLD score (69.38), a similar DOPE score to other top combinations (-44379.79), and the second highest number of clusters (11) of all other GOLD ranked solutions reported. To further evaluate hOAT3 model 1, a Ramachandran plot was generated using the program PROCHECK v9.17 allowing visualization of all bond angles. Favorable bond angles appear in the red and yellow regions whereas disallowed angles are located in the white areas (Figure 3.4). Only four residues, Leu3, Arg65, Ser159, and Tyr216 were identified as forming unfavorable bond angles in this model. These residues are positioned on the outskirts of the *in silico* model, i.e. well outside the putative ES binding domain, and thus likely exert no direct influence on the hOAT3-ES binding complex in this model. It was also of interest to visualize all top ES solutions docked, to better validate the top model chosen (Figure 3.5). The top ES pose is displayed as a space-filling molecule to distinguish from all other ES molecules docked. This molecule is positioned centrally within hOAT3, clustered amongst numerous additional ES molecules that were separately docked. This provides further validation that the top ES pose (2) is an appropriate representation of the GOLD docking results generated, in addition providing further support to a clear single, centralized binding region. Thus, hOAT3 model 1 was selected as the best representation of hOAT3 in the occluded state with ES (Figure 3.6). As shown,

the generated hOAT3 model has 12 predicted TMDs with intracellular amino and carboxyl termini, with multiple TMDs contributing to the binding pocket. ES is represented with a space filling model while individual amino acids are represented with lines.

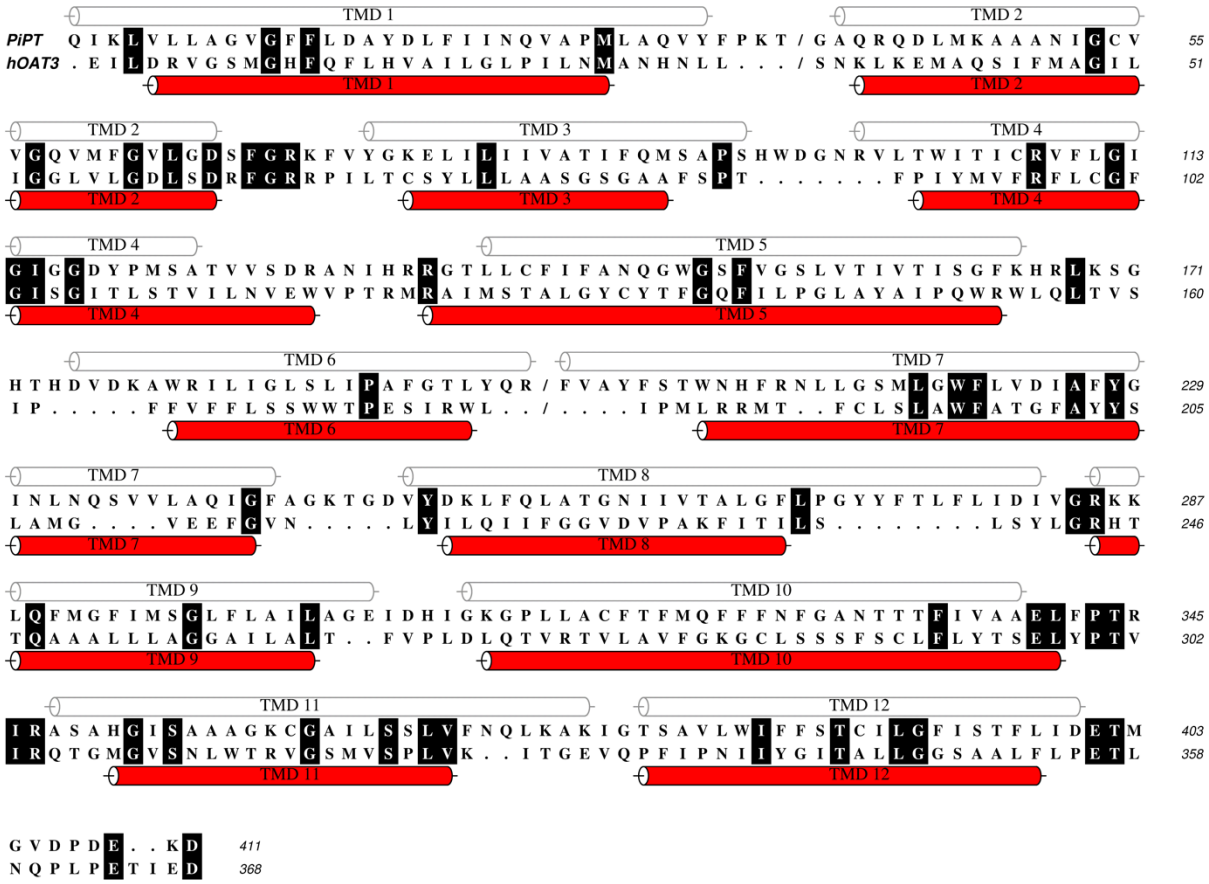

Figure 3.3 Peptide Sequence Alignment Between PiPT and hOAT3

Final peptide sequence alignment between PiPT (top) and hOAT3 (bottom). TMD regions for PiPT (white) documented and confirmed through crystallization of the protein. TMD regions for hOAT3 were initially predicted through PredictProtein v1 software, then regions were determined (red) upon final model generation. White letters indicate conserved amino acid residues between target and template. Image generated using the program ALINE v1.0.025.

Table 3.3 Summary of evaluative parameters and ranking for the top 15 hOAT3 models

GOLD Rank	GOLD Score	Model ID	Best hOAT3-ES Pose	DOPE Score	# of Clusters
1	69.38	1	2	-44379.79	11
2	68.05	23	7	-44802.35	5
3	66.61	44	8	-44684.35	4
4	66.36	97	4	-44953.14	6
5	63.76	59	28	-45154.92	1
6	61.97	6	27	-44260.03	1
7	61.54	40	15	-45136.84	2
8	61.25	37	9	-45301.54	4
9	60.33	35	1	-44745.46	14
10	59.26	88	21	-44779.84	1
11	59.12	48	10	-44982.47	3
12	58.73	9	13	-44662.20	2
13	57.62	66	5	-44582.02	6
14	55.34	18	31	-44978.31	1
15	54.53	73	6	-44853.34	5

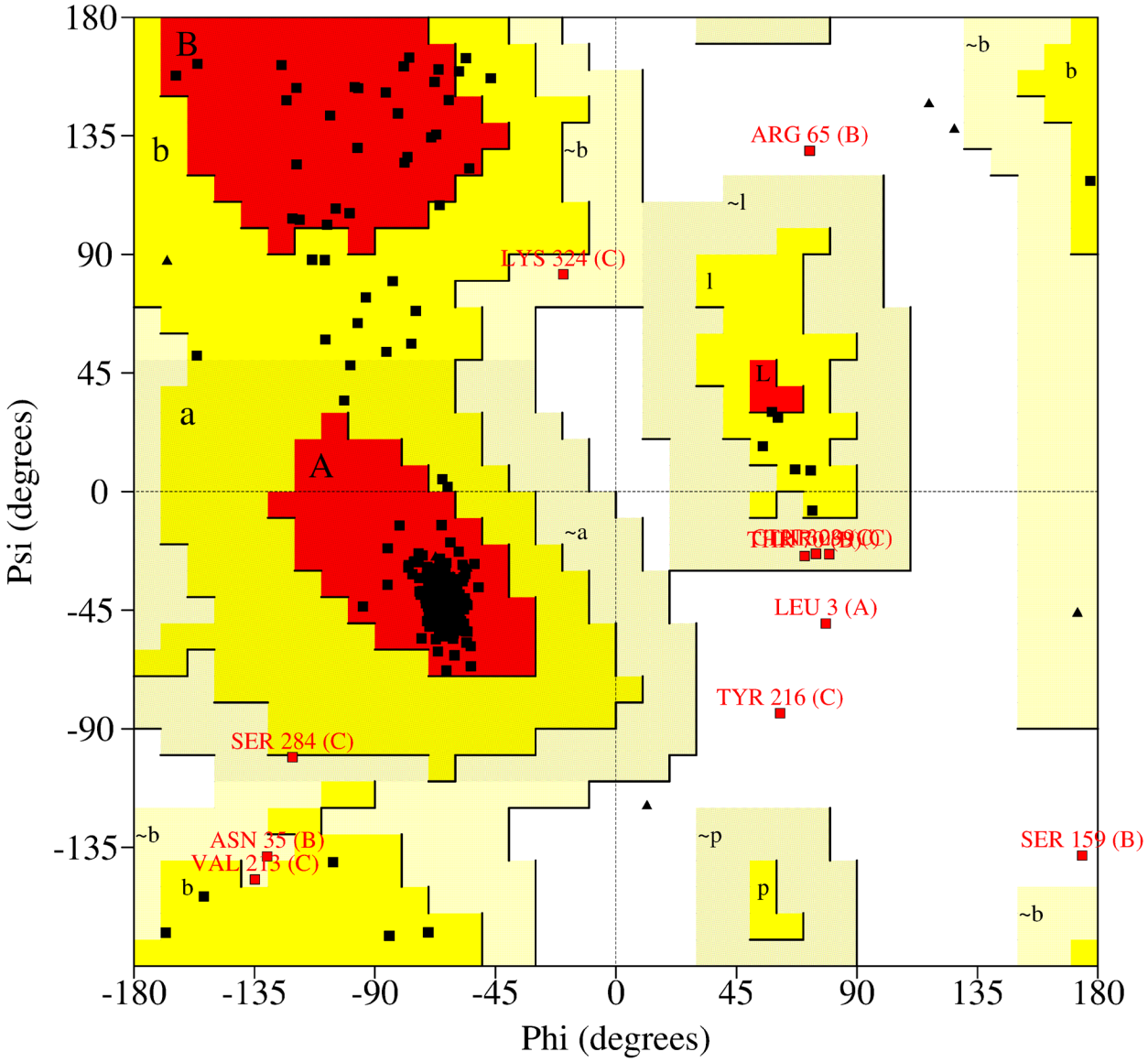

Figure 3.4 Ramachandran Plot of Top hOAT3 Homology Model

Axes indicate degree value of rotatable bonds present between neighboring amino acid residues with specific model generated. High percentage of amino acid residues were reported within favorable regions (98.7%), with remaining residues (LEU3, ARG65, SER159, TYR216) in unfavorable regions. Plot generated using PROCHECK.

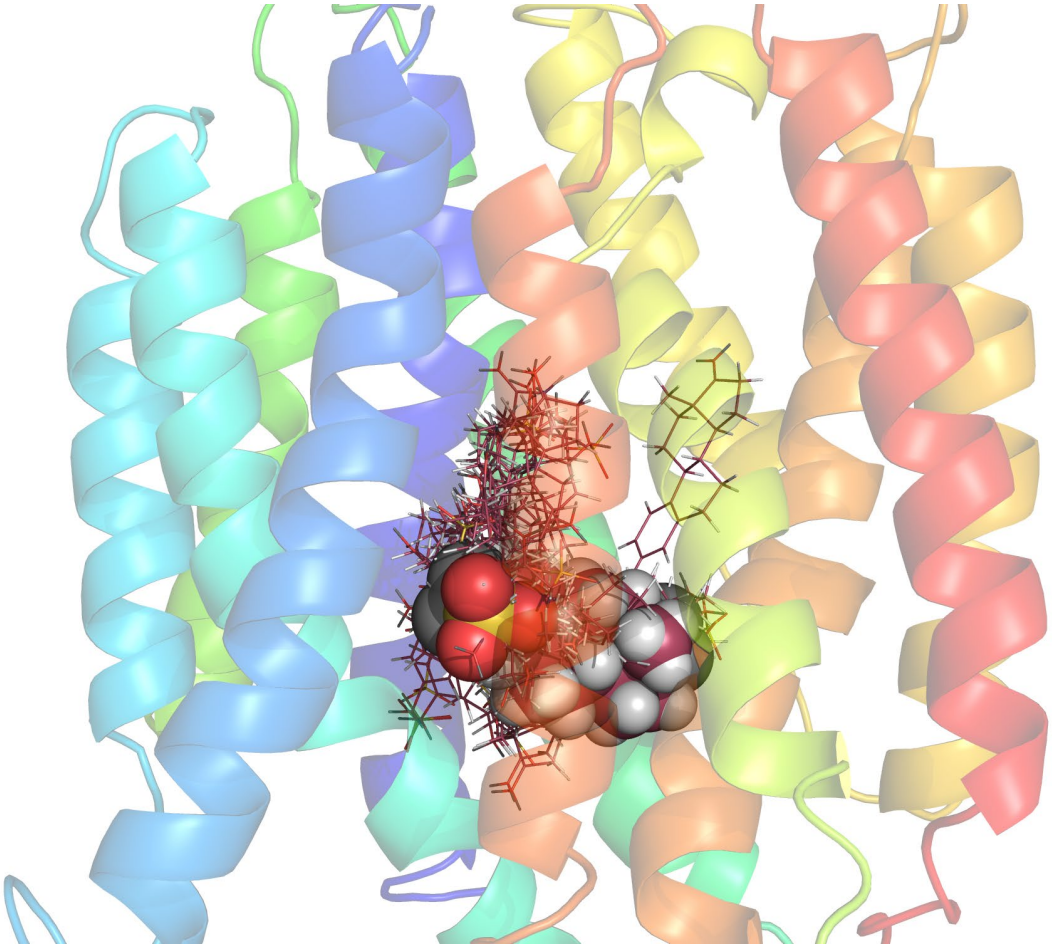

Figure 3.5 Summary of All ES Docked Poses with hOAT3

Summary of all ES locations upon successful GOLD docking studies. The ES locations for all modeling studies are indicated as line molecules. The top ES location (pose 2) is shown as a space filling molecule. The multicolored helices represent the 12 TMD regions for hOAT3. Image file generated using PyMOL 1.8.

Using PyMOL v1.8, further analysis was focused within the suggested binding pocket to determine which amino acid contacts within the transporter are critical to ES recognition (Figure 3.7 A & B). Five amino acids with potential ES interactions were identified, specifically Tyr342, Phe426, Phe430, Leu431, and Arg454. The nature of the proposed interactions between each residue and ES are summarized in Table 3.4. An edge-face aromatic interaction was predicted for Tyr342. Phe426, Phe430 and Leu431 were proposed to exhibit hydrophobic interactions. Finally, a bidentate hydrogen bond interaction was identified for Arg454. To directly examine these predicted amino acid–ES interactions, conservative and non-conservative substitutions were introduced at each position and effects on transporter function examined *in vitro*.

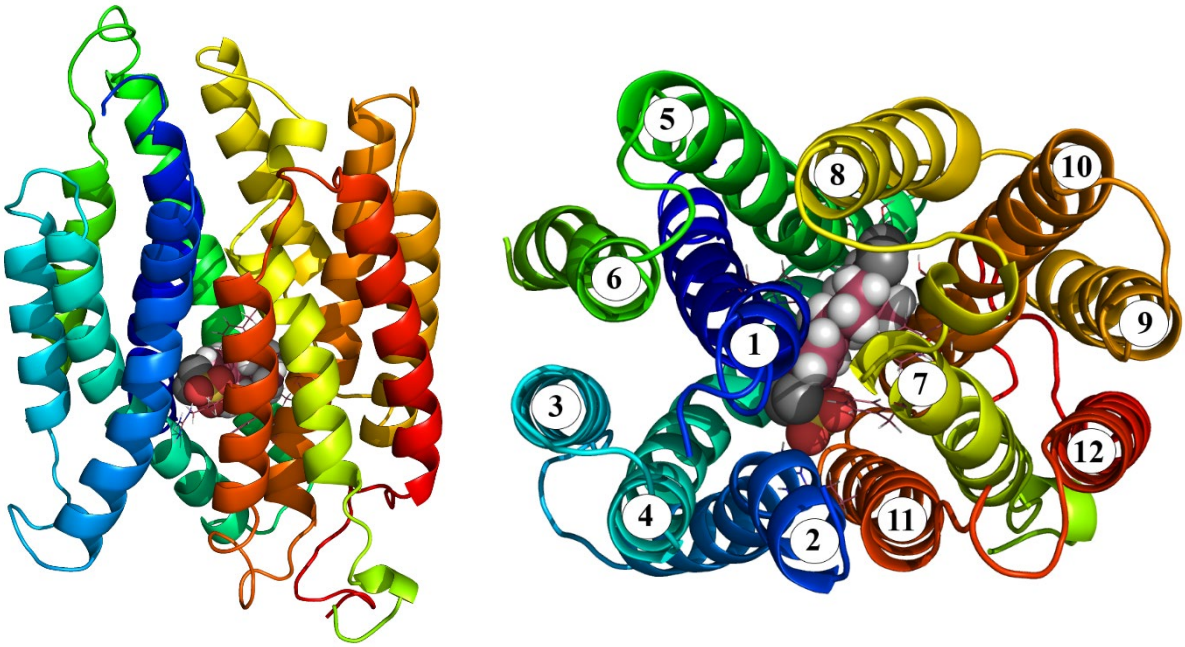

Figure 3.6 Three-Dimensional *in silico* hOAT3-ES Model

Three-dimensional side view (left) and top view (right) of the generated hOAT3-ES binding complex. The multicolored helices represent the 12 TMD regions for hOAT3 and are numbered in the top view. A space filling representation of ES is shown with putative interacting amino acids indicated as line molecules. Image files generated using PyMOL 1.8.

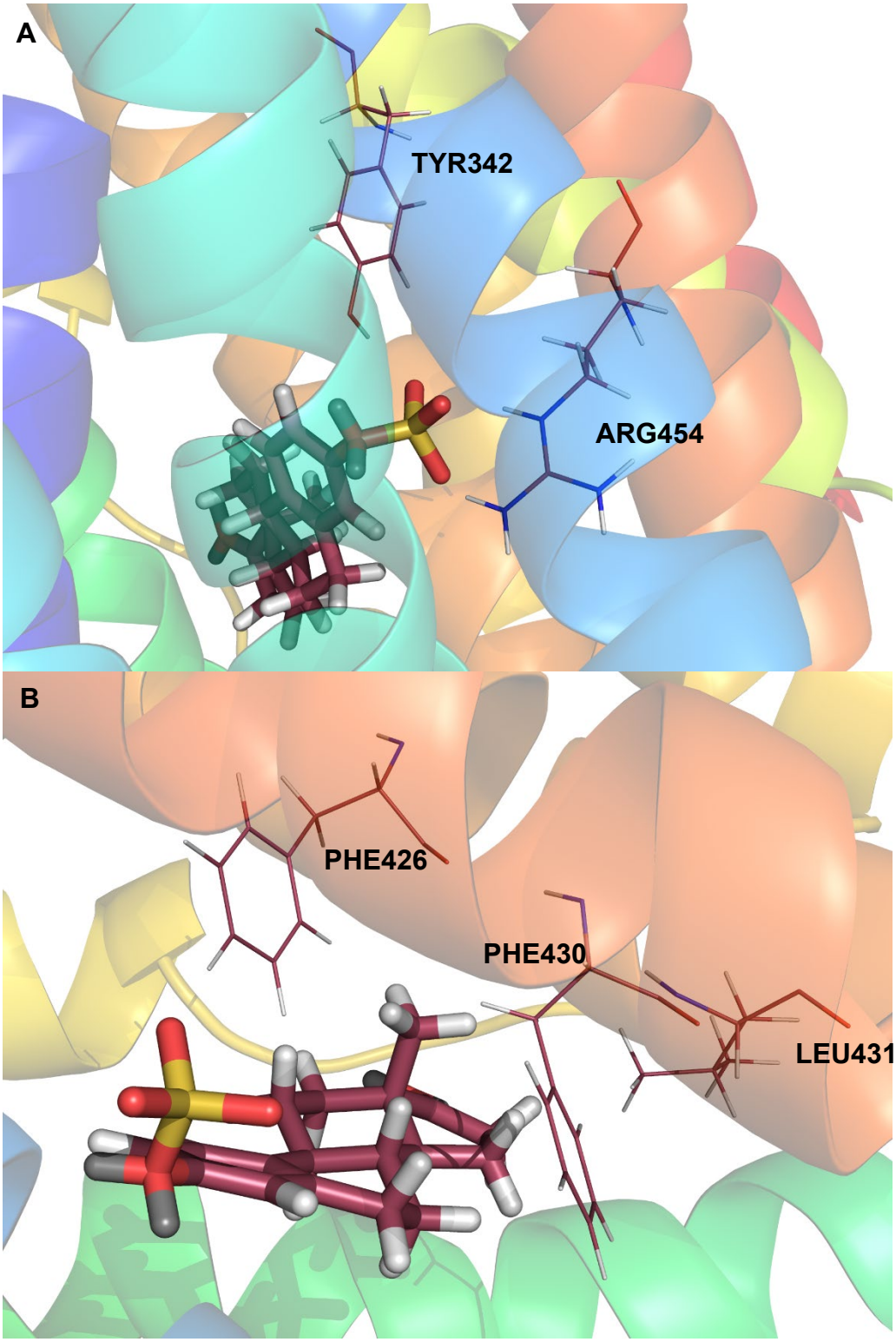

Figure 3.7 A & B Different Rotational Views of the hOAT1-ES Binding Complex

The five amino acids predicted to be important for ES binding and transport are indicated. Image files generated using PyMOL 1.8.

Table 3.4 Summary of putative ES-hOAT3 complex forming amino acids, the predicted nature of each interaction and generated conservative and non-conservative hOAT3 mutations

TMD	Amino Acid	Interaction	Conservative	Non-conservative
7	Tyr342	Edge-Face Aromatic	Phe	Ala
10	Phe426	Hydrophobic	Tyr	Ser
10	Phe430	Hydrophobic	Tyr	Ser
10	Leu431	Hydrophobic	Ile	Ala
11	Arg454	Salt Bridge featuring Bidentate Hydrogen Bond	Lys	Ala

Interactions proposed are based on each amino acid's orientation with the docked substrate. Conservative and non-conservative substitutions were based on physiochemical properties of amino acids amongst other supportive information [16].

In Vitro Testing

The identity of all hOAT3 mutant constructs was confirmed by DNA sequencing prior to functional examination. Representative chromatograms for both a hOAT3 conservative (Tyr342Phe) and non-conservative (Tyr342Ala) mutation are shown. In Figure 3.8 panel A the WT ‘TAT’ codon for tyrosine is clearly observed, while in panel B the codon has been mutated to ‘TTT’ which codes for phenylalanine. Similarly, in Figure 3.9 it can be seen that the WT tyrosine codon has been altered to ‘GCT’ which codes for alanine. Confirmed mutant constructs were stably-transfected into HEK 293 cells.

A

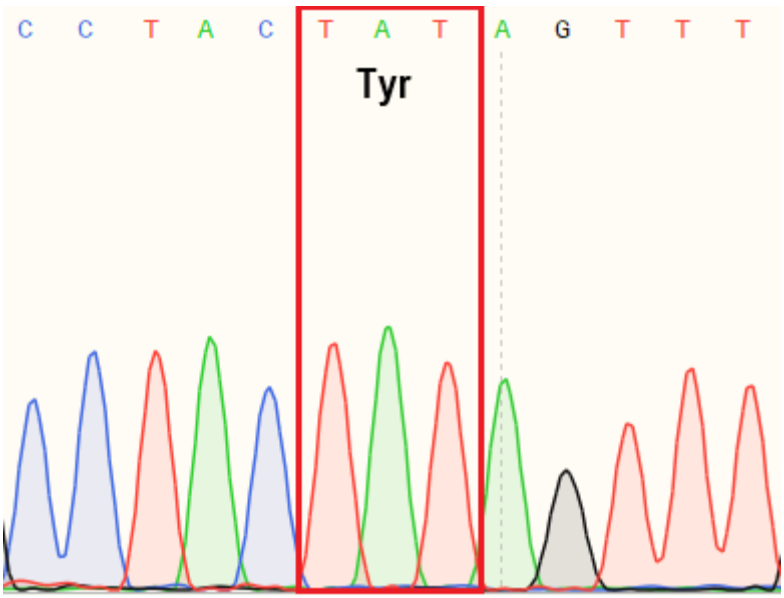

B

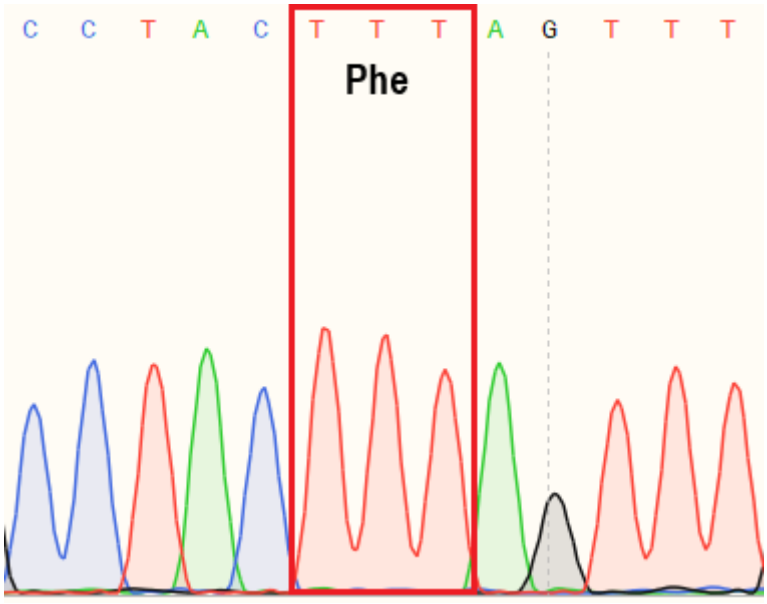

Figure 3.8 Representative Chromatogram for DNA Sequencing Confirmation of hOAT3 Conservative Mutants.

The chromatogram for hOAT3 WT (A) and hOAT3 Tyr342Phe (B) sequence. The triplet codon region highlighted shows position of mutation. The three letter amino acid codon string is translated and displayed within the highlighted section. Image generated using SnapGene.

A

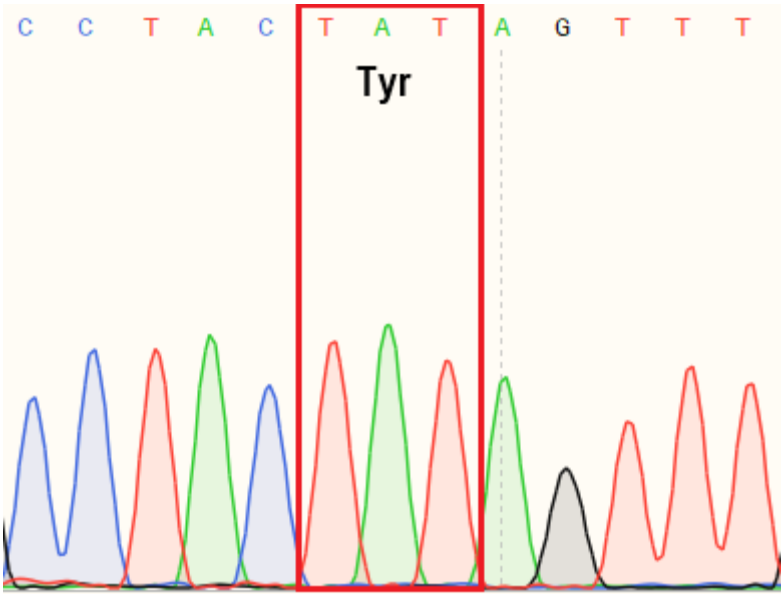

B

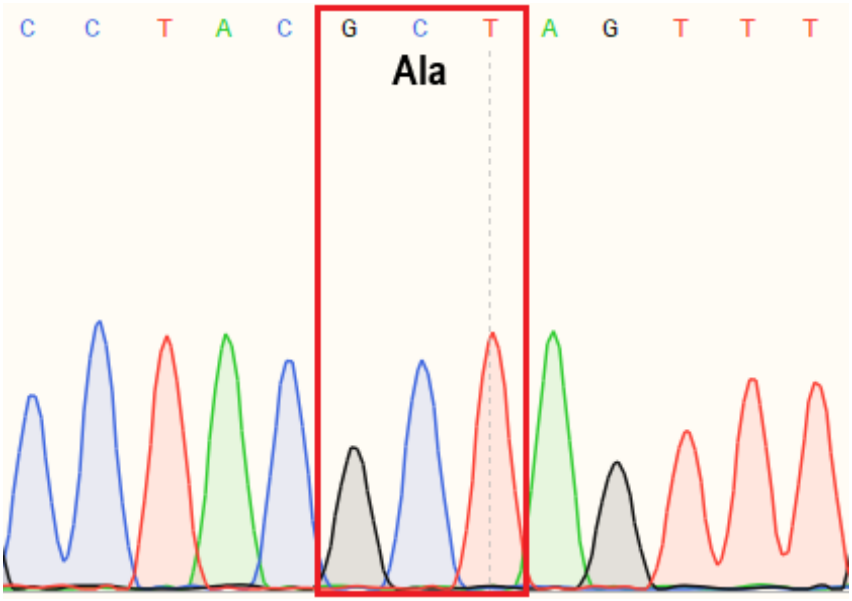

Figure 3.9 Representative Chromatogram for DNA Sequencing Confirmation of hOAT3 Non-conservative Mutants.

The chromatogram for hOAT3 WT (A) and hOAT3 Tyr342Ala (B) sequence. The triplet codon region highlighted shows position of mutation. The three letter amino acid codon string is translated and displayed within the highlighted section. Image generated using SnapGene.

After establishing stably-expressing WT and mutated hOAT3 cell lines, initial accumulation assays were performed to quantify ES transport activity. Cells were exposed to ES (5μM) in the absence or presence of the inhibitor probenecid (Figure 3.10). As shown, hOAT3 WT cells showed marked accumulation of ES (~17 fold) compared to HEK 293 parental cells (192.6 ± 5.9 vs. 11.0 ± 2.5 pmol/mg protein/10 min, respectively). The known hOAT3 inhibitor probenecid (500μM) showed virtually complete inhibition of hOAT3-mediated ES uptake, as accumulation was comparable between probenecid exposed hOAT3 WT cells and HEK 293 parental cells (9.9 ± 0.8 vs. 7.6 ± 0.5 pmol/mg protein/10 min, respectively). Cell accumulation assay demonstrated that substitutions Phe426Tyr (100.2 ± 4.7 pmol/mg protein/10 min), Phe430Tyr (338.6 ± 7.2 pmol/mg protein/10 min), Phe430Ser (155.3 ± 5.7 pmol/mg protein/10 min), Leu431Ile (27.7 ± 2.7 pmol/mg protein/10 min) and Arg454Ala (21.7 ± 7.2 pmol/mg protein/10 min) all retained ES transport activity as compared to HEK 293 parental cells. Two conservative (Tyr342Phe, Arg454Lys) and three non-conservative (Tyr342Ala, Phe426Ser, Leu431Ala) substitutions abolished ES transport mediated by hOAT3. To determine if hOAT3 mutant cell lines were considered transport active or inactive, equal variance ANOVA with Dunnett's multiple comparison between hOAT3 mutant cell lines and HEK 293 parental background cells was performed. Three cell lines (Phe426Tyr, Phe430Tyr, Phe430Ser) were found to be statistically different from HEK 293 ($p < 0.0001$), along with Leu431Ile ($p < 0.001$) and Arg454Ala ($p < 0.05$), suggesting these five are transport active mutants. However, despite reaching statistical significance under these conditions, it is clear that the Leu431Ile and Arg454Lys cell lines did not exhibit significant inhibitor-sensitive ES uptake (i.e., no hOAT3 transporter-mediated uptake) and it was concluded

these should be treated as false positives, and they were not considered active mutants. The remaining cell lines (Tyr342Phe, Tyr342Ala, Phe426Ser, Leu431Ala, Arg454Lys) were not statistically different from the parent ($p > 0.05$), and were thus treated as inactive mutants.

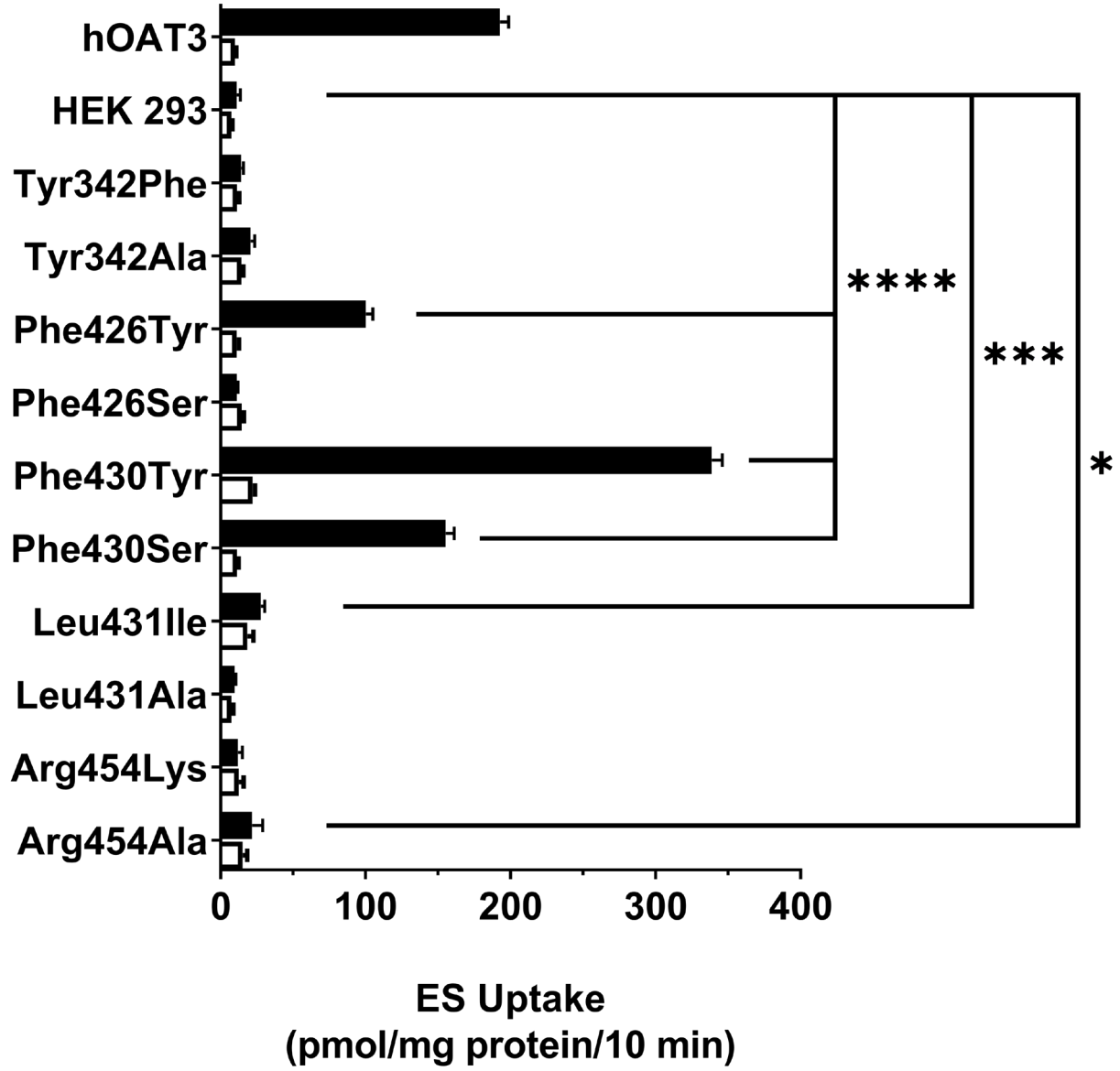

Figure 3.10 Initial ES Transport Activity Assay Assessment of hOAT3 Mutants

Initial accumulation assay with 5μM ES in the absence (black) and presence (white) of 500μM probenecid. Y-axis labels indicate the hOAT3 protein expressed in the stable cell line tested including hOAT3 WT (hOAT3), parental background (HEK 293), and the generated conservative and non-conservative hOAT3 mutants. Accumulation was performed over a 10 min period and corrected by protein content. Values reported as mean ± SD of triplicate samples. Significance indicated by ****$p < 0.0001$, ***$p < 0.001$, *$p < 0.05$ as determined by one-way ANOVA followed by Dunnett's t-test in comparison to HEK 293 without probenecid.

For the true active hOAT3 mutant cell lines, further kinetic analysis was conducted to determine if mutant cells exhibited changes in ES affinity (K_m) as compared to hOAT3 WT. Cells were exposed to increasing concentrations of ES (1μM – 100μM) for one minute and representative plots are shown in Figure 3.11. All constructs exhibited saturable transport activity and final K_m estimates are summarized in Table 3.5. As shown, K_m estimates for ES on the hOAT3 mutants Phe426Tyr, Phe430Tyr and Phe430Ser all trended higher, i.e., showed decreased affinity (13.4 ± 2.9, 13.6 ± 0.2 μM, and 26.8 ± 5.0 respectively). However, only the Phe430Ser mutant (26.8 ± 5.0 μM) had a statistically significant increase in K_m as compared to hOAT3 WT (9.1 ± 2.6 μM, $p < 0.05$).

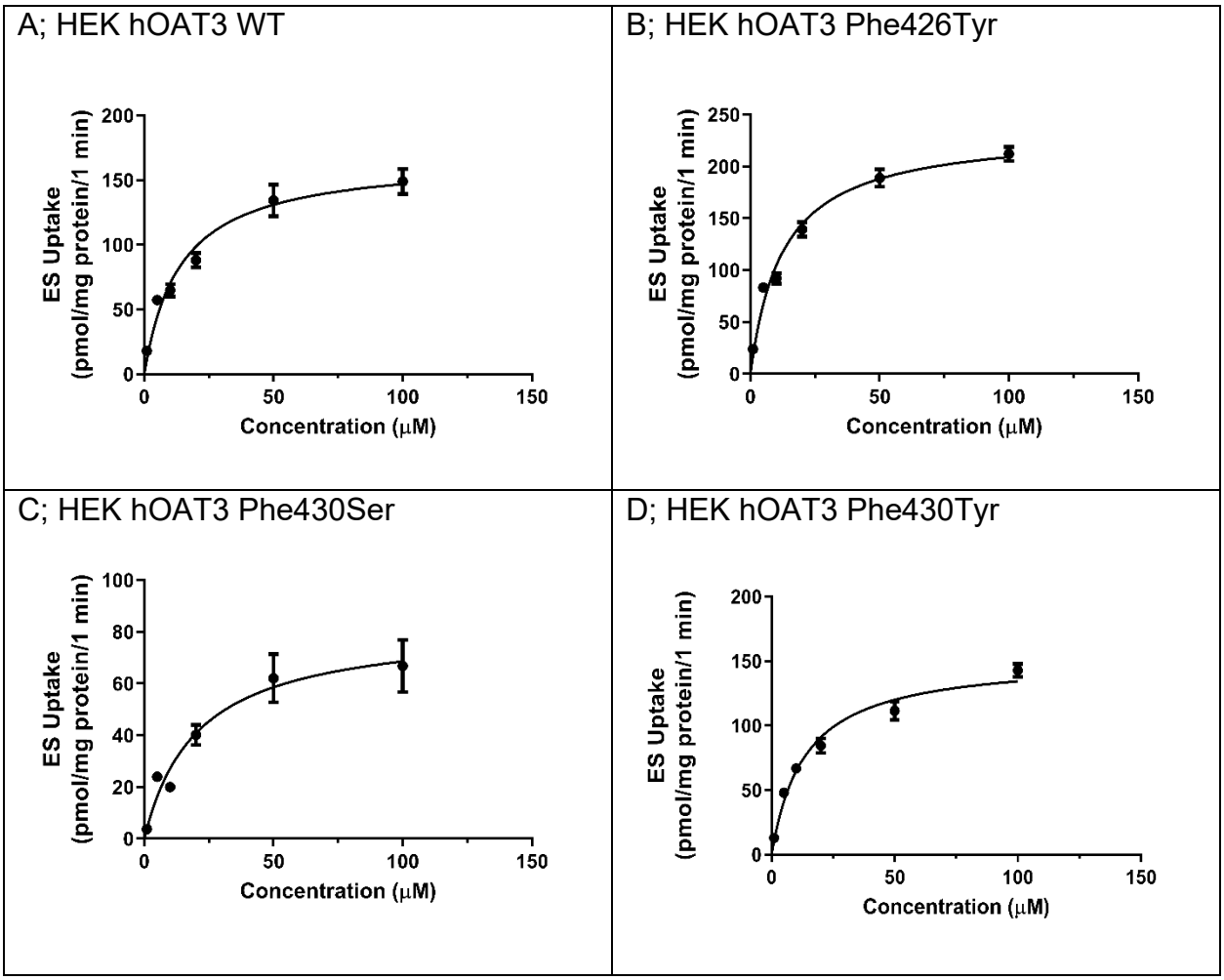

Figure 3.11 Saturation Analysis Conducted for hOAT3 WT and Active Mutants

One minute uptake of increasing concentrations of ES (1μM – 100μM) spiked with radiolabeled [^{3}H] ES (0.25 μCi/mL) in (A) HEK hOAT3 WT, (B) HEK hOAT3 Phe426Tyr, (C) HEK hOAT3 Phe430Ser, and (D) HEK hOAT3 Phe430Tyr cell lines. Data were corrected for background measured in HEK 293 control cells. K_m values were determined using Michaelis-Menten nonlinear regression using GraphPad Prism. Experiments within each cell line were repeated a minimum of three times in triplicate with final K_m estimates reported as mean ± SE. Each panel consists of a representative curve, with values plotted as mean ± SD.

Table 3.5 Estimated K_m for hOAT3 WT and hOAT3 active mutants

Transporter	K_m (μM)	N
hOAT3 WT	9.1 ± 2.6	3
hOAT3 Phe426Tyr	13.4 ± 2.9	3
hOAT3 Phe430Tyr	13.6 ± 0.2	3
hOAT3 Phe430Ser	26.8 ± 5.0*	5

Values are reported as mean ± SE. * denotes statistically different from WT.

Genomic Integration of hOAT3 Mutant Constructs

To confirm successful transfections of transport inactive cell lines, genomic DNA from each transfected cell lines was isolated and used as template for PCR. Primers consisted of the plasmid sequence specific T7 primer and the hOAT3 reverse 1 sequencing primer (Table 3.2) which should yield full length (~2,000bp) amplification of the hOAT3 insert. As shown in Figure 3.12, the expected product band was detected in every instance, except for non-transfected HEK 293 negative control (lane 2), confirming successful genome integration of all constructs during transfection.

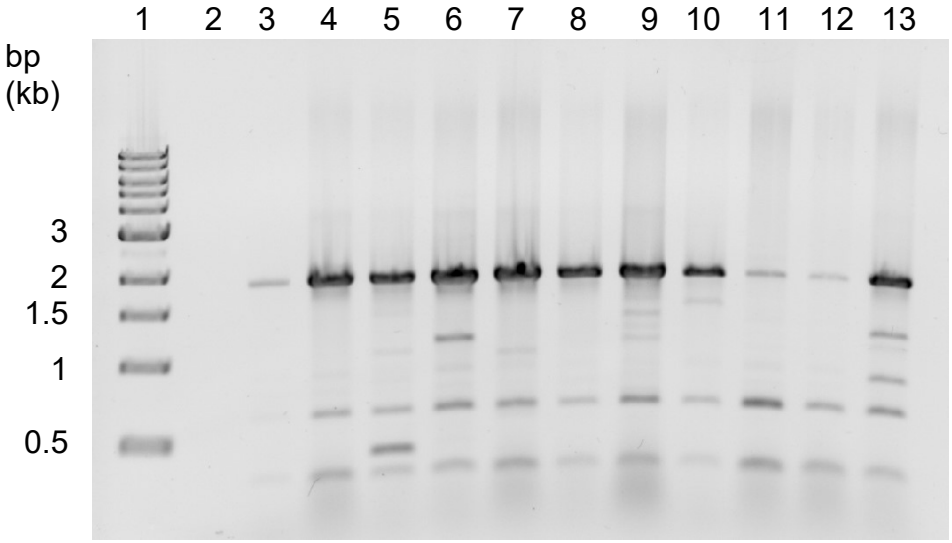

Figure 3.12 Confirmation of Construct Integration into Genomic DNA

Confirmation of successful genomic integration of mutant hOAT3 constructs. Lanes are as follows: (1) 1kb Ladder, (2) HEK 293, (3) hOAT3 WT, (4) hOAT3 Tyr342Phe, (5) hOAT3 Tyr342Ala, (6) hOAT3 Phe426Tyr, (7) hOAT3 Phe426Ser, (8) hOAT3 Phe430Tyr, (9) hOAT3 Phe430Ser, (10) hOAT3 Leu431Ile, (11) hOAT3 Leu431Ala, (12) hOAT3 Arg454Lys, (13) hOAT3 Arg454Ala.

3D. DISCUSSION

Although it has been over two decades since the first discovery of OATs, information is still lacking in regards to the structural components that impact compound recognition at the molecular level. Thus far, attempts to crystallize SLC22 family members have been unsuccessful, thus, homology modeling has been employed. Recently, however, a protein within the MFS, PiPT, was crystallized and represents a suitable template for hOAT3 modeling studies. PiPT belongs to the same transporter superfamily, shares higher protein sequence identity (17%) and similarity (31%) with hOAT3 than GlpT (16% and 27%, respectively) upon BLAST analysis, and is more closely related evolutionarily as it is a eukaryotic protein whereas GlpT is prokaryotic. Therefore, in this work molecular modeling studies were conducted using PiPT as template.

One hundred models were constructed to represent the proposed alignment between PiPT and hOAT3, which aids in distinguishing small bond angles and torsional rotations over the course of the model building procedure. Of these potential 1,000 combinations generated, the top 15 results are reported in Table 3.3. The best combinations between hOAT3 and ES are listed in descending order of “GOLD Rank”. Selecting which model and pose combination to continue with was based on GOLD scores, DOPE scores, and number of clusters. Based upon these criteria, hOAT3 model 1 was selected (out of 100), and the best pose of ES within this model was number 2. Further evaluation of model 1 was conducted via Ramachandran plot analysis. Such analysis provides an additional detailed check on the stereochemistry of the protein structure in the proposed model (Figure 3.4). This plot provides assessment of the overall quality of the structure and also highlights regions which may require further investigation

[12]. As indicated, in model 1, 98.7% of the residues exist in “allowable” or “favorable” conformations and only four residues, Leu3, Arg65, Ser159, and Tyr216, were identified as having inappropriate bond angles between neighboring amino acids. Further visual inspection of the model confirmed these four residues reside towards the outer surface of the protein, a significant distance from the putative ES binding domain identified herein. Therefore, these residues were viewed as likely being non-influential to the final hOAT3-ES result. Finally, when all 1,000 ES docking results were observed as a group it was clear a single, centralized binding region emerged and the top ES pose (i.e, pose 2, displayed as a space-filling molecule to distinguish from all other ES molecules docked) is positioned within this centrally located region within hOAT3 (Figure 3.5). Thus, model 1 was selected (Figure 3.6).

Side (left) and top (right) views of the generated hOAT3 model illustrate the 12 TMD regions, along with the proposed binding pocket ES occupies (indicated by the grey space-filling cluster). Initial investigation revealed amino acid residues predicted to interact with ES, and they are labeled and visualized in Figure 3.7 A & B. One residue, Tyr342, may exhibit an edge-face aromatic interaction, as the dense positive charge about the edge of the benzene ring of the tyrosine is orientated toward the electronegative sulfate within the ES (Table 3.4). Arg454 has the potential for hydrogen bonding, as the guanidinium group aligns with the electronegative sulfate group of ES (Figure 3.7 A). Three residues, Phe426, Phe430, and Leu431, may exhibit hydrophobic interactions, i.e., the nonpolar properties of the listed residues associate with the tetracyclic ring within ES, thus forming in a hydrophobic pocket (Figure 3.7 B).

In order to test whether the residues identified in the current study truly impact hOAT3-ES interactions, conservative and non-conservative amino acid substitutions were introduced (Table 3.4). Initial transport activity assays confirmed five hOAT3 mutants, Phe426Tyr, Phe430Tyr, Phe430Ser, $p < 0.0001$; Leu431Ile, $p < 0.001$; Arg454Ala, $p < 0.05$) exhibited ES accumulation that was significantly greater than HEK 293 parental background (Figure 3.10). However, Leu431Ile and Arg454Ala, were identified as false positives in that they did not support significant inhibitor-sensitive ES uptake. All other mutants were determined to be transport inactive, as ES accumulation was not significantly different from background. Three non-conservative substitutions (Tyr342Ala, Phe426Ser, Leu431Ala) led to inactivity. This was likely due to the drastic change of the initial amino acid to either alanine or serine, residues devoid of a physiochemical influencing functional group, thus limiting the potential interaction with the substrate, ES. Two conservative substitutions, Tyr342Phe and Arg454Lys, where also inactive, potentially indicating the importance of tyrosine and arginine at these positions; e.g. the edge-face Pi system (Tyr342) and the hydrogen bond (Arg454) between them and ES is crucial for ES translocation and altering these residues disrupts substrate recognition.

While the three active hOAT3 mutants recognized and transported ES to some degree, it was unknown whether mutation led to altered affinity for ES. Therefore, these mutants were subjected to saturation (kinetic) analysis in order to estimate the K_m for ES and directly compare this to the hOAT3 WT K_m (Figure 3.11). The hOAT3 WT K_m for ES determined in these studies was 9.1 ± 2.6μM, which is in good agreement with the previous literature [40]. Estimated K_m values for both Phe426Tyr and Phe430Tyr trended

higher (13.4 ± 2.9 and 13.6 ± 0.2μM, respectively), while Phe430Ser had a significantly larger K_m value of 26.8 ± 5.0μM, indicating the importance of phenylalanine at this position for efficient ES translocation (Figure 3.11 and Table 3.5). Further studies will investigate if multiple substitutions within the same molecule (i.e., double or triple mutants) will result in further changes in transporter affinity.

Several explanations exist for the lack of ES transport activity by Tyr342Phe, Tyr342Ala, Phe426Ser, Leu431Ala, and Arg454Lys; 1) failed integration of full length hOAT3-cDNA into the genomic DNA during transfection, 2) substitution disrupted of the native amino acid truly impacted substrate recognition based on a critical interaction with ES, or 3) substitution disrupted proper folding and/or targeting of the protein to the plasma membrane following translation. Genomic integration of intact cDNA for all hOAT3 constructs was confirmed by PCR (Figure 3.12), demonstrating at the very least successful genomic integration. In order to examine targeting of inactive hOAT3 mutants to the membrane surface, multiple techniques were considered, similar to the approach used with hOAT1. Techniques include: developing a hOAT3-GFP plasmid, developing a hOAT3-c-Myc plasmid for continued IHC analysis, and generating stable HEK cell lines expressing hOAT3-c-Myc plasmid followed by detection through Western blotting. However, due to lack of targeting success for hOAT1, progress was halted for hOAT3 until a successful method for membrane targeting of hOAT1 is confirmed and validated, then it would be feasible to shift toward hOAT3. There are additional published methods which validated targeting of hOAT3 to the membrane [34], however, the hOAT3 antibody was generated “in-house” therefore not available commercially. Future studies to prove membrane targeting include the use of biotinylation in conjunction with a commercial

antibody to target hOAT3 or a targeted proteomics approach for detection/quantification [32,33].

In summary, a novel *in silico* homology model for hOAT3 based on the solved structure of PiPT was successfully constructed and validated. Upon successful docking of the prototypical substrate, ES, into the generated hOAT3 model, residues Tyr342, Phe426, Phe430, Leu431, and Arg454 (involving three separate TMDs) were identified as potentially critical to ES recognition. Preliminary data demonstrated that non-conservative substitution to alanine or serine led to complete loss of transport activity in all but one hOAT3 mutant (Phe430Ser). Conservative substitutions at positions 426 and 430 did not significantly alter transport affinity for ES, demonstrating a degree of tolerance at these positions in hOAT3 without loss of transporter function. The significantly reduced transport affinity for the non-conservative substitutions at position 430 suggests that there is less flexibility at this position or that phenylalanine is required at this position for effective ES transport. Future work will be focused on confirming non-functional hOAT3 mutants in regards to membrane targeting efforts to further strengthen our conclusions. Once confirmed, hOAT3 modeling studies could pave the way to optimizing drug design, by serving as a preliminary tool to assess initial validation of new chemical entities, in addition to predicting drug-drug interactions, prior to investing marked time, money, and effort in the pursuit of an investigational drug product.

CHAPTER 4 – MODELING ACROSS hOAT1-3

Virtual Screening of a Structurally Diverse Dataset of OAT Interacting Compounds

4A. INTRODUCTION

The SLC22 transporter family consists of organic cation, anion, and zwitterion transporters. Within this family lies OAT1 (SLC22A6) and OAT3 (SLC22A8), two OATs which were previously mentioned in Chapters 2 and 3, as well as OAT2 (SLC22A7), initially identified in rat liver [41] followed by mRNA isolation within human kidney and liver [42]. Sun et al. reported that hOAT2 had 39% and 38% identity among deduced amino acid sequences of hOAT1 and hOAT3, as compared to the 51% identity hOAT1 and hOAT3 share. These differences in shared identity may be the basis for differing substrate/inhibitor profiles amongst hOAT1-3, as well as account for greater overlap between hOAT1 and 3 vs hOAT2 in substrate recognition. For example, does probenecid, a pan inhibitor of hOAT1-3, exhibit conserved contacts amongst all three paralogs, while PAH, a preferred hOAT1 substrate, exhibits strong contacts within the hOAT1 model that are absent in hOAT2 and 3. Thus, it was of interest to generate a dataset of structurally diverse OAT family substrates/inhibitors to screen across the constructed hOAT1, 2 and 3 homology models to (1) determine if there were common contacts shared between compounds within each transporter model and (2) determine if there were notable commonalities/differences in contacts across hOAT1-3 for the structurally diverse dataset. Such information may partially explain certain variations in compound recognition and affinity across OAT paralogs.

Homology models for hOAT1 and hOAT3 have been previously generated using PiPT as template, using PAH and ES as the prototypical substrates. This *in silico* model building information was used as a guide for generating a hOAT2 homology model, once again with PiPT as template. Further evaluation of the generated hOAT1-3 models were conducted by additional docking of structurally diverse compounds. These compounds include the antiviral agent, acyclovir; the β-lactam antibiotic, penicillin G; the non-steroidal anti-inflammatory drug, salicylate; the prototypical inhibitor for OATs, probenecid; the counter ion used to drive anion exchange on OATs, alpha-ketoglutarate (α-KG); the fluorescent moiety, fluorescein; along with PAH and ES, the prototypical substrates for hOAT1 and hOAT3, respectively. Each compound was individually docked within the hOAT1-3 homology models and amino acid residues deemed critical within the prospective binding complexes were identified. This analysis of docking known compounds with varying structures within hOAT1-3 provided further information regarding additional residues which may mediate transporter binding interactions.

4B. MATERIALS AND METHODS

Molecular Model Building – The recently solved crystal structure for PiPT was identified as the most suitable currently available template molecule and its sequence was downloaded from PBD (PDB ID: 4J05). The hOAT2 FASTA protein sequence was downloaded from UniProt (UniProtKD ID: Q9Y694). Looped regions between TMD 1 & 2 and 6 & 7 in the final crystalized form of PiPT were excluded based on their inability to resolve these regions [6]. In order to properly align the target (hOAT2) peptide sequence with the known template (PiPT) peptide sequence, hOAT2 secondary structures, including potential TMD helices, were predicted using PredictProtein v1 [7]. Looped regions between TMD 1 & 2 and 6 & 7 were excluded from hOAT2 due to lack of resolved sequence within the PiPT crystal structure. The curated sequences were aligned using the multiple sequence alignment software ClustalX v2 [8], followed by manual modifications to avoid repetitive regions of non-alignment within predicted transmembrane helices, which would negatively impact the model building. The final alignment for PiPT-hOAT2 was visualized using ALINE v1.0.025 [9]. Based on this alignment, one hundred comparative homology models were generated, using the software MODELLER v9.17 [10]. The stereochemical integrity of the generated models was evaluated through DOPE scoring v9.17 [11,26] and Ramachandran plots (PROCHECK v9.17, [12]), both of which ensure bond lengths, angles, and torsions within the *in silico* model were within acceptable and feasible limits. Note that hOAT1 and hOAT3 homology models were previously described in Chapter 2 & 3, respectively.

Substrate Docking – The ionized, energy minimized structures for the following compounds were generated (Figure 4.1) using the computer-aided molecular modeling design tool SYBYL-X 2.1 [13]. Proper confirmation and atom type for the sketched *in silico* molecules were evaluated and followed by energy minimization based on Gasteiger-Huckel charges. Ligand docking studies were initiated using the docking algorithm GOLD v5.4 provided from the Cambridge Crystallographic Data Centre [14]. Briefly, GOLD configuration files were generated individually which referenced the previously generated one hundred hOAT1 - 3 models as the corresponding “receptor” and the *in silico* compound as the “ligand”. A spherical region 30Å in diameter was designated, which virtually encapsulated the entire transporter. One thousand possible combinations were evaluated, and the top combination was selected based on GOLD score, DOPE score, and number of clusters. The specific hOAT - compound combinations were then visually inspected using SYBYL-X v2.1, which allows 3-D manipulation, thus permitting identification of amino acids deemed potentially critical for the formation of the compound-transporter complex. Further validation of these predicted critical amino acids was obtained using the empirical molecular modeling system HINT [15], which evaluates and scores the binding interactions between the specific hOAT transporter and the compound docked.

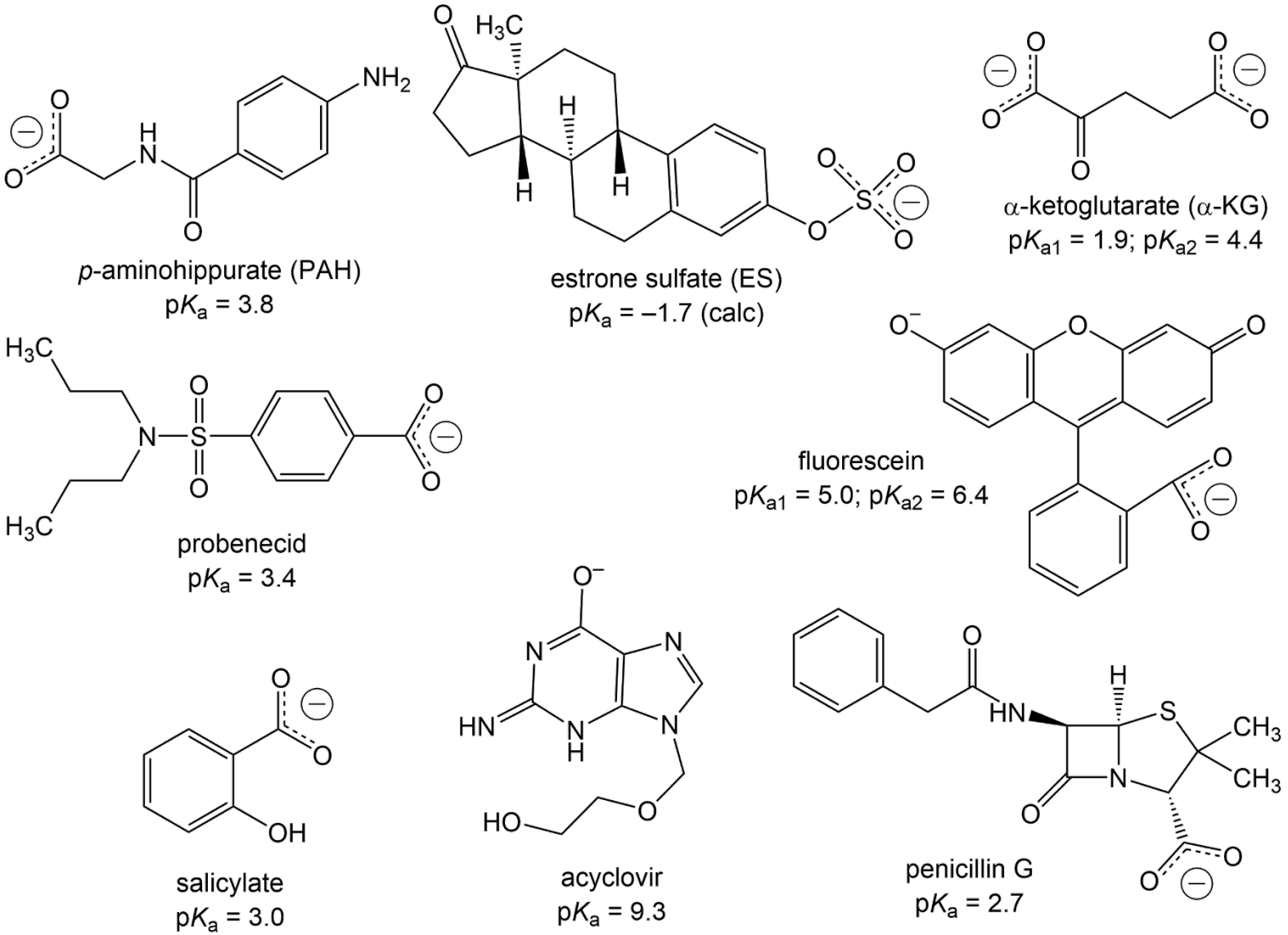

Figure 4.1 Structurally Diverse Compound Dataset Docked into hOAT1-3 Homology Models at pH 7.4

4C. RESULTS

Comparative Modeling of hOAT1, 2, & 3

An initial BLAST search of the non-redundant protein sequences database was performed to identify a suitable template for homology modeling. As mentioned previously, PiPT shares 33% sequence similarity and 19% sequence identity with hOAT1, and 31% sequence similarity and 17% sequence identity with hOAT3, both larger percentages then the previously utilized GlpT (27% and 16%). As for hOAT2, PiPT shares 33% sequence similarity and 19% sequence identity, signifying PiPT as a more appropriate template than GlpT, which shares 30% similarity and 18% identity with hOAT2. In addition, PiPT offers further advantages as a template molecule such as being a eukaryotic protein, inclusion in the MFS, a 12 TMD structure divided into two domains, and being crystallized in the occluded state therein maximizing the interaction within the compound-transporter complex. Thus, PiPT was selected to serve as the template.

All three hOATs and PiPT are predicted to have large sequence loops between TMDs 1 & 2 and 6 & 7. Due to their flexibility, these loops are not resolved in the PiPT crystal structure, thus there are no corresponding residues to model. Previous sequence curation was performed for hOAT1 and hOAT3, thus the procedure was repeated for hOAT2. Therefore, before alignment of hOAT2 and PiPT peptide sequences, the hOAT2 sequence (UniProtKB ID: Q9Y694) was truncated from Ala54 - Glu139 (between TMDs 1 & 2) and Leu286 – Phe338 (between TMDs 6 & 7). The final sequence alignment is shown in Figure 4.2, indicating the TMDs for PiPT (white) and hOAT2 (green) as well as exact positioned identities (white letters). This alignment file was fed into MODELLER, generating 100 separate *in silico* homology models for hOAT2.

Next, docking studies were conducted using GOLD v5.4 where each energy minimized compound was docked into each model separately, ten times, generating a total of 1,000 different combinations for each compound within each model. To determine the top compound-transporter combination, models were ranked through evaluation of their DOPE and GOLD scores, as well as cluster analysis. This process was previously summarized for hOAT1 and hOAT3 using their prototypical substrates (PAH and ES, respectively). As for hOAT2, representative analysis was performed to determine the top hOAT2-PAH combination. As shown in Table 4.1, the top hOAT2 model was number 18 with PAH pose number 10. Overall, this combination had the highest GOLD score (62.67), a similar DOPE score to other top combinations (-43299.80), and the highest number of clusters of the top five combinations (3). To further evaluate hOAT2 model 18, a Ramachandran plot was generated using the program PROCHECK v9.17 allowing visualization of all bond angles. Favorable bond angles appear in the red and yellow regions whereas disallowed angles are located in the white areas (Figure 4.3). Only one residue, Arg183, was identified as forming unfavorable bond angles in this model. This residue was positioned on the outskirts of the *in silico* model, i.e. well outside the putative PAH binding domain, and thus unlikely to exert direct influence on the hOAT2-PAH binding complex in this model. Thus, hOAT2 model 18 was selected as the best representation of hOAT2 in the occluded state with PAH. This process was repeated for hOAT1, 2, and 3 for each ionized, energy minimized compound (Figure 4.1), and top hOAT model and compound combinations were selected (Figures 4.4 – 4.6). Each compound is represented as a space filling molecule in a separate color and panel, specifically acyclovir (yellow), α-KG (grey), ES (pink), fluorescein (green), PAH (orange),

penicillin G (red), probenecid (purple) and salicylate (blue). Potential individual amino acid contacts are represented with lines. hOAT1-PAH and hOAT3-ES homology models are absent from Figures 4.4 and 4.6 since modeling was previously conducted in Chapters 2 and 3.

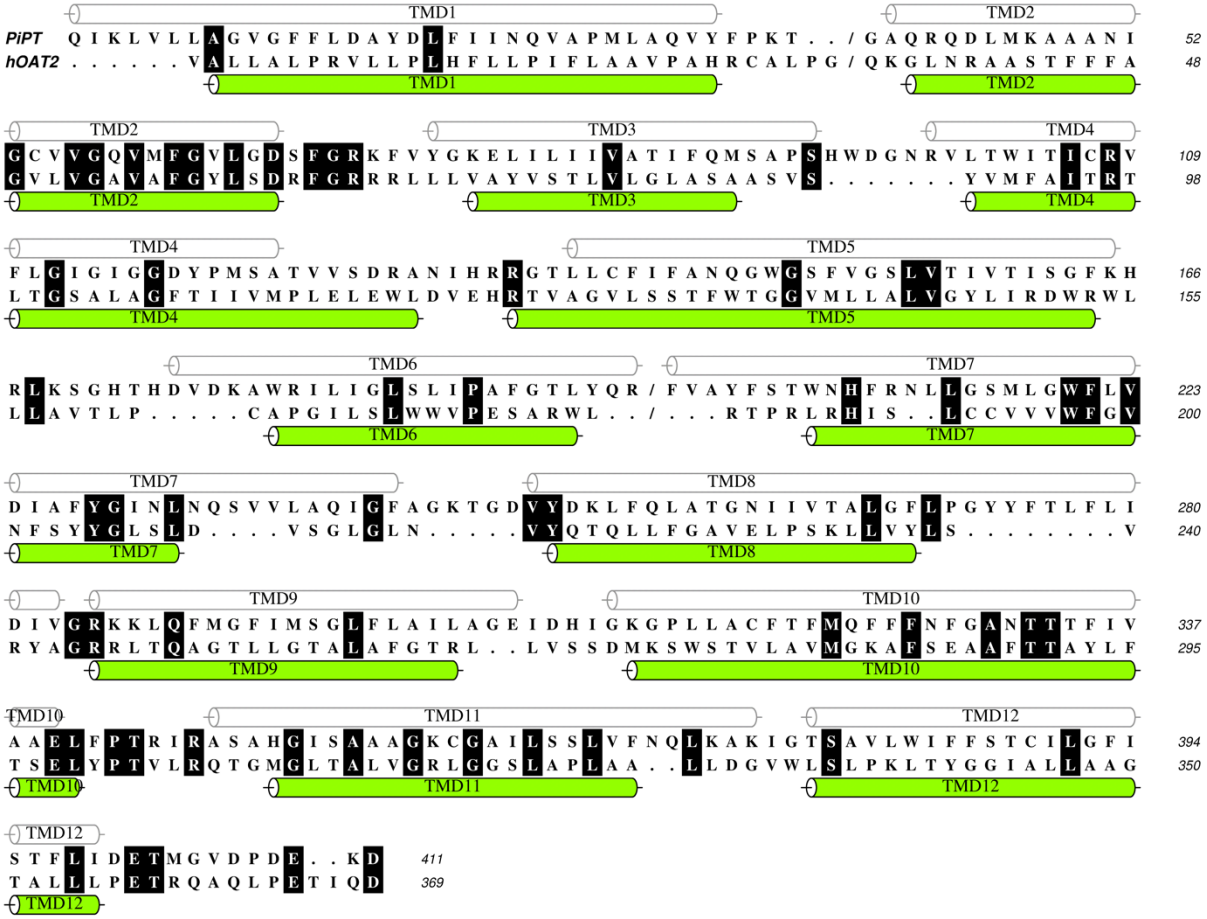

Figure 4.2 Peptide Sequence Alignment Between PiPT and hOAT2

Final peptide sequence alignment between PiPT (top) and hOAT2 (bottom). TMD regions for PiPT (white) documented and confirmed through initial crystallization of the protein. TMD regions for hOAT2 were initially predicted through PredictProtein v1 software, then regions were determined (green) upon final model generation. White letters indicate conserved amino acid residues between target and template. Image generated using the program ALINE v1.0.025.

Table 4.1 Summary of evaluative parameters and ranking for the top 15 hOAT2 models

GOLD Rank	GOLD Score	Model ID	Best hOAT2-PAH Pose	DOPE Score	# of Clusters
1	62.67	18	10	-43299.80	3
2	59.57	29	21	-42779.56	2
3	58.68	72	14	-42883.64	2
4	57.89	55	8	-43178.04	3
5	57.60	46	38	-43666.20	1
6	56.92	61	3	-42813.39	6
7	56.20	32	6	-42801.71	4
8	55.76	93	17	-43566.15	2
9	55.35	66	5	-43196.99	4
10	55.25	88	1	-42366.45	7
11	55.07	64	11	-43690.71	3
12	54.07	85	20	-43167.59	2
13	53.55	35	12	-43004.50	3
14	53.24	70	28	-42987.27	1
15	53.11	60	4	-42980.82	5

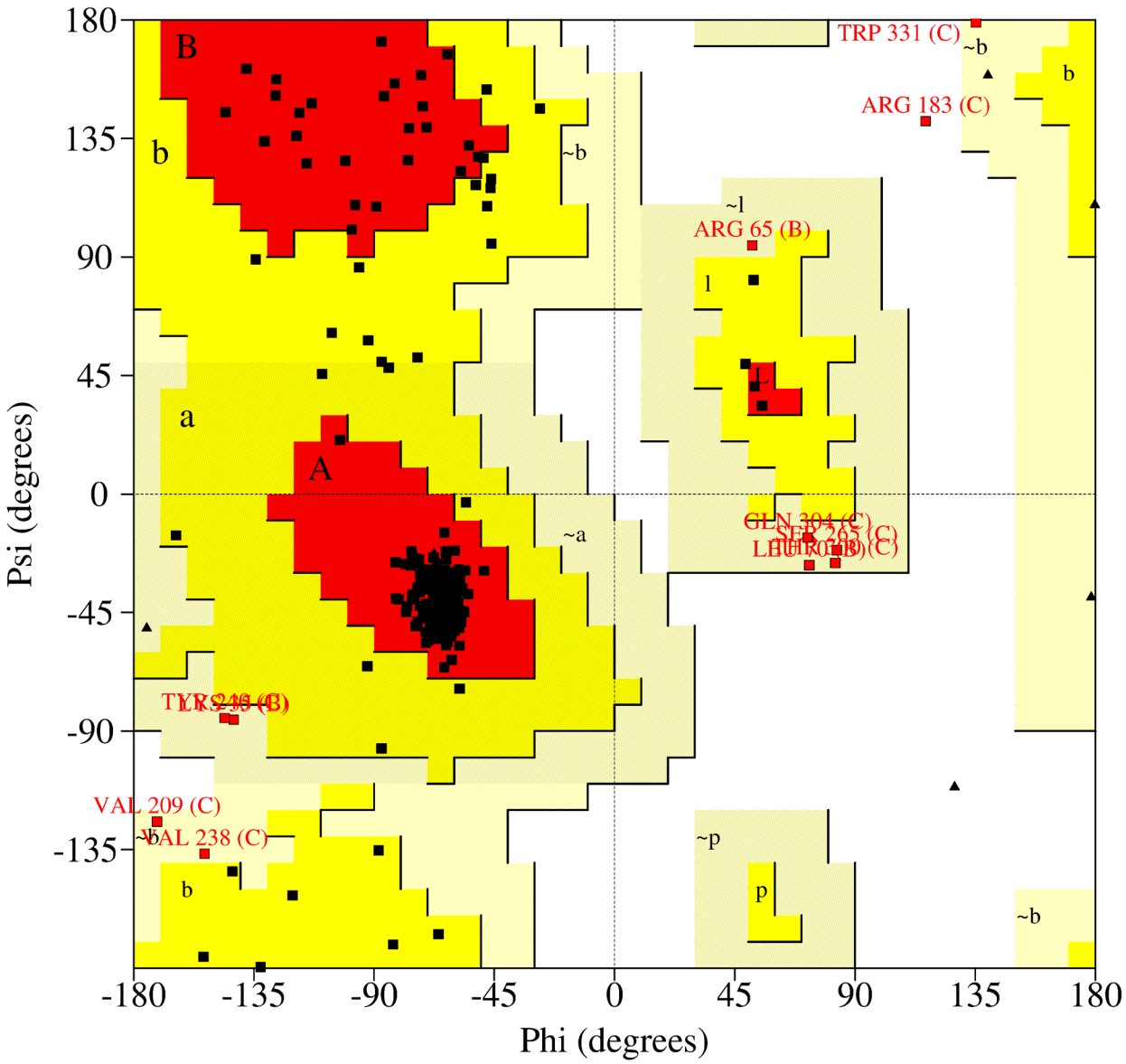

Figure 4.3 Ramachandran Plot of Top hOAT2 Homology Model

Axes indicate degree value of rotatable bonds present between neighboring amino acid residues with specific model generated. High percentage of amino acid residues were reported within favorable regions (99.7%), with remaining residue (ARG183) in unfavorable region. Plot generated using PROCHECK.

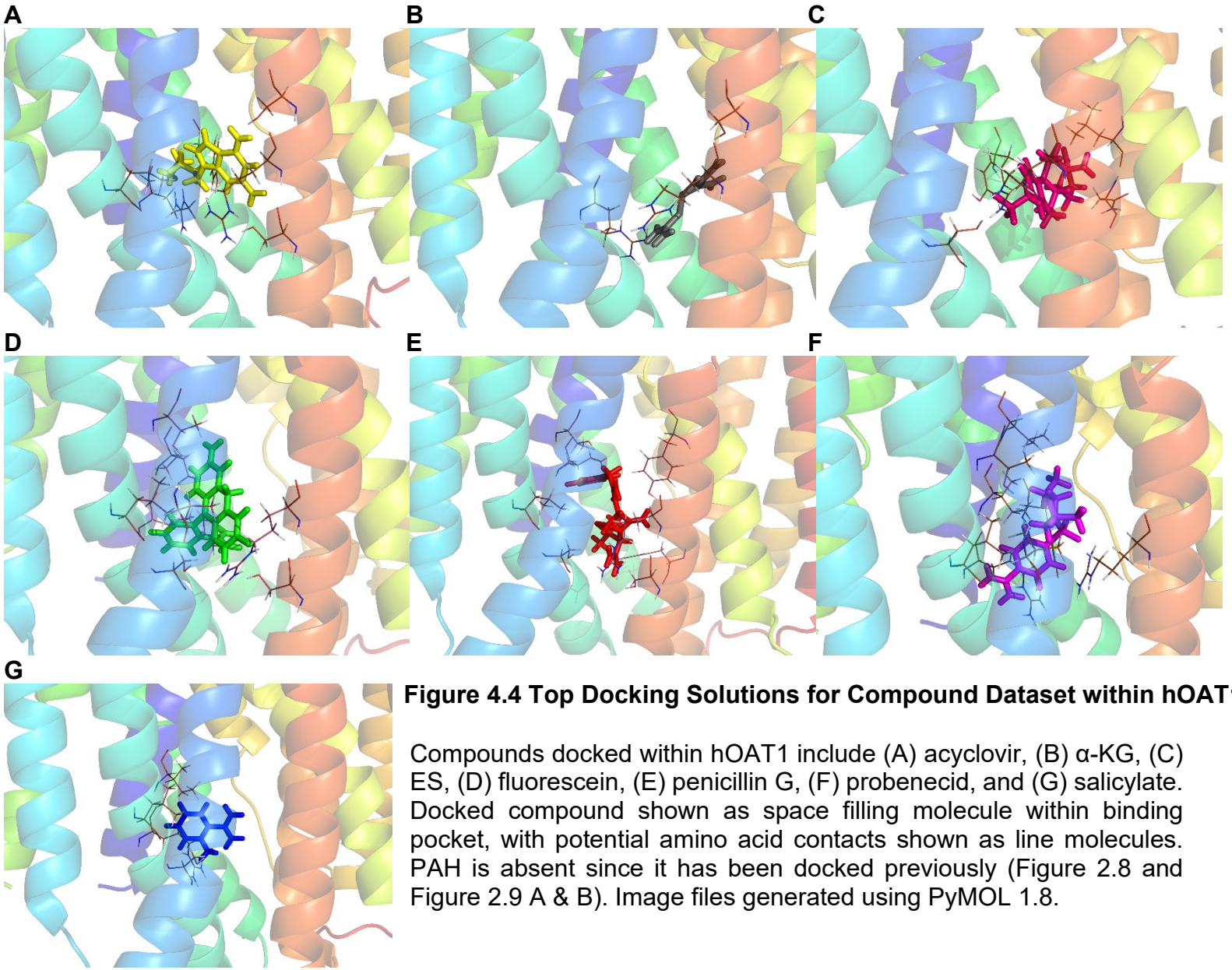

Figure 4.4 Top Docking Solutions for Compound Dataset within hOAT1

Compounds docked within hOAT1 include (A) acyclovir, (B) α-KG, (C) ES, (D) fluorescein, (E) penicillin G, (F) probenecid, and (G) salicylate. Docked compound shown as space filling molecule within binding pocket, with potential amino acid contacts shown as line molecules. PAH is absent since it has been docked previously (Figure 2.8 and Figure 2.9 A & B). Image files generated using PyMOL 1.8.

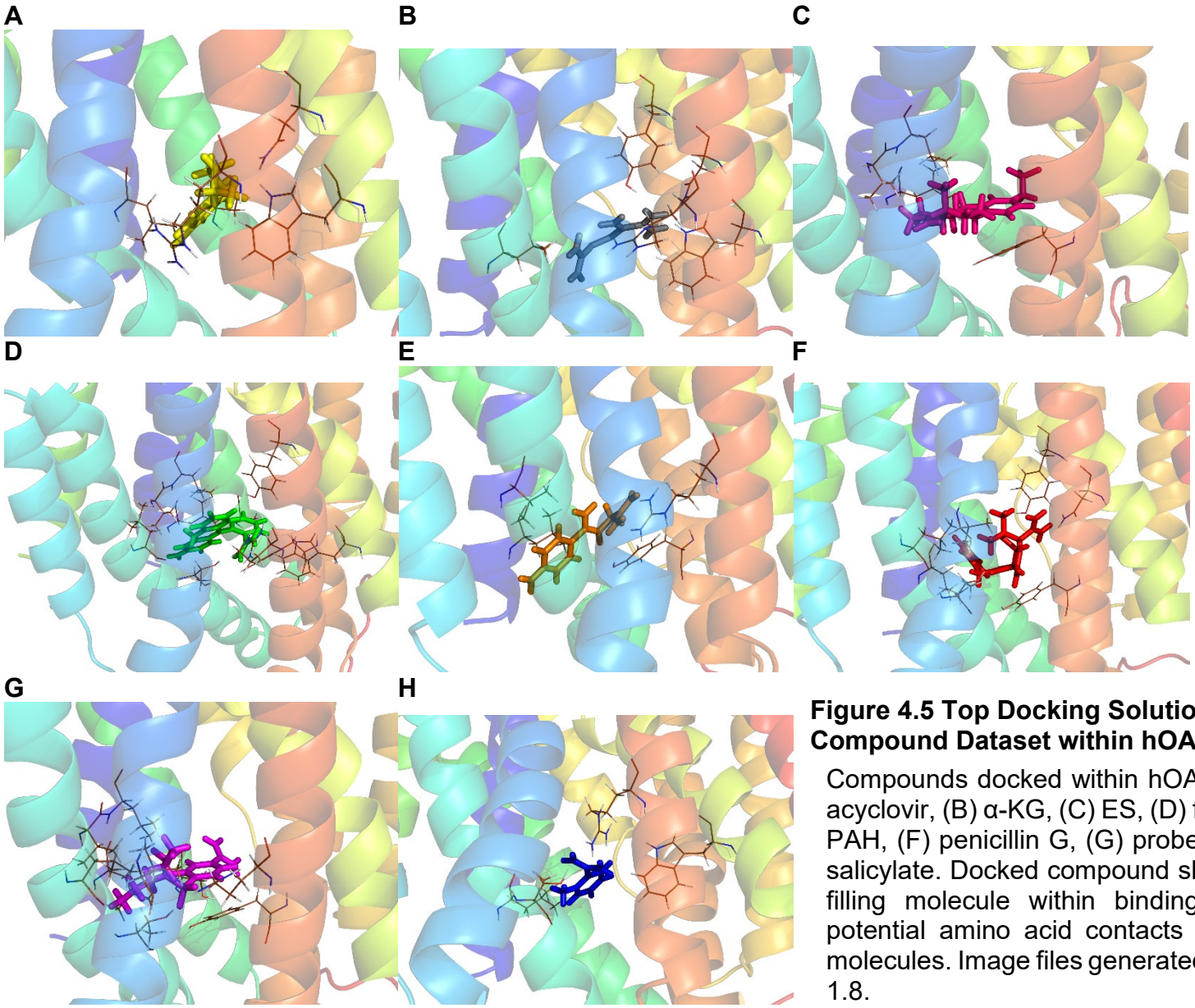

Figure 4.5 Top Docking Solutions for Compound Dataset within hOAT2

Compounds docked within hOAT2 include (A) acyclovir, (B) α-KG, (C) ES, (D) fluorescein, (E) PAH, (F) penicillin G, (G) probenecid, and (H) salicylate. Docked compound shown as space filling molecule within binding pocket, with potential amino acid contacts shown as line molecules. Image files generated using PyMOL 1.8.

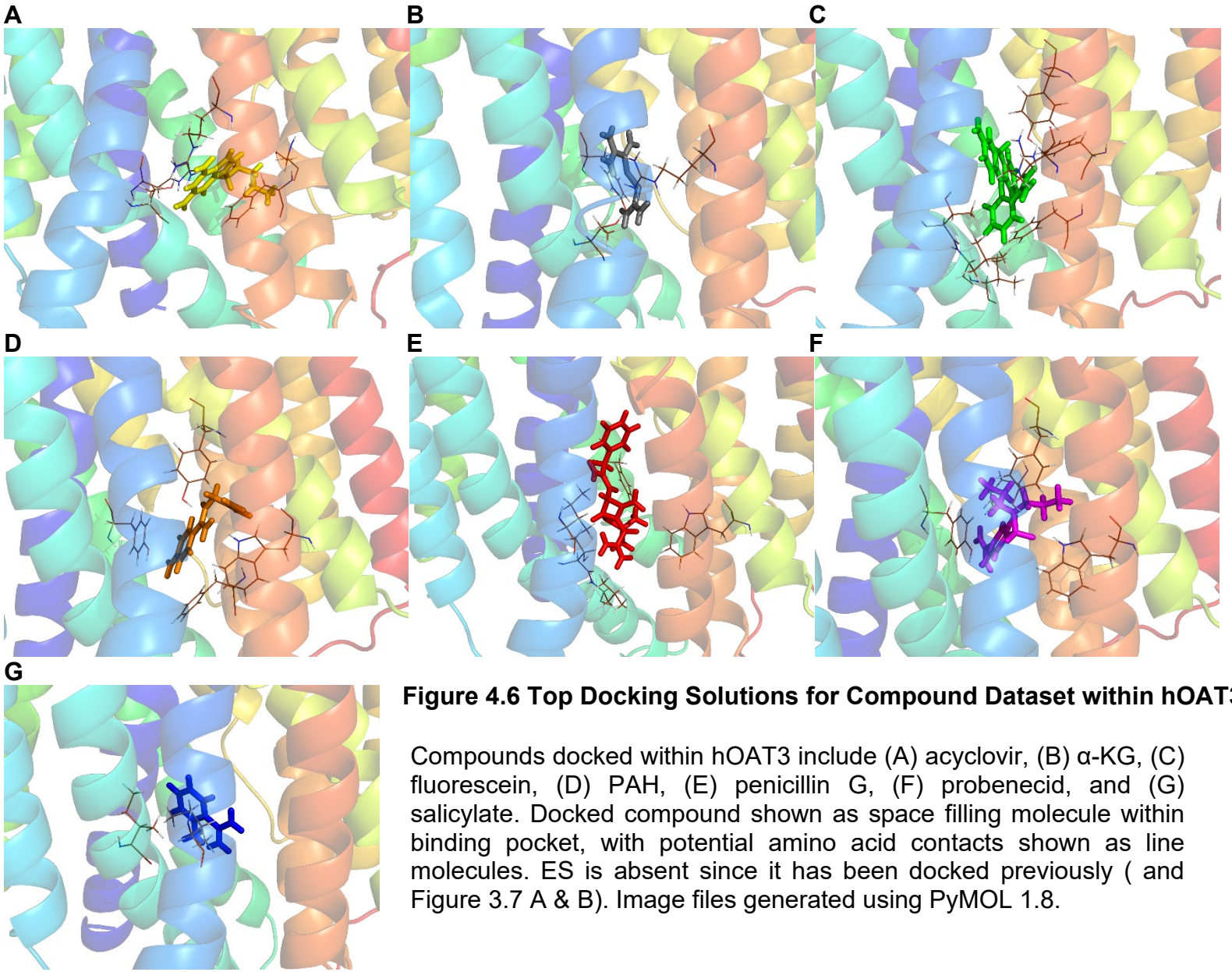

Figure 4.6 Top Docking Solutions for Compound Dataset within hOAT3

Compounds docked within hOAT3 include (A) acyclovir, (B) α-KG, (C) fluorescein, (D) PAH, (E) penicillin G, (F) probenecid, and (G) salicylate. Docked compound shown as space filling molecule within binding pocket, with potential amino acid contacts shown as line molecules. ES is absent since it has been docked previously (and Figure 3.7 A & B). Image files generated using PyMOL 1.8.

Using PyMOL v1.8, further analysis was focused within the suggested binding pocket to determine which amino acid contacts within the transporter are likely to be critical to compound recognition. Amino acids with potential compound interactions were identified, and the nature of the proposed interactions are summarized (Tables 4.2 – 4.4). Amino acid residues predicted to interact with the respective transporter are indicated by a check mark. Amino acid residues interacting with three or more compounds are highlighted yellow. Published compounds known to interact with hOAT1 (blue) and hOAT3 (red) are shown in Tables 4.2 and 4.4. Docking of the eight compounds in the hOAT1 model identified thirteen unique contacts across the dataset. Four of the five amino acids identified for PAH, Arg15, Ile19, Tyr230, and Arg466, interact with two or more other compounds, possibly indicating the importance of these residues in hOAT1 compound recognition. In particular, Arg15 and Arg466 were identified for all examined compounds that interact with hOAT1 (blue, Table 4.2). Eleven out of the twelve unique residues identified within hOAT2 interacted with three or more compounds. Leu26 was found to interact with every compound listed, thus this position could be highly important in hOAT2 compound recognition (Table 4.3). For hOAT3, fifteen unique contacts were identified. Three of the five potential amino acid contacts identified with ES, Tyr342, Phe430 and Arg454, also interact with two additional compounds, emphasizing the importance of these residues in hOAT3 compound recognition. Within the compounds known to interact with hOAT3 (red), Tyr342 was identified as a critical contact for both probenecid and ES, while Arg454 was identified as a critical contact for both ES and α-KG. ES and penicillin G did not share any similar binding contacts, which could be explained by the differences in structure; ES has a bulky tetracyclic ring and a sulfate

functional group while penicillin G has smaller, dispersed rings in addition to a carboxyl functional group.

Table 4.2 Summary of hOAT1 GOLD docking studies

hOAT1 Docking Studies									
Residue	**TMD**	**PAH**	**ES**	**α-KG**	**Probenecid**	**Acyclovir**	**Salicylate**	**Penicillin G**	**Fluorescein**
Arg15	1	✓		✓	✓	✓	✓		✓
Ile19	1	✓			✓		✓	✓	✓
Thr22	1				✓			✓	✓
Leu23	1				✓				
Val145	2				✓				✓
Leu199	4				✓	✓	✓	✓	✓
Ser203	4		✓				✓	✓	✓
Tyr230	5	✓	✓		✓	✓			
Leu434	10		✓						
Asn439	10	✓	✓						
Ser462	11					✓		✓	✓
Arg466	11	✓	✓	✓	✓	✓			✓
Ser469	11			✓		✓			

Compounds docked within *in silico* hOAT1 model. Check mark indicates potential amino acid contact. Yellow highlight indicates amino acid interacts with three or more compounds. Blue highlight indicates compounds known to interact with hOAT1.

Table 4.3 Summary of hOAT2 GOLD docking studies

hOAT2 Docking Studies									
Residue	**TMD**	**PAH**	**ES**	**α-KG**	**Probenecid**	**Acyclovir**	**Salicylate**	**Penicillin G**	**Fluorescein**
Leu26	1	✓	✓	✓	✓	✓	✓	✓	✓
Val29	1	✓	✓		✓				✓
Leu30	1		✓		✓				✓
Val155	2				✓			✓	
Leu209	4				✓			✓	✓
Thr213	4				✓		✓	✓	✓
Ser237	5				✓	✓			✓
Trp354	7			✓		✓	✓		✓
Asn358	7			✓		✓		✓	
Tyr362	7			✓				✓	✓
Tyr450	10	✓	✓		✓			✓	✓
Arg474	11	✓		✓	✓	✓	✓		✓

Compounds docked within *in silico* hOAT2 model. Check mark indicates potential amino acid contact. Yellow highlight indicates amino acid interacts with three or more compounds.

Table 4.4 Summary of hOAT3 GOLD docking studies

hOAT3 Docking Studies									
Residue	**TMD**	**PAH**	**ES**	**α-KG**	**Probenecid**	**Acyclovir**	**Salicylate**	**Penicillin G**	**Fluorescein**
His15	1					✓			
Ile133	2						✓	✓	
Ile187	4						✓		
Thr191	4			✓				✓	✓
Leu192	4							✓	✓
Val195	4								✓
Tyr218	5	✓		✓	✓			✓	
Trp334	7	✓			✓			✓	
Tyr342	7	✓	✓		✓				
Leu422	10				✓				
Phe426	10		✓						
Ser427	10					✓			
Phe430	10	✓	✓			✓			
Leu431	10		✓						
Arg454	11		✓	✓		✓			

Compounds docked within *in silico* hOAT3 model. Check mark indicates potential amino acid contact. Yellow highlight indicates amino acid interacts with three or more compounds. Red highlight indicates compounds known to interact with hOAT3.

4D. DISCUSSION

Due to the limitations of technology in the past, visual representation of a protein's structure was constrained to a two-dimensional view. With the first discovery of OATs in rodent and human [3,43], gene sequences were represented as either individual nucleotides or amino acids. To predict how the protein spanned the phospholipid bilayer, membrane topology predictions were performed using Kyte-Doolittle hydropathy analysis, a graphical representation which plots the hydrophilicity and hydrophobicity of individual amino acids which together makeup a protein [44]. While such analysis was adequate at the time, there has been increased use and development of technology in the 21st century. New and innovative methods are using computer-based systems to drive pharmaceutical based research. Among these advancements, homology modeling techniques have emerged based on the ability to generate three-dimensional *in silico* homology models for unresolved proteins, and thus was explored for OATs.

hOAT1-3 homology models were generated, followed by the docking of multiple structurally diverse compounds. There have been numerous publications regarding compounds which interact with OATs, including antiviral agents, such as acyclovir [45–47], β-lactam antibiotics, such as penicillin [47,48], non-steroidal anti-inflammatory drugs, such as salicylate [28,34,49,50], a uricosuric agent and OAT inhibitor, probenecid [28,47,51], the counter ion used to drive anion exchange via OATs, α-KG [42,52], the fluorescent moiety, fluorescein [28,42], as well as PAH [27,28,34,42] and ES [53–55], the prototypical substrates for hOAT1 and hOAT3, respectively. The ionized form of each compound was sketched and energy minimized in SYBYL-X v2.1 (Figure 4.1) then separately docked into each model. A top compound-transporter solution was determined

for hOAT1 (Figure 4.4), hOAT2 (Figure 4.5), and hOAT3 (Figure 4.6). Each compound was colored as such: acyclovir (yellow), α-KG (grey), ES (pink), fluorescein (green), PAH (orange), penicillin G (red), probenecid (purple), and salicylate (blue). hOAT1-PAH and hOAT3-ES homology models are absent from Figure 4.4 and Figure 4.6 due to extensive modeling studies previously performed (Chapter 2 and Chapter 3).

Amino acid contacts for each compound were identified and reported (Table 4.2 – 4.4). Amino acid contacts for hOAT1 were identified in TMDs 1, 2, 4, 5, 10 and 11, with three or more residues identified in TMDs 1 and 11 (Table 4.2), suggesting these TMD regions are highly involved in hOAT1 compound recognition. Four of the five residues identified for PAH, Arg15, Ile19, Tyr230 and Arg466, were identified with two or more compounds, suggesting the importance of these positions in hOAT1-PAH recognition and continued testing of these positions through *in vitro* efforts. Tyr230, a residue identified in a previous hOAT1 modeling publication [1], was identified for three known hOAT1 compounds, PAH, probenecid and acyclovir, suggesting the importance of tyrosine's benzene ring, which possesses the ability to form edge-face aromatic interactions, for hOAT1 compound recognition. Additionally, Arg15 and Arg466 were identified for all known hOAT1 compounds docked, suggesting a guanidinium group within these positions is very important in hOAT1 compound recognition. Residue Asn439 was identified to interact with only two compounds, PAH and ES, suggesting further analysis at this position be deprioritized. However, hOAT1 Asn439Gln and Asn439Ala mutants were identified as PAH transport inactive (Figure 2.12). Additionally, the interaction between Asn439 and PAH was a hydrogen bond, a strong intermolecular force. Future work requires docking of additional compounds to validate Asn439 as a critical contact.

Residues Thr22, Leu199, Ser203 and Ser462 were identified after docking penicillin G and fluorescein, but were not identified with PAH. This suggests structurally divergent OAT substrates may utilize different contact points to achieve membrane translocation via the transporter. Amino acid contacts for hOAT2 were identified in TMDs 1, 2, 4, 5, 7, 10, and 11, with three or more residues identified in TMDs 1 and 7 (Table 4.3), suggesting these TMD regions are highly involved in hOAT2 compound recognition. Eleven of the twelve residues were identified to interact with three or more compounds, suggesting that it is unclear which contacts are most important in hOAT2 compound recognition. While every docked compound in Table 4.3 has been reported to interact with hOAT2, there are no verified prototypical substrates for hOAT2, or much transport data at all regarding hOAT2, including kinetic parameters, thus making it difficult to provide informed hOAT2 docking conclusions. However, LEU26 stands out in that it was identified for all eight dataset compounds, the only position to do so. Human OAT2 also has the greatest number of suggested contacts for probenecid amongst these three paralogs. Once a prototypical hOAT2 substrate is determined, more informed suggestions and continued validation through *in vitro* efforts can be performed. Amino acid contacts for hOAT3 were identified in TMDs 1, 2, 4, 5, 7, 10, and 11, with three or more residues identified in TMDs 4 and 10 (Table 4.3). Three of the five residues identified for ES, Tyr342, Phe430 and Arg454, were identified with two or more other compounds, suggesting the importance of these positions in hOAT3 ES recognition and continued testing of these positions through *in vitro* efforts. Two residues, Phe426 and Leu431, were only identified in ES docking studies, possibly indicating unique contact profiles for various substrate structures and again suggesting OATs are able to interface with such a broad array of structurally diverse

compounds by providing flexibility in contacts along its 'translocation pathway'. These positions, along with Phe430, are important in forming hydrophobic interactions. Additionally, Tyr 342 and Arg454 were identified across two known hOAT3 compounds: ES and probenecid (Tyr342) & ES and α-KG (Arg454), suggesting the benzene ring (tyrosine) and the guanidinium group (arginine) are important for hOAT3 compound recognition. No common contacts were identified between ES and penicillin G, potentially due to the difference in compound structure: ES contains a bulky tetracyclic ring and a sulfate functional group while penicillin G has two dispersed rings and a carboxyl functional group. Position Tyr218 was identified to interact with three out of four known hOAT3 compounds, α-KG, probenecid, and penicillin G, but not identified to interact with ES. α-KG, probenecid, and penicillin G all possess a carboxy functional group, which is absent in ES. Therefore, Tyr218 may influence compound recognition if the compound possesses a carboxyl functional group.

A similar number of contacts were identified upon hOAT1 (five), hOAT2 (four), and hOAT3 (four) PAH docking studies. Since PAH is the prototypical substrate for hOAT1 (K_m ~ 8.9 – 14.5 μM, [27,28]) and a weak substrate for hOAT2 (K_m ~ NA, [42]) and hOAT3 (K_m ~ 87.2 μM, [34]), amino acid interactions were evaluated to identify correlations. Of the five hOAT1-PAH contacts identified, hydrogen bonding (Arg15, Asn439 and Arg466), hydrophobic (Ile19), and edge-face aromatic (Tyr230) interactions were identified. Similar interactions were identified for hOAT2 and hOAT3: hydrogen bonding (hOAT2: Arg474; hOAT3: Trp334), hydrophobic (hOAT2: Leu26 and Val29), and edge-face aromatic (hOAT2: Tyr450; hOAT3: Tyr218, Tyr342 and Phe430) Due to these similarities, it is unclear as to why such marked differences in PAH affinity exist across the three paralogs.

A similar number of contacts were identified upon hOAT1 (five), hOAT2 (four), and hOAT3 (five) ES docking studies. Since ES is the prototypical substrate for hOAT3 (K_m ~ 6 μM, [54]) and a weak substrate for hOAT1 (K_m ~ NA, [53]) and hOAT2 (K_m ~ NA, [55]), individual amino acid interactions were evaluated to potentially explain these differences in affinity. hOAT3-ES interactions include edge facing pi-system (Tyr342), hydrophobic (Phe426, Phe430, and Leu431) and hydrogen bonding (Arg454). As for hOAT1 and hOAT2, similar interactions were identified: edge-face aromatic (hOAT1: Tyr230; hOAT2: Tyr450), hydrophobic (hOAT1: Leu434 and Asn439; hOAT2: Leu26, Val29 and Leu30), and hydrogen bonding (hOAT1: Ser203 and Arg466). Once again, it is unclear as to why differences in ES affinity exist across paralogs. A similar comparison was conducted by assessing α-KG docking results. hOAT2 (five) had more contacts recognized as compared to hOAT1 (three) and hOAT3 (three). Although used as the counter ion to drive anion exchange on OATs, α-KG has no reported kinetic parameters for hOAT1, 2, or 3. For hOAT2-α-KG, two instances of hydrogen bonding (Asn358 and Arg474), two instances of an edge-facing pi-system (Trp354 and Tyr362), and one instance of the hydrophobic effect (Leu26) were identified. For hOAT1-α-KG, two instances of hydrogen bonding (Arg15 and Arg466) and one instance of the hydrophobic (Ser469) were identified, with no instances of an edge-face aromatic interactions. As for hOAT3-α-KG, edge-facing pi system (Thr191 and Tyr218) and hydrogen bonding (Arg454) were identified, however there were no instances of extensive hydrophobic interactions. This suggests the importance of an additional edge-face aromatic and hydrogen bond interaction in α-KG recognition, however this is only speculative due to the lack of kinetic estimates and further mutational studies are required. Finally, probenecid has been used

as the prototypical inhibitor in OAT studies based on its strong inhibitory effect for hOAT1 (K_i ~ 4 μM, [28]) and hOAT3 (K_i ~ 4 μM, [47]), and weaker inhibitory potential for hOAT2 (K_i ~ 766 μM, [51]). Numerous contacts were identified in hOAT1 (eight), hOAT2 (nine), and hOAT3 (four) docking studies. Five hOAT1 contacts (Ile19, Thr22, Leu23, Val145, and Leu199) and six hOAT2 contacts (Leu26, Val29, Leu30, Val155, Leu209, and Ser237) were identified as contributing to hydrophobic interactions, suggesting the importance of this interaction in probenecid recognition. Three instances of edge-face aromatic were identified in hOAT3 (Tyr218, Trp334, and Tyr342), suggesting the cyclic features within these residues aid with hOAT3-probenecid recognition. Based on the sheer number and strength of contacts identified, it is not surprising that probenecid is a strong OAT inhibitor.

In summary, novel *in silico* homology models for hOAT1-3 based on the solved structure of PiPT were successfully constructed and validated. Numerous structurally diverse compounds which have been published to interact with OATs were docked within the generated models. Amino acid contacts were primarily found in TMDs 1, 2, 4, 5, 10, and 11, suggesting that these TMDs are important in compound recognition. Four of the five residues identified in hOAT1-PAH docking studies interacted with two or more compounds, indicating the importance of these residues in hOAT1 substrate recognition. For hOAT2, eleven of the twelve amino acid contacts identified interacted with three of more compounds, suggesting initial positions to investigate for continued hOAT2 substrate recognition studies. Three of the five residues identified in hOAT3-ES docking studies interacted with two or more compounds, indicating the importance of these residues in hOAT3 substrate recognition. Similar residue counts and residue interactions

were identified after PAH, ES and α-KG docking studies across paralogs. Numerous, strong interactions were identified after probenecid docking studies, validating that probenecid is indeed a strong OAT inhibitor. These preliminary docking studies provide an initial starting point for continued analysis using these hOAT1-3 homology models. Future work involves docking the library of FDA compounds to further develop, validate, and compare results across hOAT1-3 homology models.

CHAPTER 5 – FUTURE APPLICATION

There has been a recent surge in additional techniques to further characterize compound interactions with SLC transporters, specifically through utilizing homology modeling supplemented with *in vitro* validation. Having the ability to assess whether a compound could interact with an ADME-relevant transporter, specifically through use of an *in silico* model, could expedite the early stages of drug discovery, in addition to potentially uncovering further information regarding ligand-transporter interactions [25]. Therefore, using these *in silico* models could be beneficial to 1) screen the FDA library of drug molecules to predict interacting drugs, 2) screen a large compound dataset to predict novel interacting molecules *in silico* followed by testing *in vitro* to identify new leads, or 3) potentially uncover key structural components as a means of informed rational drug design.

The generated models can be used for further assessment of key amino acid contacts and binding regions via docking of additional compounds. Docking the dataset of FDA compounds, for example, then comparing the strength of each drug's interaction with the OATs could elucidate common themes defining ligand-OAT interactions, e.g., which structural features specifically interact with OATs. Identifying compounds with similar structural characteristics could result in identification of novel interacting drugs, perhaps even aid in predicting potential clinical drug-drug interactions.

Additional screening of a large commercial compound dataset could be used to predict novel molecules for continued testing *in vitro* as potential lead compounds for further development that specifically target OATs. For some molecules, this could provide a viable elimination pathway for the potential lead, which in turn benefits the compounds'

safety profile by diminishing the potential for drug toxicity due to prolonged exposure. Alternatively, designing a potential OAT inhibitor to block elimination could also be pursued, especially if prolonging the drug's exposure in systemic circulation is necessary to reach efficacious drug concentration levels for a therapeutic effect.

Additional rational drug design strategies could be implemented as a result of continued modeling. Using known OAT substrates or inhibitors, there is potential to identify therapeutic vs OAT-interacting regions of the molecules which can then be exploited to design a more efficacious drug. Through the synthesis of a series of compounds with targeted modifications of specific functional groups, these various physiochemical features controlling each aspect can be probed by evaluating differences in accumulation levels and transport affinity. By identifying the separate therapeutic and OAT-interacting regions of a compound, there may be the potential to reduce renal elimination, increase half-life and decrease a patient dose or dose frequency, thus leading to increased patient compliance and benefit, in turn leading to safer and more cost-effective drug designs.

The current study is paving the way toward an innovative method to gather new information involving the binding complex location, and molecular level interactions, to aid in assessing the underlying mechanism of transport for hOAT1-3. Initial investigation of identified residues of the prototypical substrates for hOAT1 (PAH) and hOAT3 (ES) may offer insight to transporter-substrate recognition within each respective transporter in addition to other SLC22 family members. These preliminary studies offer a method for continued assessment of and screening for potential substrates/inhibitor, increasing our

ability to predict and avoid clinical drug-drug interactions, which in turn can lead to safer and more efficient drug design.

LIST OF REFERENCES

[1] Perry JL, Dembla-Rajpal N, Hall LA, et al. A three-dimensional model of human organic anion transporter 1: Aromatic amino acids required for substrate transport. *J Biol Chem*. **2006**, *281*, 38071-38079.

[2] Wang L, Sweet DH. Renal organic anion transporters (SLC22 family): expression, regulation, roles in toxicity, and impact on injury and disease. *AAPS J*. **2013**, *15*, 53-69.

[3] Hosoyamada M, Sekine T, Kanai Y, et al. Molecular cloning and functional expression of a multispecific organic anion transporter from human kidney. *Am J Physiol*. **1999**, *276*, F122-8.

[4] Race JE, Grassl SM, Williams WJ, et al. Molecular Cloning and Characterization of Two Novel Human Renal Organic Anion Transporters (hOAT1 and hOAT3). *Biochem Biophys Res Commun*. **1999**, *514*, 508-514.

[5] Martí-Renom MA, Stuart AC, Fiser A, et al. Comparative protein structure modeling of genes and genomes. *Annu Rev Biophys Biomol Struct*. **2000**, *29*, 291-325.

[6] Pedersen BP, Kumar H, Waight AB, et al. Crystal structure of a eukaryotic phosphate transporter. *Nature*. **2013**, *496*, 533-536.

[7] Yachdav G, Rost B. PredictProtein. https://www.predictprotein.org/. Published 2013. Accessed March 19, 2017.

[8] Larkin M a, Blackshields G, Brown NP. ClustalW2 and ClustalX version 2. *Bioinformatics*. **2007**, *23*, 2947-2948.

[9] Bond CS, Schüttelkopf AW. ALINE: A WYSIWYG protein-sequence alignment editor for publication-quality alignments. *Biol Crystallogr*. **2009**, *65*, 510-512.

[10] Webb B, Sali A. Comparative protein structure modeling using MODELLER. *Curr Protoc Bioinforma*. **2014**, *47*, 5.6.1-5.6.32.

[11] Shen M, Sali A. Statistical potential for assessment and prediction of protein structures. *Protein Sci*. **2006**, *15*, 2507-2524.

[12] Laskowski RA, MacArthur MW, Moss DS, et al. PROCHECK: a program to check the stereochemical quality of protein structures. *J Appl Crystallogr*. **1993**, *26*, 283-291.

[13] Tripos. SYBYL Expert Molecular Modeling Environment. www.tripos.com. Published 2013. Accessed October 10, 2017.

[14] Centre CCD. GOLD User Guide: A Component of the CSD-Discovery Suite. https://www.ccdc.cam.ac.uk/. Published 2019. Accessed October 10, 2017.

[15] Kellogg GE, Semus SF, Abraham DJ. HINT: A new method of empirical hydrophobic field calculation for CoMFA. *J Comput Aided Mol Des*. **1991**, *5*, 545-552.

[16] Bordo D, Argos P. Suggestions for “safe” residue substitutions in site-directed mutagenesis. *J Mol Biol*. **1991**, *217*, 721-729.

[17] Novoradovsky A, Zhang V, Ghosh M, et al. Computational principles of primer design for site directed mutagenesis. *NSTI-Nanotech*. **2005**, *1*, 532-535.

[18] *QIAprep ® Miniprep Handbook For Purification of Molecular Biology Grade DNA Sample & Assay Technologies.* Germantown, Maryland: QIAGEN; 2015.

[19] Scientific T. Lipofectamine 2000. https://www.thermofisher.com/us/en/home/references/protocols/cell-culture/transfection-protocol/lipofectamine-2000.html#procedure. Published 2006. Accessed May 30, 2020.

[20] Wang L, Sweet DH. Potential for food-drug interactions by dietary phenolic acids on human organic anion transporters 1 (SLC22A6), 3 (SLC22A8), and 4 (SLC22A11). *Biochem Pharmacol*. **2012**, *84*, 1088-1095.

[21] VanWert AL, Sweet DH. Impaired clearance of methotrexate in organic anion transporter 3 (Slc22a8) knockout mice: A gender specific impact of reduced folates. *Pharm Res*. **2008**, *25*, 453-462.

[22] Abràmoff MD, Magalhães PJ, Ram SJ. Image processing with imageJ. *Biophotonics Int*. **2004**, *11*, 36-41.

[23] Hong M, Zhou F, You G. Critical amino acid residues in transmembrane domain 1 of the human organic anion transporter hOAT1. *J Biol Chem*. **2004**, *279*, 31478-31482.

[24] Schlessinger A, Yee SW, Sali A, et al. SLC classification: An update. *Clin Pharmacol Ther*. **2013**, *94*, 19-23.

[25] Türková A, Zdrazil B. Current Advances in Studying Clinically Relevant Transporters of the Solute Carrier (SLC) Family by Connecting Computational Modeling and Data Science. *Comput Struct Biotechnol J*. **2019**, *17*, 390-405.

[26] Eramian D, Shen M, Devos D, et al. A composite score for predicting errors in protein structure models. *Protein Sci*. **2006**, *15*, 1653-1666.

[27] Ho ES, Lin DC, Mendel DB, et al. Cytotoxicity of antiviral nucleotides adefovir and cidofovir is induced by the expression of human renal organic anion transporter 1.

J Am Soc Nephrol. **2000**, *11*, 383-393.

[28] Cihlar T, Ho ES. Fluorescence-based assay for the interaction of small molecules with the human renal organic anion transporter. *Anal Biochem*. **2000**, *283*, 49-55.

[29] Sweet DH, Miller DS, Pritchard JB. Localization of an organic anion transporter-GFP fusion construct (rROAT1-GFP) in intact proximal tubules. *Am J Physiol*. **1999**, *276*, F864-73.

[30] Sweet DH, Miller DS, Pritchard JB. Basolateral localization of organic cation transporter 2 in intact renal proximal tubules. *Am J Physiol - Ren Physiol*. **2000**, *279*, 826-834.

[31] Kuze K, Graves P, Leahy A, et al. Heterologous expression and functional characterization of a mouse renal organic anion transporter in mammalian cells. *J Biol Chem*. **1999**, *274*, 1519-1524.

[32] Uchida Y, Toyohara T, Ohtsuki S, et al. Quantitative Targeted Absolute Proteomics for 28 Transporters in Brush-Border and Basolateral Membrane Fractions of Rat Kidney. *J Pharm Sci*. **2016**, *105*, 1011-1016.

[33] Kamiie J, Ohtsuki S, Iwase R, et al. Quantitative atlas of membrane transporter proteins: Development and application of a highly sensitive simultaneous LC/MS/MS method combined with novel in-silico peptide selection criteria. *Pharm Res*. **2008**, *25*, 1469-1483.

[34] Cha SH, Sekine T, Fukushima JI, et al. Identification and characterization of human organic anion transporter 3 expressing predominantly in the kidney. *Mol Pharmacol*. **2001**, *59*, 1277-1286.

[35] In Vitro Drug Interaction Studies — Cytochrome P450 Enzyme- and Transporter-Mediated Drug Interactions Guidance for Industry. https://www.fda.gov/regulatory-information/search-fda-guidance-documents/vitro-drug-interaction-studies-cytochrome-p450-enzyme-and-transporter-mediated-drug-interactions. Published 2020. Accessed February 1, 2020.

[36] Laskin OL, de Miranda P, King DH, et al. Effects of probenecid on the pharmacokinetics and elimination of acyclovir in humans. *Antimicrob Agents Chemother*. **1982**, *21*, 804-807.

[37] Eraly SA, Vallon V, Vaughn DA, et al. Decreased renal organic anion secretion and plasma accumulation of endogenous organic anions in OAT1 knock-out mice. *J Biol Chem*. **2006**, *281*, 5072-5083.

[38] Cihlar T, Lin DC, Pritchard JB, et al. The antiviral nucleotide analogs cidofovir and adefovir are novel substrates for human and rat renal organic anion transporter 1. *Mol Pharmacol*. **1999**, *56*, 570-580.

[39] Aslamkhan AG, Thompson DM, Perry JL, et al. The flounder organic anion transporter fOat has sequence, function, and substrate specificity similarity to both mammalian Oat1 and Oat3. *Am J Physiol - Regul Integr Comp Physiol*. **2006**, *291*, 1773-1780.

[40] VanWert AL, Gionfriddo MR, Sweet DH. Organic anion transporters: Discovery, pharmacology, regulation and roles in pathophysiology. *Biopharm Drug Dispos*. **2010**, *31*, 1-71.

[41] Sekine T, Cha SH, Tsuda M, et al. Identification of multispecific organic anion transporter 2 expressed predominantly in the liver. *Fed Eur Biochem Soc*. **1998**, *429*, 179-182.

[42] Sun W, Wu RR, van Poelje PD, et al. Isolation of a family of organic anion transporters from human liver and kidney. *Biochem Biophys Res Commun*. **2001**, *283*, 417-422.

[43] Sweet DH, Wolff NA, Pritchard JB, et al. Expression Cloning and Characterization of ROAT1. **1997**, *272*, 30088-30095.

[44] Kyte J, Doolittle RF. A simple method for displaying the hydropathic character of a protein. *J Mol Biol*. **1982**, *157*, 105-132.

[45] Takeda M, Khamdang S, Narikawa S, et al. Human organic anion transporters and human organic cation transporters mediate renal antiviral transport. *J Pharmacol Exp Ther*. **2002**, *300*, 918-924.

[46] Cheng Y, Vapurcuyan A, Shahidullah M, et al. Expression of organic anion transporter 2 in the human kidney and its potential role in the tubular secretion of guanine-containing antiviral drugs. *Drug Metab Dispos*. **2012**, *40*, 617-624.

[47] Tahara H, Shono M, Kusuhara H, et al. Molecular cloning and functional analyses of OAT1 and OAT3 from cynomolgus monkey kidney. *Pharm Res*. **2005**, *22*, 647-660.

[48] Deguchi T, Kusuhara H, Takadate A, et al. Characterization of uremic toxin transport by organic anion transporters in the kidney. *Kidney Int*. **2004**, *65*, 162-174.

[49] Khamdang S, Takeda M, Noshiro R, et al. Interactions of human organic anion transporters and human organic cation transporters with nonsteroidal anti-inflammatory drugs. *J Pharmacol Exp Ther*. **2002**, *303*, 534-539.

[50] Takeda M, Khamdang S, Narikawa S, et al. Characterization of methotrexate transport and its drug interactions with human organic anion transporters. *J Pharmacol Exp Ther*. **2002**, *302*, 666-671.

[51] Enomoto A, Takeda M, Shimoda M, et al. Interaction of human organic anion

transporters 2 and 4 with organic anion transport inhibitors. *J Pharmacol Exp Ther*. **2002**, *301*, 797-802.

[52] Hagos Y, Krick W, Braulke T, et al. Organic anion transporters OAT1 and OAT4 mediate the high affinity transport of glutarate derivatives accumulating in patients with glutaric acidurias. *Pflugers Arch Eur J Physiol*. **2008**, *457*, 223-231.

[53] Ueo H, Motohashi H, Katsura T, et al. Human organic anion transporter hOAT3 is a potent transporter of cephalosporin antibiotics, in comparison with hOAT1. *Biochem Pharmacol*. **2005**, *70*, 1104-1113.

[54] Sakurai Y, Motohashi H, Ueo H, et al. Expression Levels of Renal Organic Anion Transporters (OATs) and Their Correlation with Anionic Drug Excretion in Patients with Renal Diseases. *Pharm Res*. **2004**, *21*, 61-67.

[55] Kobayashi Y, Ohshiro N, Sakai R, et al. Transport mechanism and substrate specificity of human organic anion transporter 2 (hOat2 [SLC22A7]). *J Pharm Pharmacol*. **2005**, *57*, 573-578.

VITA

Christopher Edward Jay is an American citizen born February 25, 1993, in Buffalo, New York. He graduated from Orchard Park High School, Orchard Park, New York in 2011. He received his Bachelor of Science in Medicinal Chemistry with a minor in Mathematics from University at Buffalo, Buffalo, New York in 2015, then joined Virginia Commonwealth University (VCU) in the Department of Pharmaceutics in 2015.

During his PhD education, Chris was a co-author of a review paper and has presented his research both at the American Association of Pharmaceutical Scientists (AAPS) PharmSci 360 in 2018 and 2019, and VCU School of Pharmacy.

With his time at VCU, Chris took part in many opportunities, both in a professional and educational sense. Chris was a summer intern within the Office of Clinical Pharmacology at the Food and Drug Administration (FDA) in Silver Spring, Maryland. He held many leadership roles within VCU including AAPS Student Chapter Vice President, in addition to President and Secretary/Historian within the Department of Pharmaceutics Graduate Student Association (PCEU GSA). Chris was devoted in his teaching assignments as well, serving as a Teaching Assistant for Laboratory Foundations, Pharmacokinetics, and Graduate Research Methods. He was presented with various honors and awards, including travel grants, the 2018 AAPS Foundation Graduate Student Fellowship, Love of Learning Award, Jyontsna and Mavji Thakker Award, and was welcomed into various honor societies including Alpha Epsilon Lambda (AEL), Rho Chi, and Phi Kappa Phi (PKP). He will be continuing his studies at VCU with the Department of Biostatistics, as he looks to receive a Master’s degree shortly after completing his PhD.

PUBLICATIONS

Lai RE, **Jay CE**, Sweet DH. Organic solute carrier 22 (SLC22) family: Potential for interactions with food, herbal/dietary supplements, endogenous compounds, and drugs. *J Food Drug Anal*. 2018;26:S45-S60.

PRESENTATIONS AND AWARDS

AAPS PharmSci 360 Poster Presentation	2019, 2018
VCU School of Pharmacy Poster Presentation	2019, 2018, 2017
VCU Biopharmaceutical Applied Statistical Symposium (BASS) Scholarship	2019
VCU Graduate Student Travel Grant	2019, 2018
VCU Peter and Sian Byron SOP Graduate Student Travel Award	2019, 2018
VCU Dean’s Award Presentation	2019
Pfizer Consumer Healthcare R&S Leading for Innovation Award	2019
AAPS Foundation Graduate Student Fellowship	2018
VCU School of Pharmacy Student Podium Presentation	2017
Jyontsna and Mavji Thakker Award	2016